WCAP-15945-NP
Revision 1 (Revision 0 not published)

November 2002

Structural Integrity Evaluation of Reactor Vessel Upper Head Penetrations to Support Continued Operation: St. Lucie Unit 1
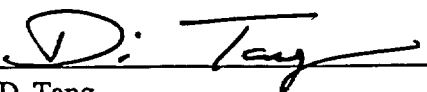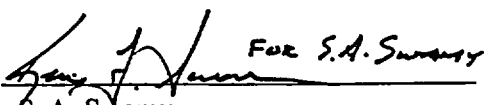
Westinghouse

WCAP-15945-NP
Revision 1 (Revision 0 not published)

Structural Integrity Evaluation of Reactor Vessel Upper Head Penetrations to Support Continued Operation: St. Lucie Unit 1

Warren H. Bamford
Chris K. Ng
Adam H. Alvarez

November 2002

Verifier: _____
D. Tang
Structural Mechanics Technology

Approved: _____ For S.A. Swamy
S. A. Swamy
Structural Mechanics Technology

TABLE OF CONTENTS

LIST OF TABLES

LIST OF FIGURES

LIST OF FIGURES (cont.)

LIST OF FIGURES (cont.)

1 INTRODUCTION

In September of 1991, a leak was discovered in the Reactor Vessel Control Rod Drive Mechanism (CRDM) head penetration region of an operating plant. This has led to the question of whether such a leak could occur at the St. Lucie Unit 1 Control Element Drive Mechanism (CEDM), In-Core Instrumentation (ICI), or head vent nozzle penetrations. Note that the designation CRDM (Westinghouse and French designs) and CEDM (Combustion Engineering Design) are synonymous. The geometry of interest is shown in Figure 1-1. Throughout this report, the penetration rows have been identified by their angle of intersection with the head. The location of head penetrations for St. Lucie Unit 1 are shown in Figure 1-2 and the angles for each penetration are identified in Table 1-1.

The CEDM leak resulted from cracking in Alloy 600 base metal, which occurred in the outermost penetrations of a number of operating plants as discussed in Section 2. This outermost CEDM location, as well as a number of intermediate CEDM penetrations, the ICI nozzles, and the head vent were chosen for fracture mechanics analyses to support continued safe operation of St. Lucie Unit 1 if such cracking were to be found. The dimensions of the CEDM penetrations are all identical, with 3.85 inch Outside Diameter (OD) and wall thickness of 0.566 inch; however, they all have a counterbore of 2.85 inches which extends from the bottom of the tube to 3.3 inches above the weld region. The ICI penetrations have an OD of 5.563 inch and a wall thickness of 0.469 inch. The ICI penetrations have a counterbore, beginning at the weld, of 4.75 in. inside diameter, leaving a thickness of 0.407 inch. For the head vent, the OD is 1.050 inches, and the wall thickness is 0.154 inch. All of these dimensions are summarized in Table 6-2.

The basis of the analyses was a detailed three-dimensional elastic-plastic finite element analysis of several penetration locations, as described in detail in Section 5. Results were obtained at a number of locations in each penetration, and used in the fracture analysis. The fracture analyses were carried out using reference crack growth rates recommended by the EPRI Materials Reliability Program (MRP). These rates are consistent with service experience. The results are presented in the form of flaw tolerance charts for both surface and through wall flaws. If indications are found, the charts will determine the allowable service life of safe operation. The service life calculated in the flaw tolerance charts are all in Effective Full Power Years (EFPY).

Note that there are several locations in this report where proprietary information has been bracketed and deleted. For each of the bracketed locations, reasons for proprietary classifications are given using a standardized system. The proprietary brackets are labeled with three different letters to provide this information. The explanation for each letter is given below:

a.   The information reveals the distinguishing aspects of a process or component, structure, tool, method, etc., and the prevention of its use by Westinghouse's competitors, without license from Westinghouse, gives Westinghouse a competitive economic advantage.

b.   The information, if used by a competitor, would reduce the competitor's expenditure of resources or improve the competitor's advantage in the design, manufacture, shipment, installation, assurance of quality, or licensing of a similar product.

c.   The information reveals aspects of past, present, or future Westinghouse or customer funded development plans and programs of potential commercial value to Westinghouse.

This flaw tolerance handbook is the latest in a series of reports prepared for many operating plants. Flaw tolerance charts have been prepared for the following plants to date:

- Point Beach Units 1 and 2
- Almaraz Units 1 and 2
- Beznau Units 1 and 2
- R. E. Ginna
- San Onofre Units 2 and 3
- Palo Verde Units 1 and 2
- Millstone Unit 2
- Waterford Unit 3
- ANO Unit 2
- North Anna Units 1 and 2
- Surry Units 1 and 2
- D. C. Cook Units 1 and 2
- Angra Unit 1
- Farley Units 1 and 2
- H. B. Robinson

The handbooks for D. C. Cook and North Anna have been submitted to the Regulatory Authority and the plants have received approval for restart. The Safety Evaluation Report for D. C. Cook is published, but that for North Anna is still pending.

Table 1-1			St. Lucie Unit 1 Head Penetration Nozzles with the Intersection Angles Identified					
Nozzle No.	Type	Angle (Degrees)	Nozzle No.	Type	Angle (Degrees)	Nozzle No.	Type	Angle (Degrees)
1	CEDM	0.0	27	CEDM	29.1	53	CEDM	37.1
2	CEDM	11.0	28	CEDM	29.1	54	CEDM	37.1
3	CEDM	11.0	29	CEDM	29.1	55	CEDM	37.1
4	CEDM	11.0	30	CEDM	29.1	56	CEDM	37.1
5	CEDM	11.0	31	CEDM	29.1	57	CEDM	37.1
6	CEDM	11.0	32	CEDM	29.1	58	CEDM	42.5
7	CEDM	11.0	33	CEDM	29.1	59	CEDM	42.5
8	CEDM	11.0	34	CEDM	35.6	60	CEDM	42.5
9	CEDM	11.0	35	CEDM	35.6	61	CEDM	42.5
10	CEDM	22.4	36	CEDM	35.6	62	CEDM	42.5
11	CEDM	22.4	37	CEDM	35.6	63	CEDM	42.5
12	CEDM	22.4	38	CEDM	35.6	64	CEDM	42.5
13	CEDM	22.4	39	CEDM	35.6	65	CEDM	42.5
14	CEDM	23.9	40	CEDM	35.6	66	CEDM	42.5
15	CEDM	23.9	41	CEDM	35.6	67	CEDM	42.5
16	CEDM	23.9	42	CEDM	38.5	68	CEDM	42.5
17	CEDM	23.9	43	CEDM	38.5	69	CEDM	42.5
18	CEDM	25.3	44	CEDM	38.5	70	ICI	54.8
19	CEDM	25.3	45	CEDM	38.5	71	ICI	54.8
20	CEDM	25.3	46	CEDM	38.5	72	ICI	54.8
21	CEDM	25.3	47	CEDM	38.5	73	ICI	54.8
22	CEDM	25.3	48	CEDM	38.5	74	ICI	54.8
23	CEDM	25.3	49	CEDM	38.5	75	ICI	54.8
24	CEDM	25.3	50	CEDM	37.1	76	ICI	54.8
25	CEDM	25.3	51	CEDM	37.1	77	ICI	54.8
26	CEDM	29.1	52	CEDM	37.1			
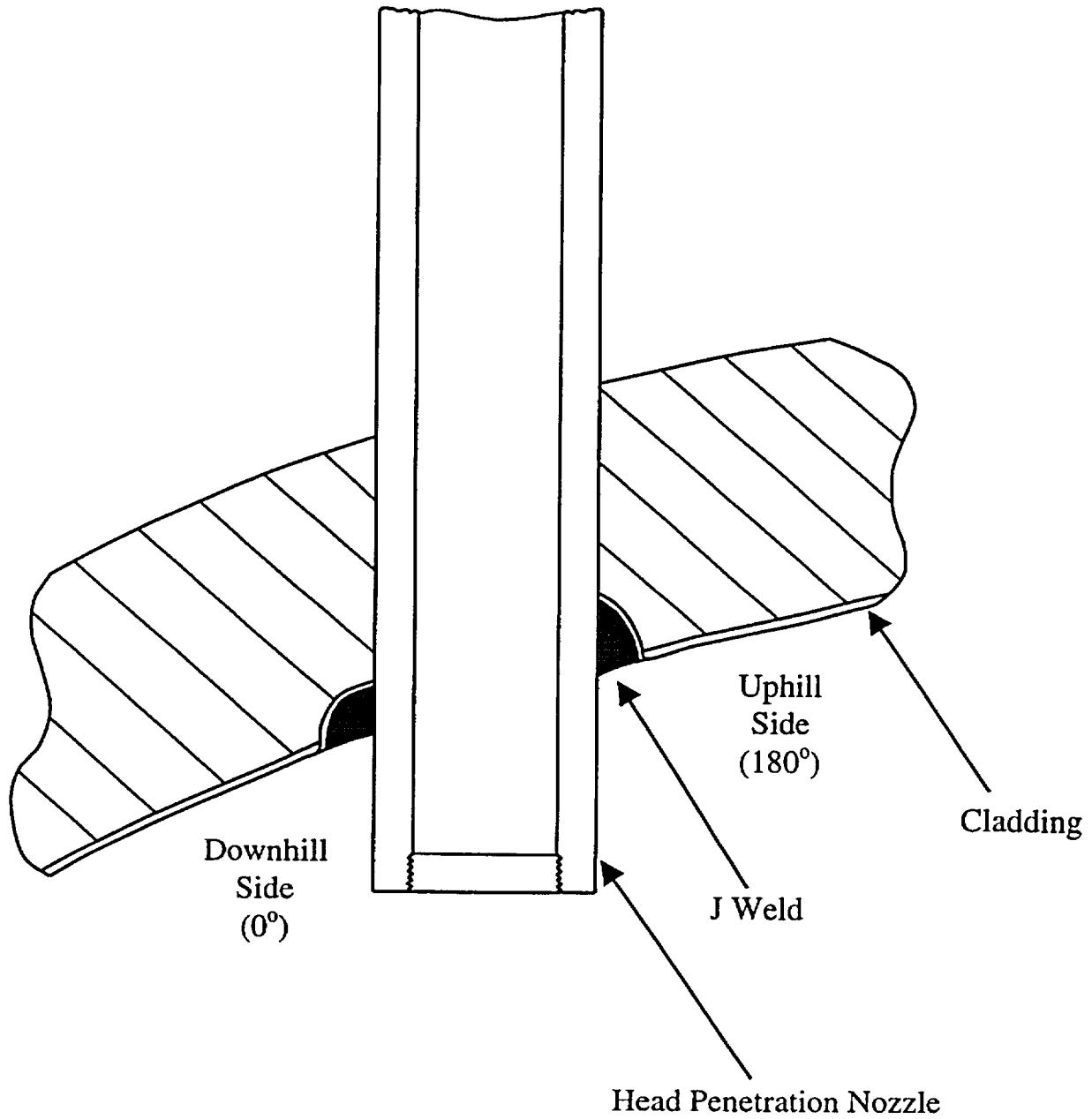
Figure 1-1 Reactor Vessel Control Element Drive Mechanism (CEDM) Penetration
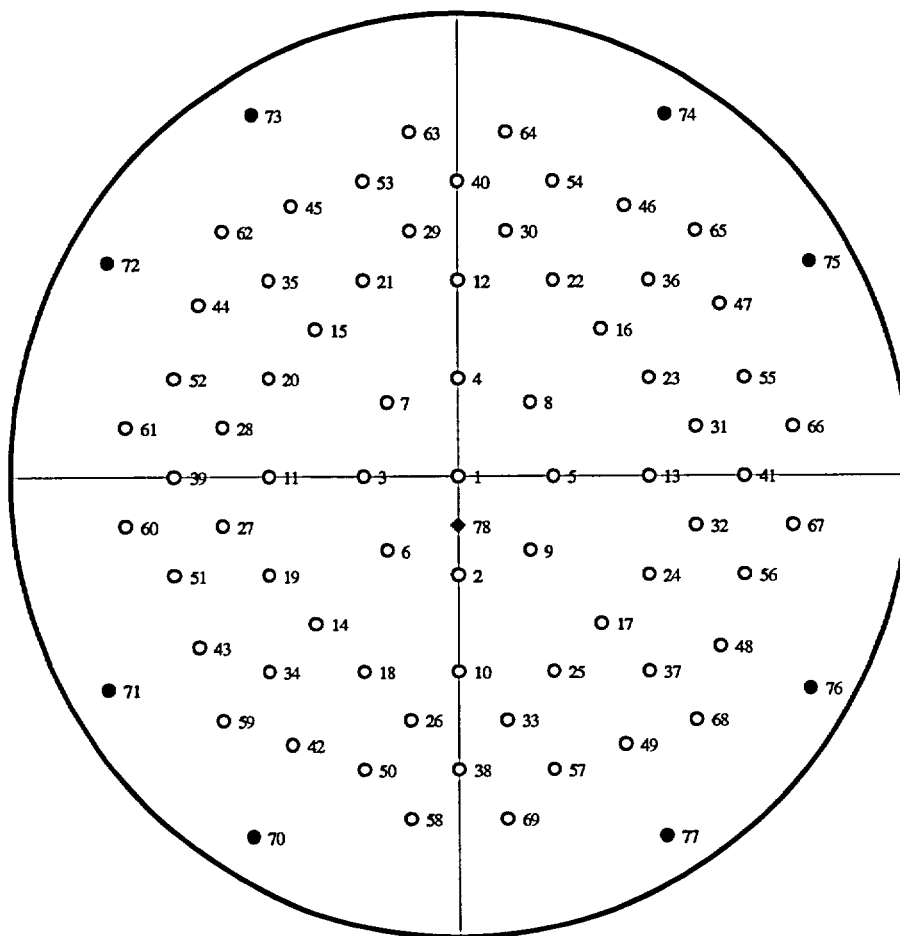
Figure 1-2 Location of Head Penetrations for St. Lucie Unit 1

2 HISTORY OF CRACKING IN HEAD PENETRATIONS

In September of 1991, leakage was reported from the reactor vessel CRDM head penetration region of a French plant, Bugey Unit 3. Bugey 3 is a 920 megawatt three-loop Pressurized Water Reactor (PWR) plant which had just completed its tenth fuel cycle. The leak occurred during a post ten year hydrotest conducted at a pressure of approximately 3000 psi (204 bar) and a temperature of 194°F (90°C). The leak was detected by metal microphones, which are located on the top and bottom heads. The leak rate was estimated to be approximately 0.7 liter/hour. The location of the leak was subsequently established on a peripheral penetration with an active control rod (H-14), as seen in Figure 2-1.

The control rod drive mechanism and thermal sleeve were removed from this location to allow further examination. A study of the head penetration revealed the presence of longitudinal cracks near the head penetration attachment weld. Penetrant and ultrasonic testing confirmed the cracks. The cracked penetration was fabricated from Alloy 600 bar stock (SB-166), and has an outside diameter of 4 inches (10.16 cm) and an inside diameter of 2.75 inches (7.0 cm).

As a result of this finding, all of the control rod drive mechanisms and thermal sleeves at Bugey 3 were removed for inspection of the head penetrations. Only two penetrations were found to have cracks, as shown in Figure 2-1.

An inspection of a sample of penetrations at three additional plants were planned and conducted during the winter of 1991-92. These plants were Bugey 4 , Fessenheim 1, and Paluel 3. The three outermost rows of penetrations at each of these plants were examined, and further cracking was found in two of the three plants.

At Bugey 4, eight of the 64 penetrations examined were found to contain axial cracks, while only one of the 26 penetrations examined at Fessenheim 1 was cracked. The locations of all the cracked penetrations are shown in Figure 2-1. At the time, none of the 17 CRDM penetrations inspected at Paluel 3 showed indications of cracking, however subsequent inspections of the French plants have confirmed at least one crack in each operating plant.

Thus far, the cracking in reactor vessel heads not designed by Babcock and Wilcox (B&W) has been consistent in both its location and extent. All cracks discovered by nondestructive examination have been oriented axially, and have been located in the bottom portion of the penetration in the vicinity of the partial penetration attachment weld to the vessel head as shown schematically in Figure 1-1.

[

]^{a,c,e}

[

]^{a,c,e}

]ᵃ,ᶜ,ᵉ

Non-destructive examinations of the leaking CRDM nozzles showed that most of the cracks were axially oriented, originating on the outside surface of the nozzles below the J-groove weld and propagating primarily in the nozzle base material to an elevation above the top of the J-groove weld. Leakage could then pass through the annulus to the top of the head where it was detected by visual inspection. In some cases the cracks initiated in the weld metal or propagated into the weld metal, and in a few cases the cracks propagated through the nozzle wall thickness to the inside surface.

[

]ᵃ,ᶜ,ᵉ

[

]a,c,e

The cracking has now been confirmed to be primary water stress corrosion cracking. Relatively high residual stresses are produced in the outermost CRDM penetrations due to the welding process. Other important factors which affect this process are temperature and time, with higher temperatures and longer times being more detrimental. It is interesting to note that no head vents have been found to have cracks. The inspection findings for the plants examined thus far are summarized in Table 2-1.

Table 2-1	Operational Information and Inspection Results for Units Examined (Results through April 30, 2002)						
Country	Plant Type	Units Inspected	K Hours	Head Temp. (°F)	Total Penetrations	Penetrations Inspected	Penetrations With Indications
France	CPO	6	80-107	596-599	390	390	23
	CPY	28	42-97	552	1820	1820	126
	1300M W	20	32-51	558-597	1542	1542	95
Sweden	3 Loop	3	75-115	580-606	195	190	8
Switzerland	2 Loop	2	148-154	575	72	72	2
Japan	2 Loop	7	105-108	590-599	276	243	0
	3 Loop	7	99	610	455	398	0
	4 Loop	3	46	590	229	193	0
Belgium	2 Loop	2	115	588	98	98	0
	3 Loop	5	60-120	554-603	337	337	6
Spain	3 Loop	5	65-70	610	325	102	0
Brazil	2 Loop	1	25	NA	40	40	0
South Africa	3 Loop	1	NA	NA	65	65	6
Slovenia	2 Loop	1	NA	NA	49	49	0
South Korea	2 Loop	3	NA	NA	49	49	3
	3 Loop	2	NA	NA	130	130	2
US	2 Loop	2	170	590	98	98	0
	3 Loop	1	NA	NA	65	20	12
	4 Loop	18	NA	NA	1149	537	35
TOTALS		117	–	–	7384	6373	318

NA = Not Available.

Note: CPO, CPY, and 1300 MW are all different models of French designed plants The CPOand CPY plants can be compared with a 3 loop plant, and the 1300 MW plant can becompared with a 4 loop plant.
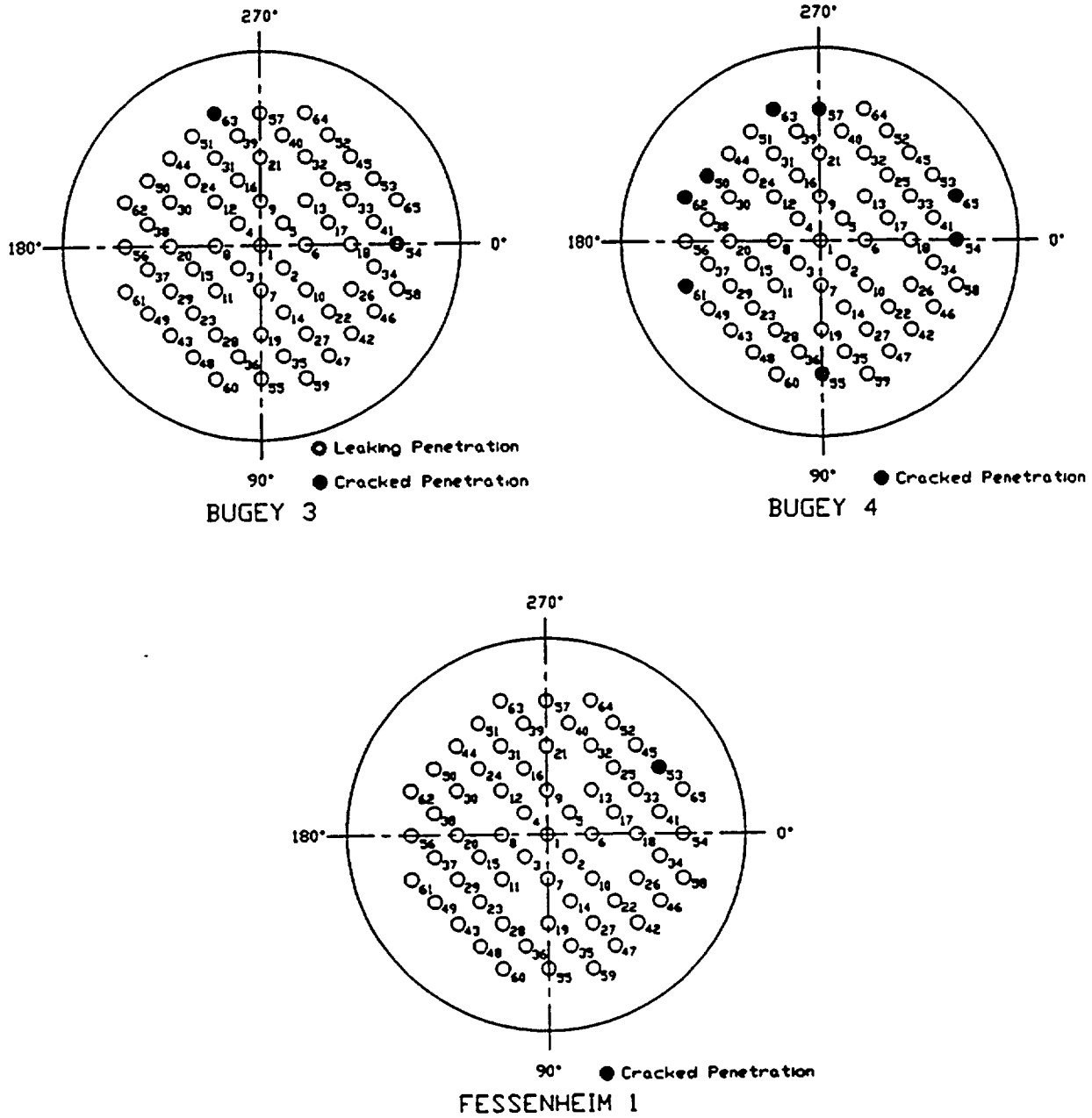
Figure 2-1 French R/V Closure Head CEDM Penetration Cracking EDF Plants – Penetrations with Cracking

3 OVERALL TECHNICAL APPROACH

The primary goal of this work is to provide technical justification for the continued safe operation of St. Lucie Unit 1 in the event that cracking is discovered during in-service inspections of the Alloy 600 reactor vessel upper head penetrations.

3.1 PENETRATION STRESS ANALYSIS

Three-dimensional elastic-plastic finite element stress analyses has been performed to determine the stresses in the head penetration region [6A, 6B, 6C]. These analyses have considered the pressure loads associated with steady state operation, as well as the residual stresses that are produced by the fabrication process.

[

$]^{a,c,e}$

3.2 FLAW TOLERANCE APPROACH

A flaw tolerance approach has been developed to allow continued safe operation until an appropriate time for repair, or the end of plant life. The approach is based on the prediction of future growth of detected flaws, to ensure that such flaws would remain stable.

If an indication is discovered during in-service inspection, its size can be compared with the flaw size considered as allowable for continued service. This "allowable" flaw size is determined from the actual loadings (including mechanical and residual loads) on the head penetration for St. Lucie Unit 1. Suitable margins to ensure the integrity of the reactor vessel as well as safety from unacceptable leakage rates should also be considered. Acceptance criteria are discussed in Section 6.5.

The time for the observed crack to reach the allowable crack size determines the length of time the plant can remain online before repair, if required. For the crack growth calculation, a best estimate is needed and no additional margins are necessary.

The results of the evaluation are presented in terms of simple flaw tolerance charts. The charts graphically show the time required to reach the allowable length or depth, which represents

additional service life before repair. This result is a function of the loadings on the particular head penetration as well as the circumferential location of the crack in the penetration nozzle.

Schematic drawings of the head penetration flaw tolerance charts are presented as Figures 3-1 and 3-2. These two types of charts can be used to provide estimates of the remaining service life before a leak would develop from an observed crack. For example, if a part-through flaw was discovered, the user would first refer to Figure 3-1, to determine the time (t_P) which would be remaining before the crack would penetrate the wall or reach the allowable depth (t_a) (e.g. a/t = 0.75). Once the crack penetrates the wall, the time (t_B) required to reach an allowable crack length would be determined from Figure 3-2. The total time remaining would then be the simple sum:

$$\text{Time remaining} = t_P + t_B$$

Another way to determine the allowable time of operation with a part-through flaw would be to use Figure 3-2 directly, in effect assuming the part-through flaw is a through-wall flaw. This approach would be more conservative than that above, and the time remaining would then be:

$$\text{Time remaining} = t_B$$
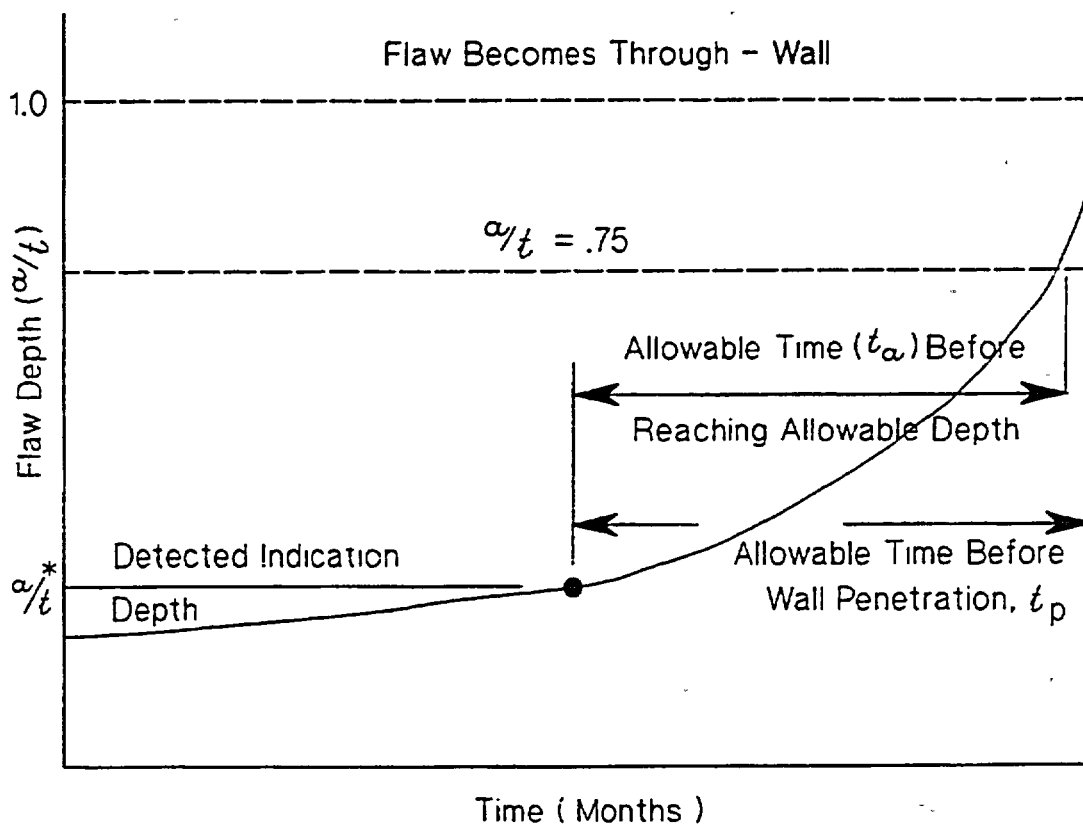
Figure 3-1 Schematic of a Head Penetration Flaw Growth Chart for Part-Through Flaws
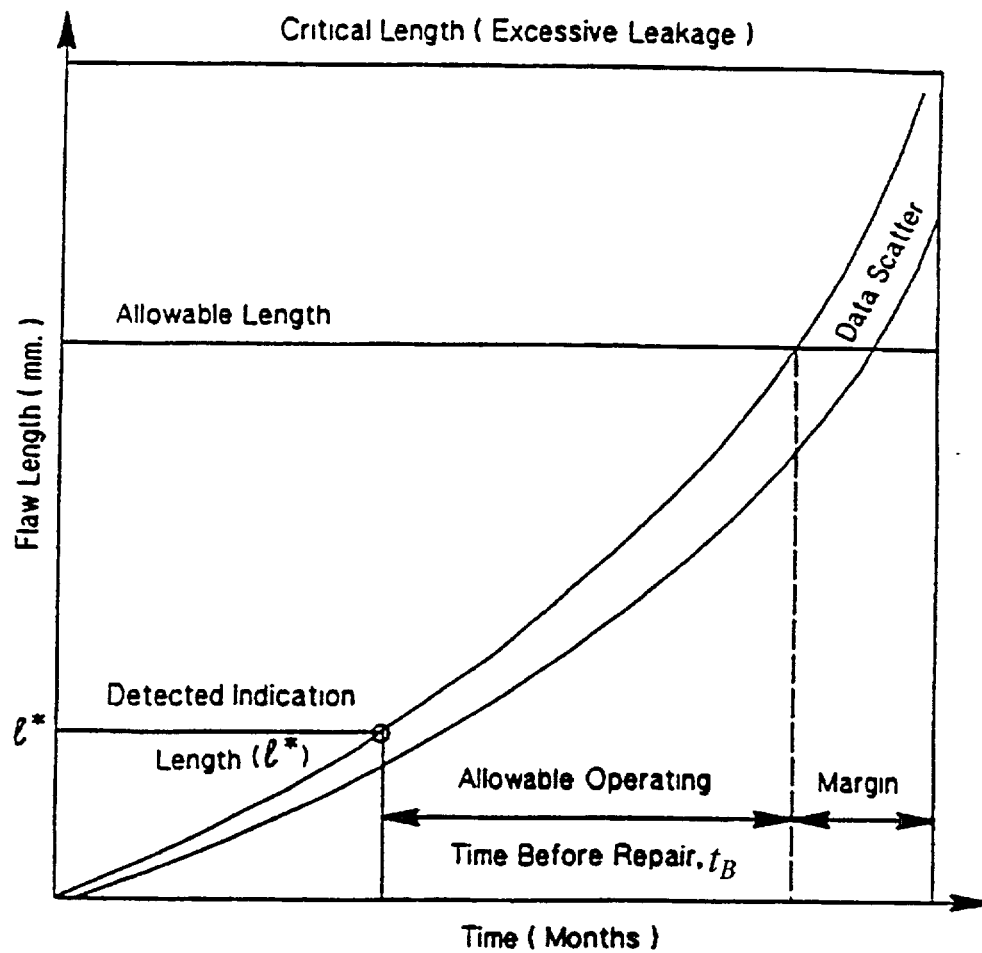
Figure 3-2 Schematic of a Head Penetration Flaw Tolerance Chart for Through-Wall Flaws

4 MATERIAL PROPERTIES, FABRICATION HISTORY AND CRACK GROWTH PREDICTION

4.1 MATERIALS AND FABRICATION

The head adapters for St. Lucie Unit 1 were manufactured by Combustion Engineering from material produced by Huntington Alloys and International Nickel in the USA. The carbon content and mechanical properties of the Alloy 600 material used to fabricate the St. Lucie Unit 1 vessel are provided in Table 4-1. The Certified Material Test Reports (CMTRs) were used to obtain the chemistry and mechanical properties for the vessel head penetrations. The CMTRs for the material do not indicate the heat treatment of the material. However, Westinghouse records indicate that the Huntington Alloy materials were annealed for one hour at a temperature of 1700° - 1800°, followed by water-quench. There is no information for the heat treatment on the International Nickel materials. Figures 4-1 and 4-2 illustrate the yield strengths and carbon content, based on percent of heats, of the head adapter penetrations in the St. Lucie Unit 1 vessel relative to a sample of the French head adapters which have experienced cracking. The general trend for the head adapter penetrations in St. Lucie Unit 1 are of a higher carbon content, higher mill annealing temperature, and lower yield strength relative to those on the French vessels. These factors should all have a beneficial effect on the material resistance to PWSCC in the head penetrations.

4.2 CRACK GROWTH PREDICTION

The cracks in the penetration region have been determined to result from primary water stress corrosion cracking in the Alloy 600 base metal and, in some cases, the Alloy 182 weld metal. There are a number of available measurements of static load crack growth rates in primary water environment, and in this section the available results will be compared and a representative growth rate established.

Direct measurements of Stress Corrosion Cracking (SCC) growth rates in Alloy 600 are relatively rare. Also, care should be used when interpreting the results because the materials may be excessively cold worked, or the loadings applied may be near or exceeding the limit load of the penetration nozzle, meaning there will be an interaction between tearing and crack growth. In these cases the crack growth rates may not be representative of service conditions.

The effort to develop a reliable crack growth rate model for Alloy 600 began in the spring of 1992, when the Westinghouse Owners Group was developing a safety case to support continued operation of plants. At the time, there was no available crack growth rate data for head penetration materials, and only a few publications existed on growth rates of Alloy 600 in any product form.

The best available publication at that time was that of Peter Scott of Framatome, who had developed a growth rate model for PWR steam generator materials [1]. His model was based on a study of results obtained by McIlree, Rebak and Smialowska [2] who had tested short steam generator tubes which had been flattened into thin compact specimens.

An equation was fitted to the data of reference [2] for the results obtained in water chemistries that fell within the standard specification for PWR primary water. Results for chemistries outside the specification were not used. The following equation was fitted to the data at 330°C (626°F):

$$\frac{da}{dt} = 2.8 \times 10^{-11} (K-9)^{1.16} \, m/\sec \qquad (4\text{-}1)$$

where:

K is in $MPa\sqrt{m}$

The next step was to correct these results for the effects of cold work. Based on work by Cassagne and Gelpi [3], Scott concluded that dividing the above equation by a factor of 10 would be appropriate to account for the effects of cold work. The crack growth law for 330°C (626°F) then becomes:

$$\frac{da}{dt} = 2.8 \times 10^{-12} (K-9)^{1.16} \, m/\sec \qquad (4\text{-}2)$$

Scott further corrected this law for the effects of temperature. This forms the basis for the PWR Materials Reliability Program (MRP) recommended crack growth rate (CGR) curve for the evaluation of SCC where a power-law dependence on stress intensity factor was assumed. The MRP recommended CGR curve was used in this report for determining the primary water stress corrosion crack growth rate and a brief discussion on this recommended curve is as follows:

[

]a,c,e

[

$$]^{a,c,e}$$

There is a general agreement that crack growth in Alloy 600 materials in the primary water environment can be modeled using a power-law dependence on stress intensity factor with differences in temperature accounted for by an activation energy (Arrhenius) model for thermally controlled processes. Figure 4-3 shows the recommended CGR curve along with the laboratory data from Huntington materials used to develop the curve.

[

$$]^{a,c,e}$$

[

$]^{a,c,e}$

The applicability of the MRP recommended model to head penetrations was recently confirmed by two independent approaches. The first was a collection of all available data from Standard Steel and Huntington Alloys materials tested over the past ten years [4H]. The results are shown in Figure 4-3, along with the Scott model for the test temperature.

The MRP crack growth curve was structured to bound 75 percent of the 26 heats for which test results were available. Fits were done on the results for each heat, and the constant term was determined for each heat. This was done to eliminate the concern that the curve might be biased from a large number of results from a single heat. The 75th percentile was then determined from these results. The MRP expert panel on crack growth endorsed the resulting curve unanimously in a meeting on March 6th and 7th 2002. This approach is consistent with the Section XI flaw evaluation philosophy, which is to make a best estimate prediction of future growth of a flaw. Margins are incorporated in the allowable flaw sizes. The entire data set is shown in Figure 4-3, where the data have been adjusted to a single temperature of 325°C.

A second independent set of data were used to validate the model, and these data were obtained from the two inspections carried out on penetration no. 75 of D.C. Cook Unit 2, which was first found to be cracked in 1994 [4G]. The plant operated for one fuel cycle before the penetration was repaired in 1996 and the flaw was measured again before being repaired. These results were used to estimate the PWSCC growth rate for both the length of the flaw and its depth. These two points are also shown in Figure 4-4, and are consistent with the laboratory data for Huntington materials. In fact, Figure 4-4 demonstrates that the MRP model is nearly an upper bound for these materials. The D.C. Cook Unit 2 penetrations were made from Huntington materials.

Since St. Lucie Unit 1 operates at a temperature of 311°C (591°F) in the head region [9], and the crack growth rate is strongly affected by temperature, a temperature adjustment is necessary. This temperature correction was obtained from study of both laboratory and field data for stress corrosion crack growth rates for Alloy 600 in primary water environments. The available data showing the effect of temperature are summarized in Figure 4-5. Most of the results shown here are from steam generator tube materials, with several sets of data from operating plants, and results from two heats of materials tested in a laboratory [4A].

Study of the data shown in Figure 4-5 results in an activation energy of 31-33 Kcal/mole, which can then be used to adjust for the lower operating temperature. This value is slightly lower than the generally accepted activation energy of 44-50 Kcal/mole used to characterize the effect of temperature on crack initiation, but the trend of the actual data for many different sources is unmistakable.

[

].[a,c,e] Therefore the following crack growth rate model was used for the St. Lucie Unit 1 head penetration for crack growth in all the cases analyzed.

$$\frac{da}{dt} = 1.40 \times 10^{-12} (K - 9)^{1.16} \text{ m/sec}$$

where:

K = applied stress intensity factor, in MPa$\sqrt{m}$

This equation implies a threshold for cracking susceptibility, K_{ISCC} = 9 MPa$\sqrt{m}$. The crack growth rate is applicable to propagation in both axial and circumferential directions.

(a,c,e)
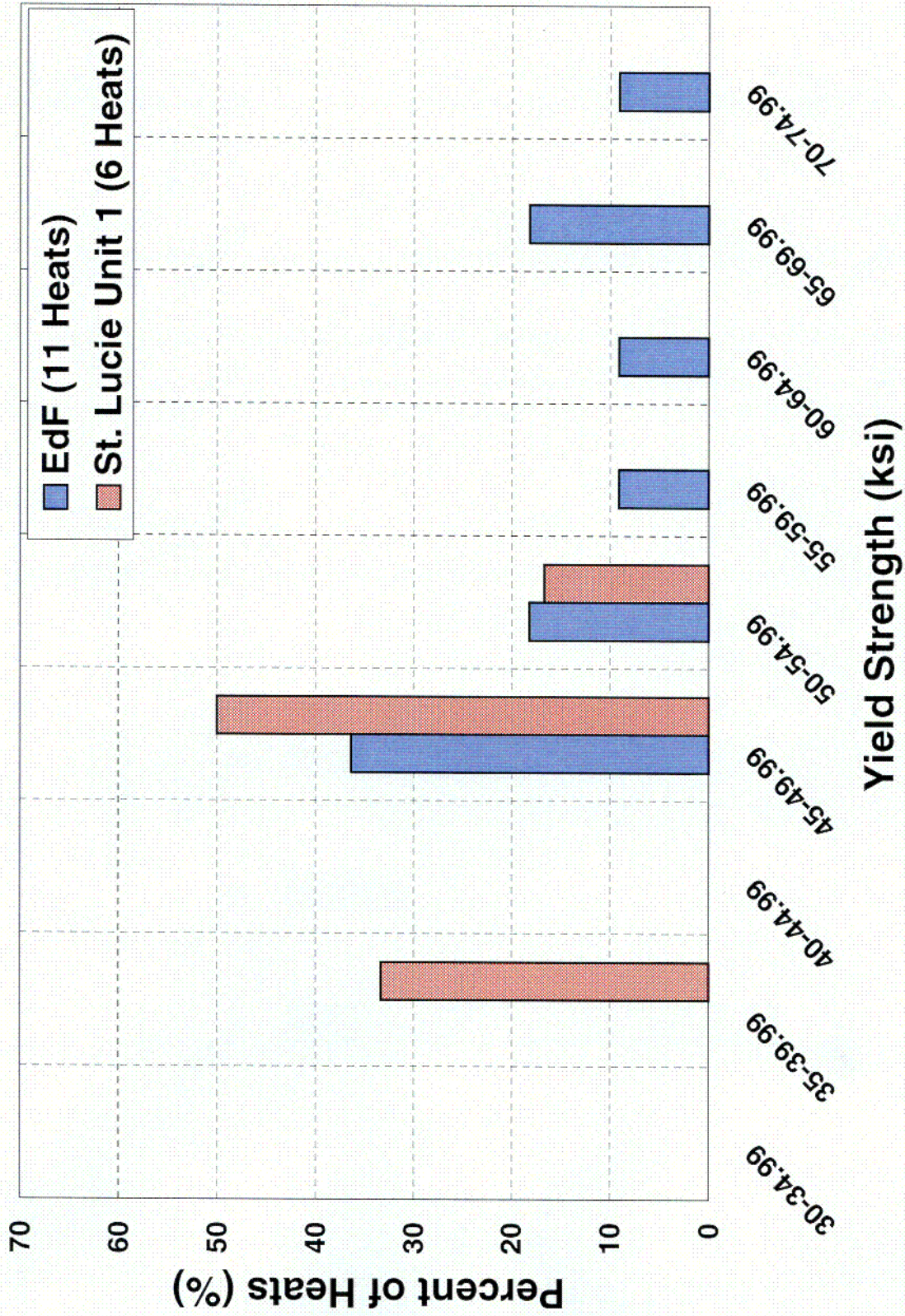
Figure 4-1 Yield Strength of the Various Heats of Alloy 600 Used in Fabricating the St. Lucie Unit 1 and French Head Penetrations
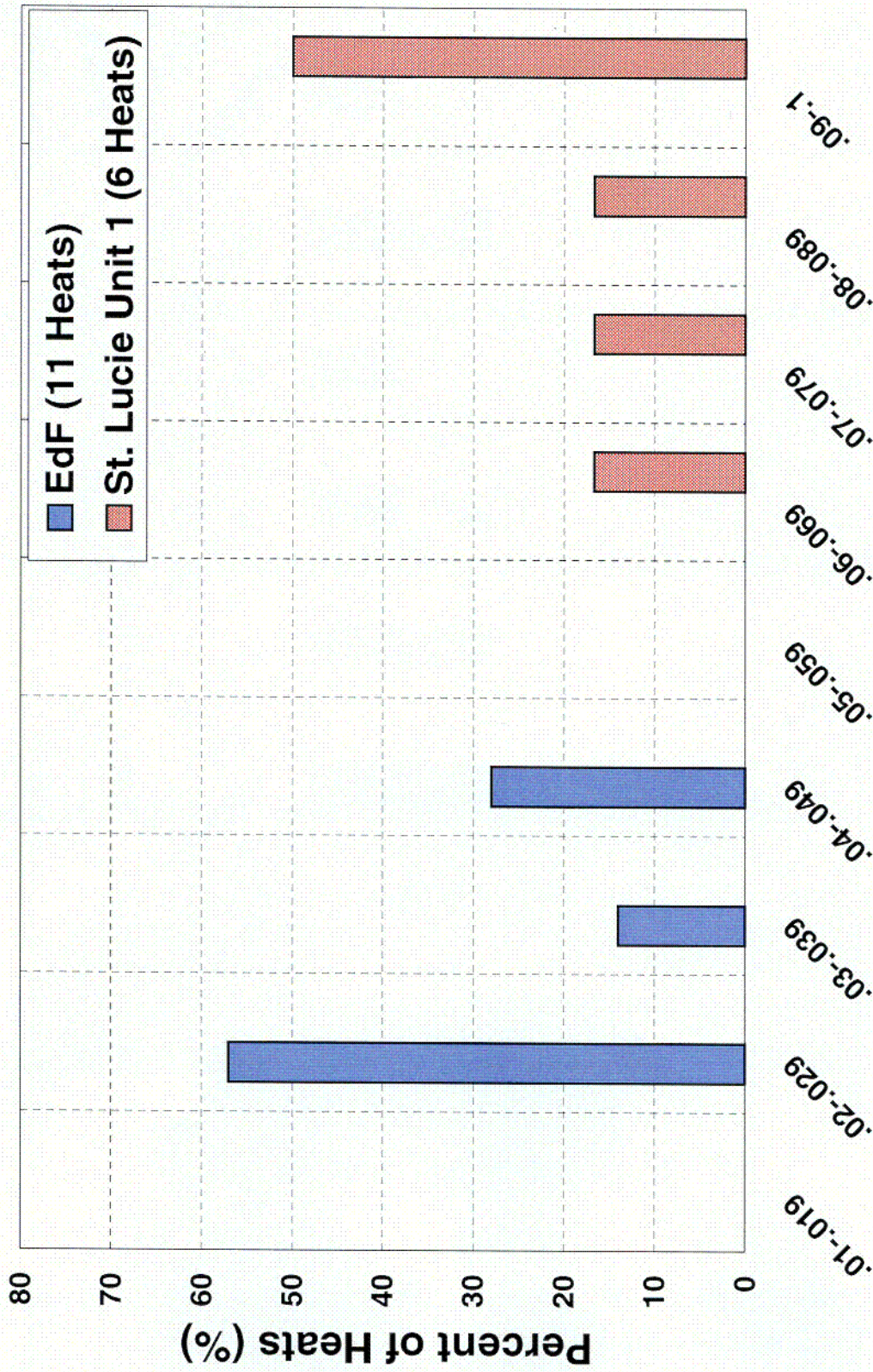
Figure 4-2 Carbon Content of the Various Heats of Alloy 600 Used in Fabricating the St. Lucie Unit 1 and French Head Penetration

C02

(a,c,e)

Figure 4-3   Screened Laboratory Data for Alloy 600 with the MRP Recommended Curve
(Note that the Modified Scott Model is also Shown)

(a,c,
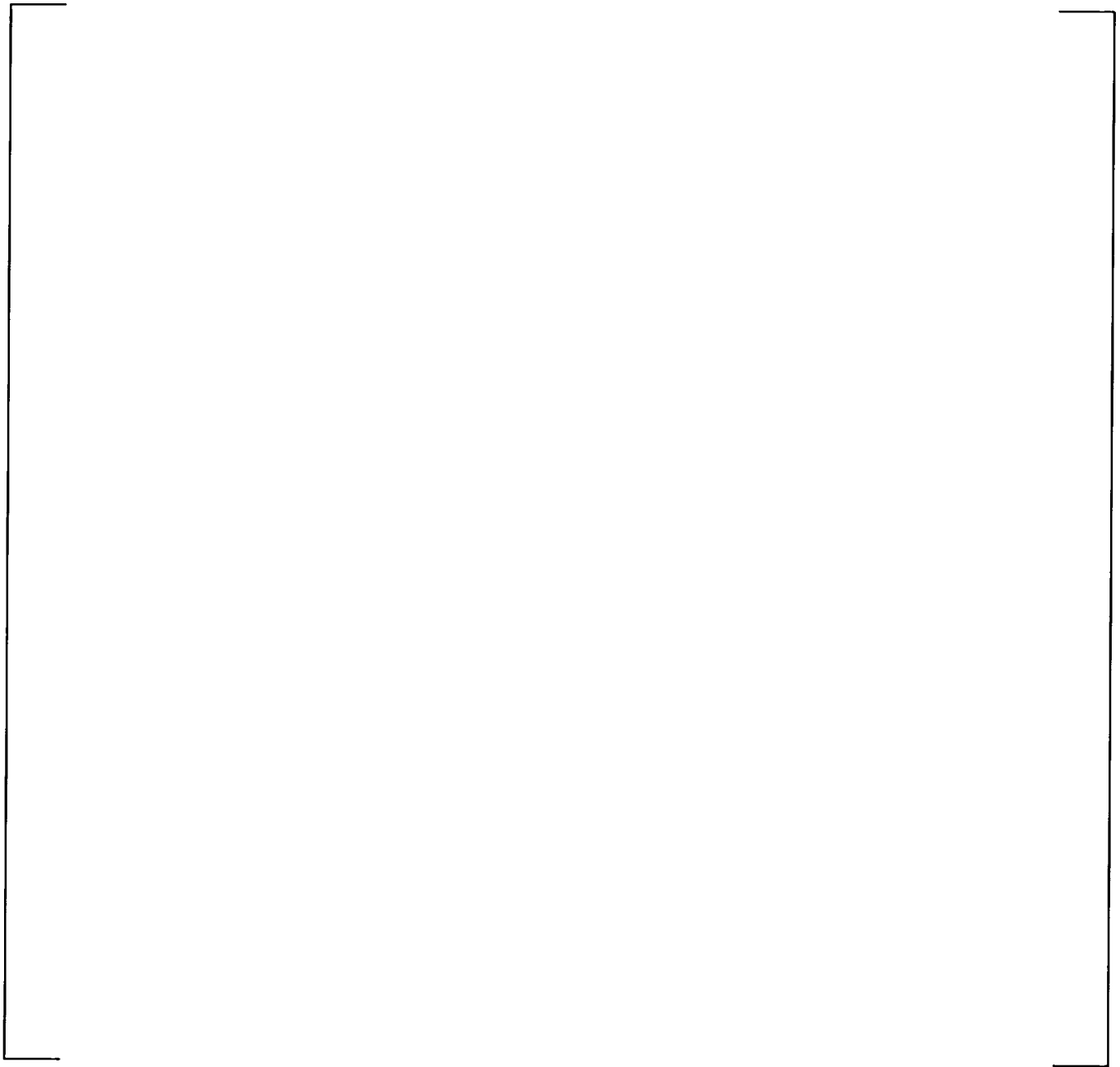
Figure 4-4   Model for PWSCC Growth Rates in Alloy 600 in Primary Water Environments (325°C), With Supporting Data from Standard Steel, Huntington, and Sandvik Materials

Figure 4-5 Summary of Temperature Effects on PWSCC Growth Rates for Alloy 600 in Primary Water
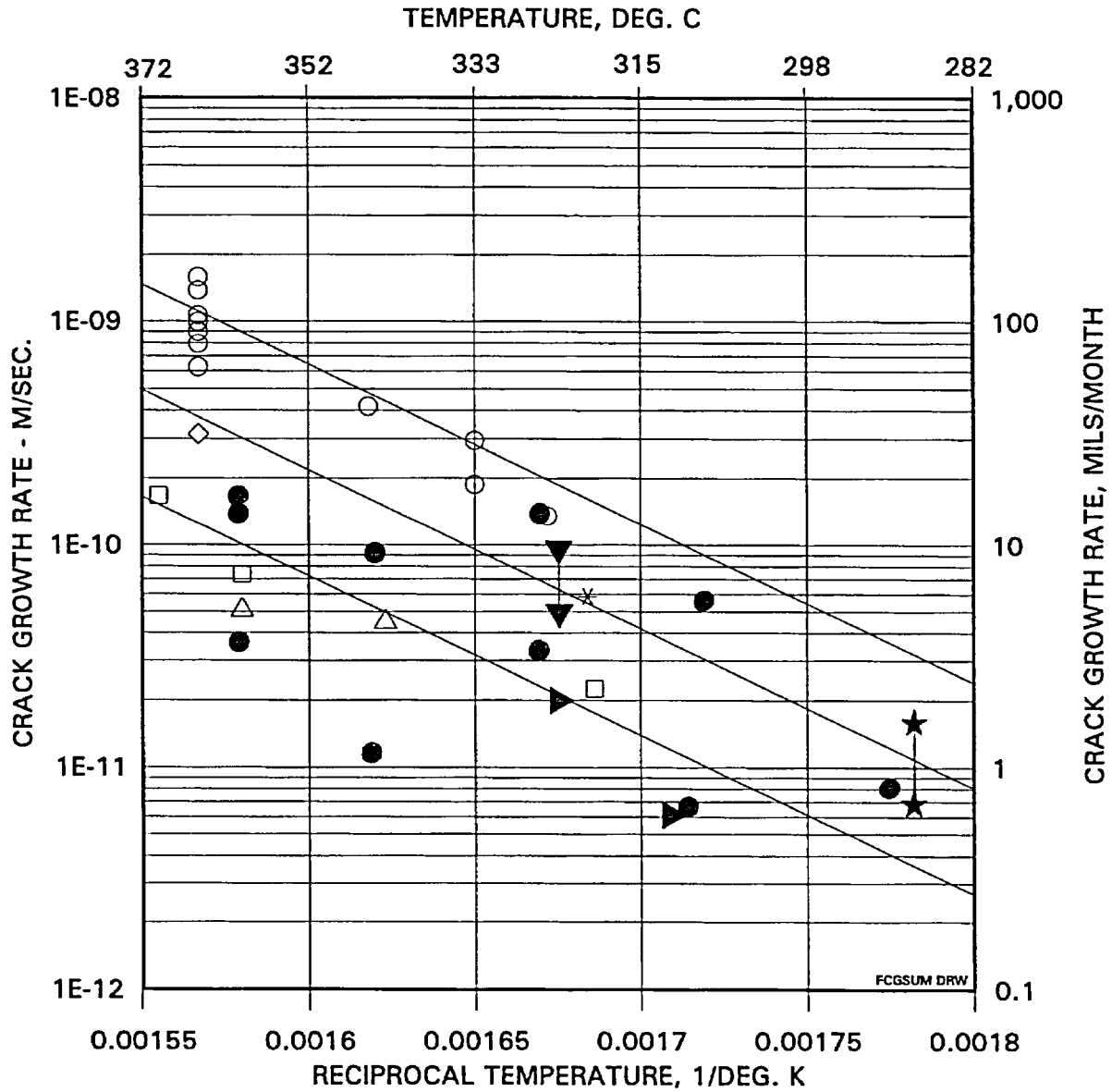
Note   All symbols are for steam generator materials, except the solid circles, which are head penetration laboratory data.

5 STRESS ANALYSIS

5.1 OBJECTIVES OF THE ANALYSIS

The objective of this analysis was to obtain accurate stresses in each of the CEDM, ICI, and head vent penetrations as well as the immediate vicinity. To do so requires a three-dimensional finite element analysis which considers all the pertinent loadings on the penetration [6A, 6B, 6C]. An investigation of deformations at the lower end of the housing was also performed using the same model. Four CEDM locations were considered: the outermost row (42.5°), rows at 37.1°, 29.1°, and the center location (0°). These locations bound the CEDM penetration angles in the St. Lucie Unit 1 reactor vessel head. In addition, the ICI penetration (angle of 54.8) and the head vent were analyzed.

The analyses were used to provide information for the flaw tolerance evaluation in Section 6. Also, the results of the stress analysis were compared to the findings from service experience to help assess the causes of the observed cracking.

5.2 MODEL

A three-dimensional finite element model comprised of isoparametric brick and wedge elements with midside nodes on each face was used to obtain the stresses and deflections. Views of the outermost CEDM, the ICI, and the head vent models are shown in Figures 5-1, 5-2, and 5-3 respectively. Taking advantage of symmetry through the vessel and penetration centerlines, only half of the penetration geometry plus the surrounding vessel were modeled. The difference between the hillside penetrations and the center penetration was that there was no differential height across the weld for the center penetration.

In the models, the lower portion of the Control Element Drive Mechanism (CEDM) penetration nozzle, In-Core Instrumentation (ICI) nozzle, the head vent, the adjacent section of the vessel closure head, and the joining weld were modeled. The vessel to penetration nozzle weld was simulated with two layers of elements. The penetration nozzle, weld metal, and cladding were modeled as Alloy 600 and the vessel head shell as carbon steel.

The only loads used in the analysis are the steady state operating loads. External loads, such as seismic loads, have been studied and have no impact since the penetration nozzles are captured by the full thickness of the reactor vessel head (about seven inches of steel) into which the penetrations are shrunk fit during construction. The area of interest is in the penetration near the attachment weld, which is unaffected by these external loads.

5.3 STRESS ANALYSIS RESULTS – OUTERMOST CEDM PENETRATION (42.5°)

Figure 5-5 presents the hoop and axial stresses for the steady state condition for the outermost penetration.

[

]^{a,c,e}

[

]^{a,c,e}

5.4 STRESS ANALYSIS RESULTS – INTERMEDIATE CEDM AND ICI PENETRATIONS

[

]^{a,c,e}

5.5 STRESS ANALYSIS RESULTS – CENTER CEDM PENETRATION

[

]^{a,c,e}

5.6 STRESS ANALYSIS RESULTS – HEAD VENT

[

]^{a,c,e}
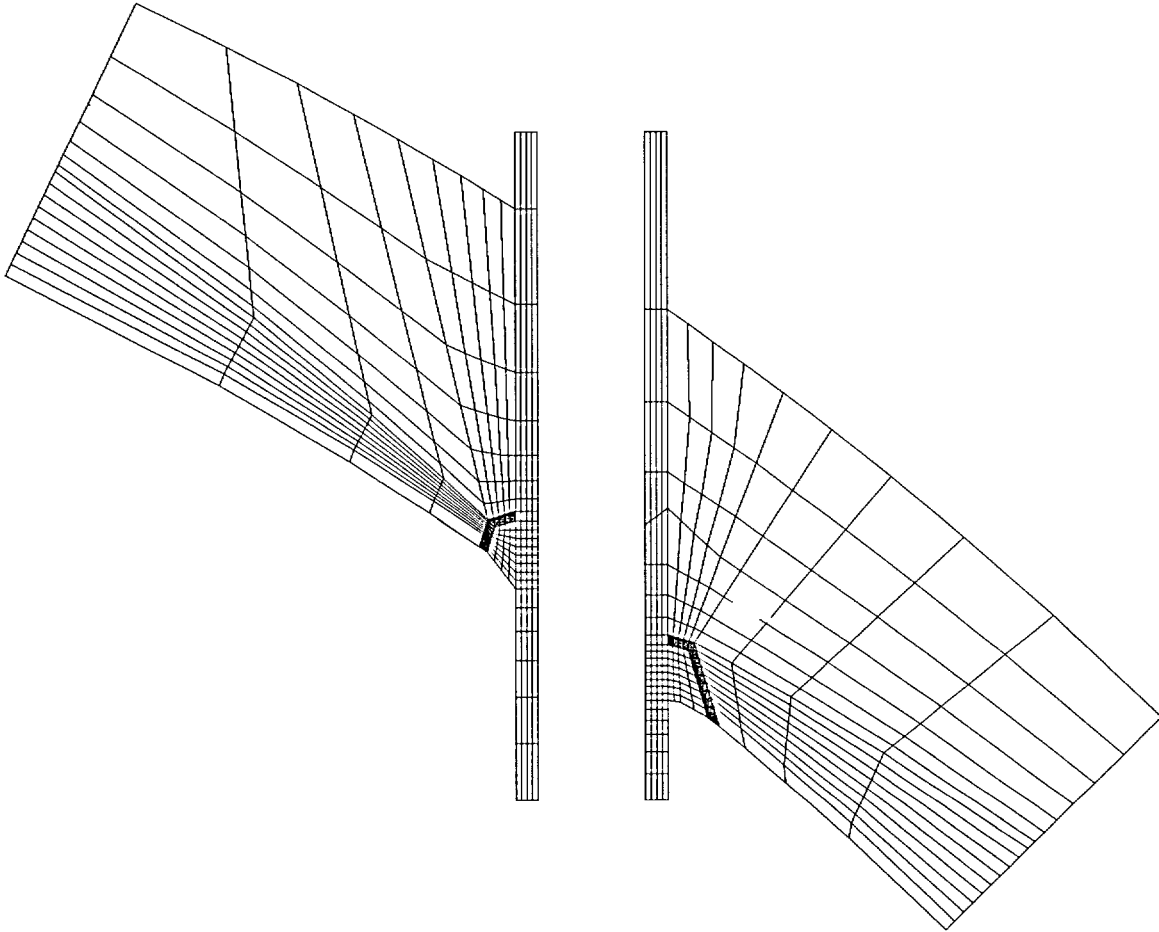
Figure 5-1 Finite Element Model of the Outermost CEDM Penetration (42.5 Degrees)
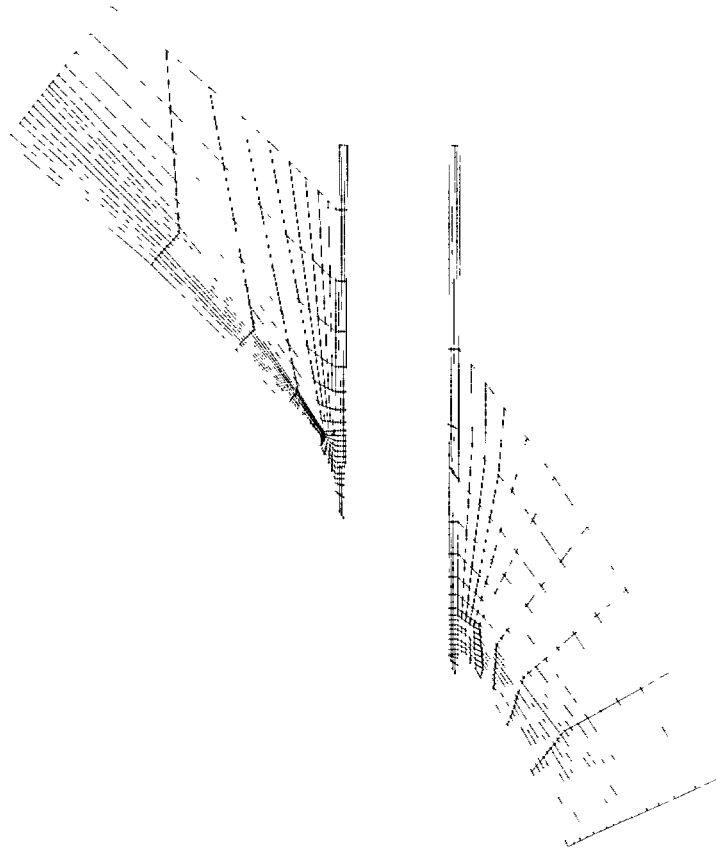
Figure 5-2 Finite Element Model of the ICI penetrations (54.8 degrees)
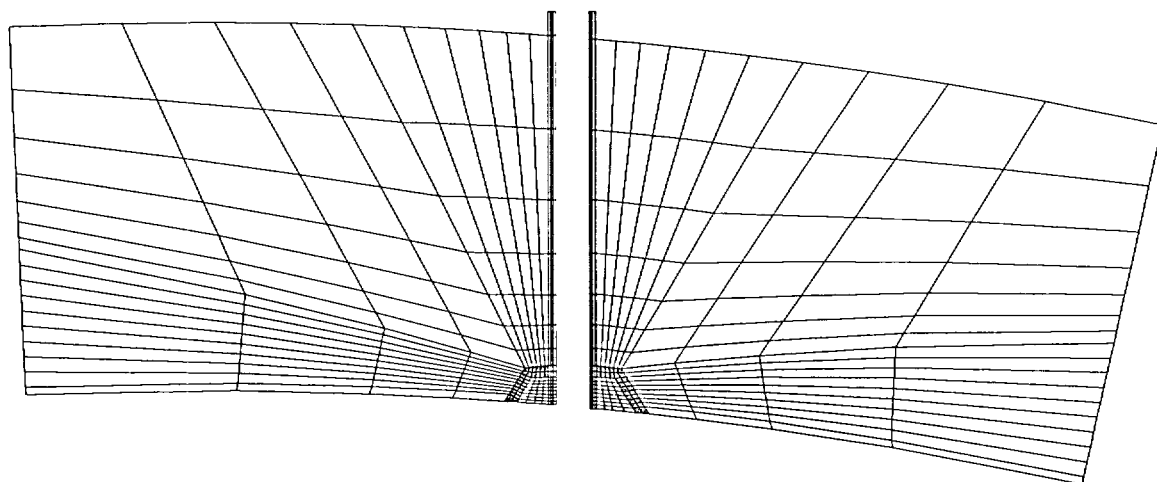
Figure 5-3 Vent Pipe Finite Element Model

ANSYS 5.7
JAN 23 2002
20:21:48
PLOT NO.   3
ELEMENTS
PowerGraphics
EFACET=1
MAT NUM

NODAL SOLUTION
TIME=4004
SY   (AVG)
RSYS=11
PowerGraphics
EFACET=1
AVRES=Mat
DMX =.449752
SMN =-43191
SMX =77378

-43191
-10000
0
10000
20000
30000
40000
50000
100000

Mil2 ICI(54.8d,CYC SS,5.563/4.625,2.5E-03,A) - Operating

ANSYS 5.7
JAN 23 2002
20:21:50
PLOT NO.   4
ELEMENTS
MAT NUM

NODAL SOLUTION
TIME=4004
SZ   (AVG)
RSYS=11
PowerGraphics
EFACET=1
AVRES=Mat
DMX =.449752
SMN =-40193
SMX =54053

-40193
-10000
0
10000
20000
30000
40000
50000
100000

Mil2 ICI(54.8d,CYC SS,5.563/4.625,2.5E-03,A) - Operating

Figure 5-4   Stress Distribution at Steady State Condition for the 54.8 Degree ICI Penetration Nozzle (Hoop Stress is the Top Figure, Axial Stress is the Bottom Figure)

C03

Mil2CEDM(42.46d,CYC SS,3.85/2.718,2.5E-03,A) - Operating

Mil2CEDM(42.46d,CYC SS,3.85/2.718,2.5E-03,A) - Operating
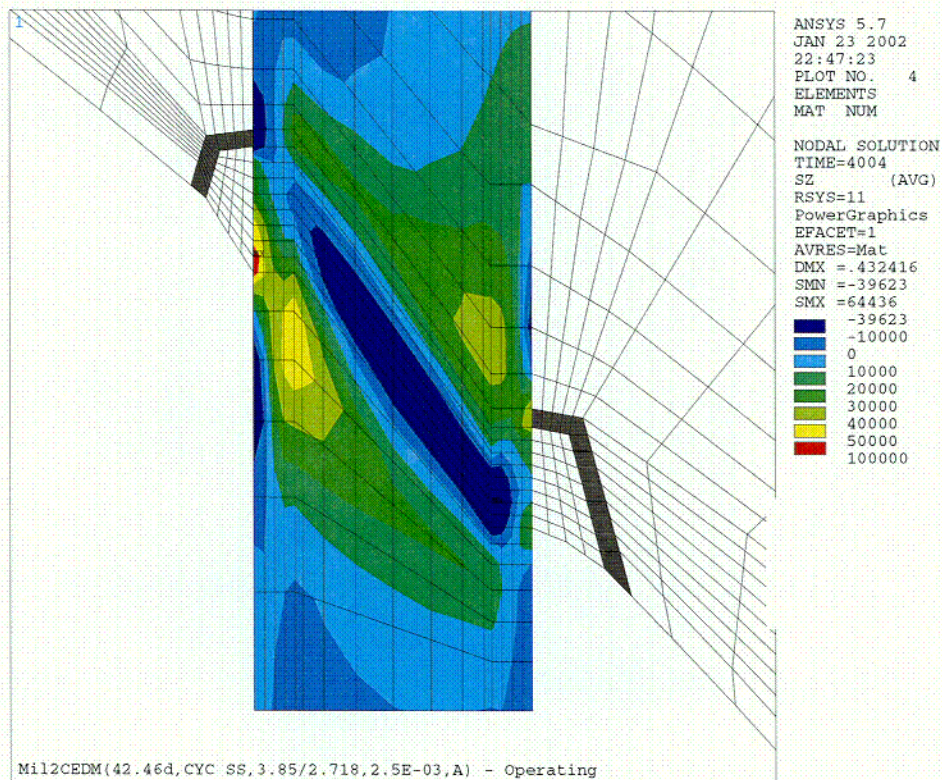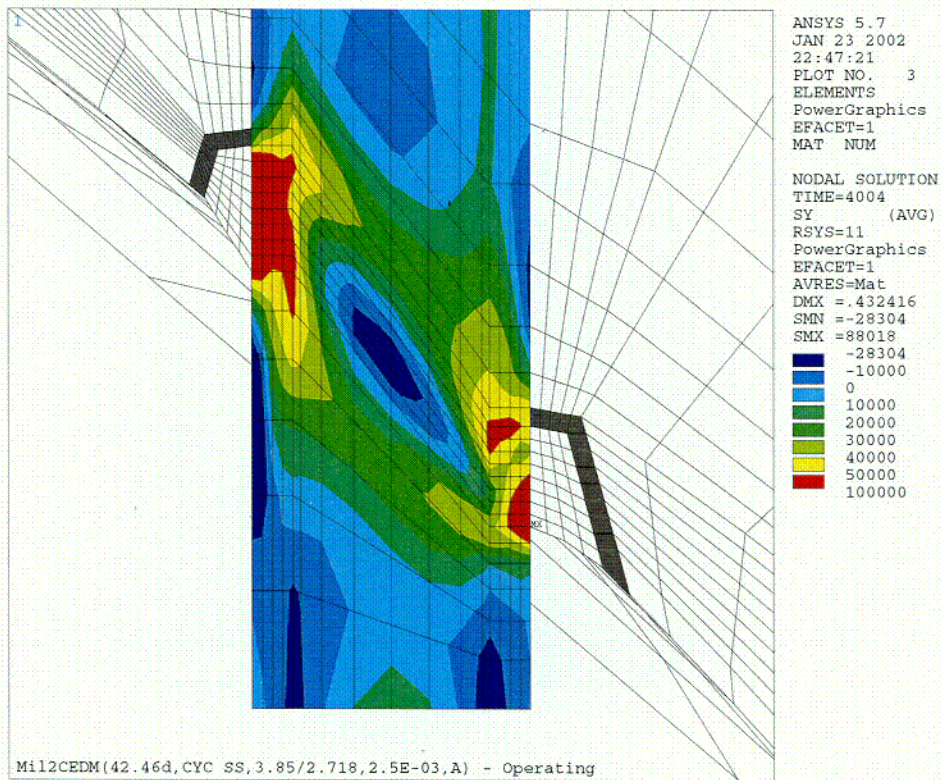
Figure 5-5 **Stress Distributions at Steady State Conditions: Outermost CEDM Penetration (42.5 Degrees) (Hoop Stress is the Top Figure; Axial Stress is the Bottom Figure)**

C04
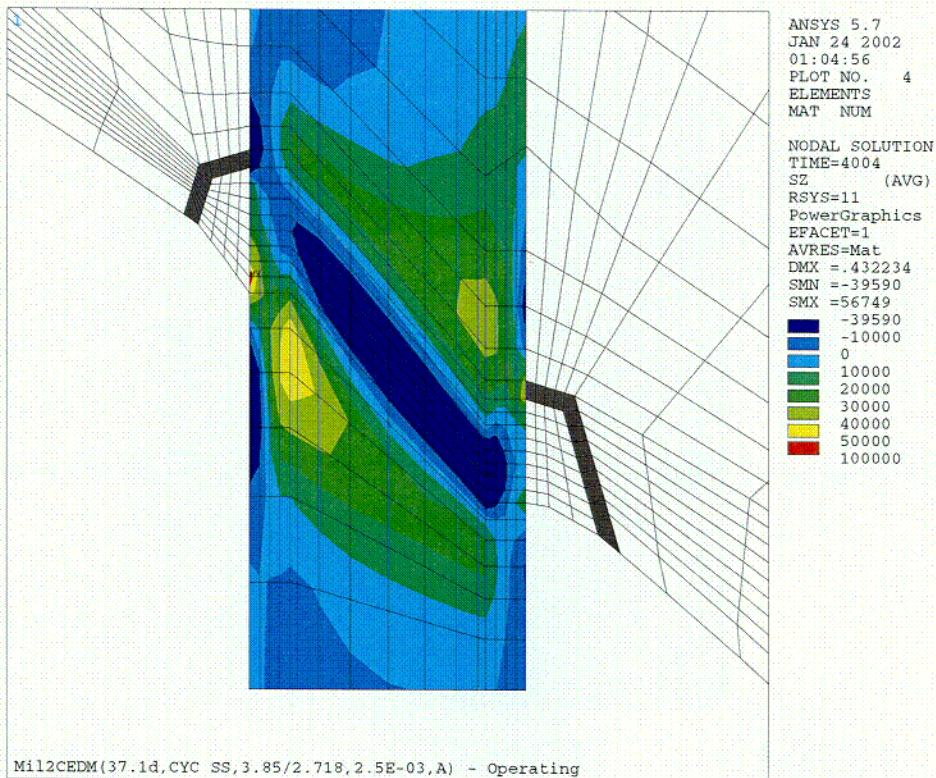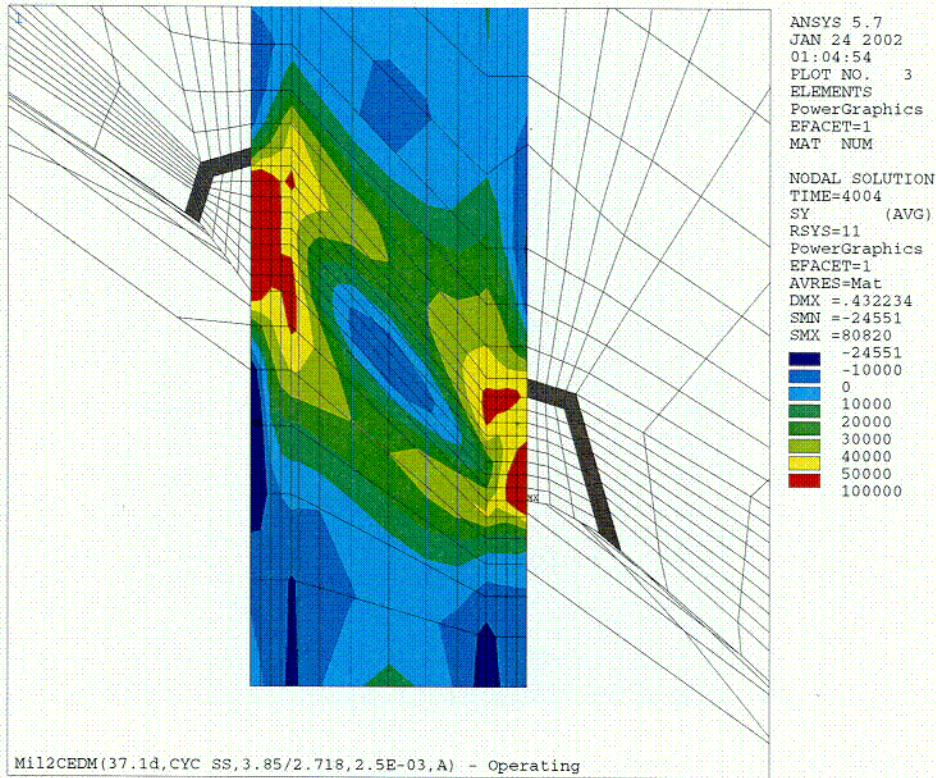
Figure 5-6   Stress Distribution at Steady State Conditions for the 37.1 Degrees CEDM Penetration (Hoop Stress is the Top Figure; Axial Stress is the Bottom Figure)

C05
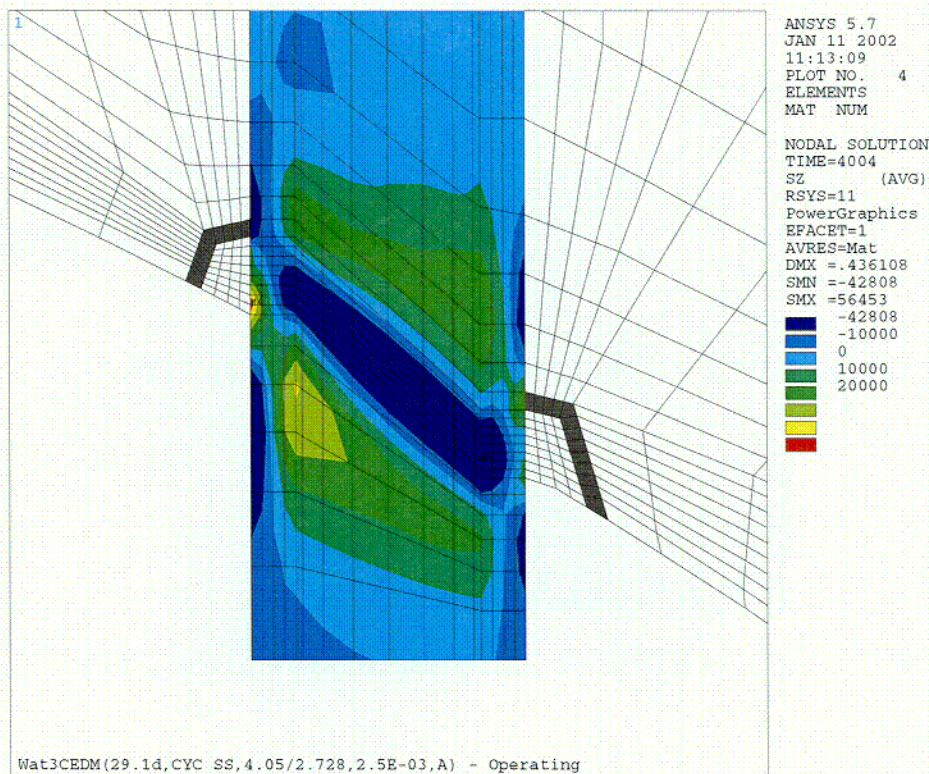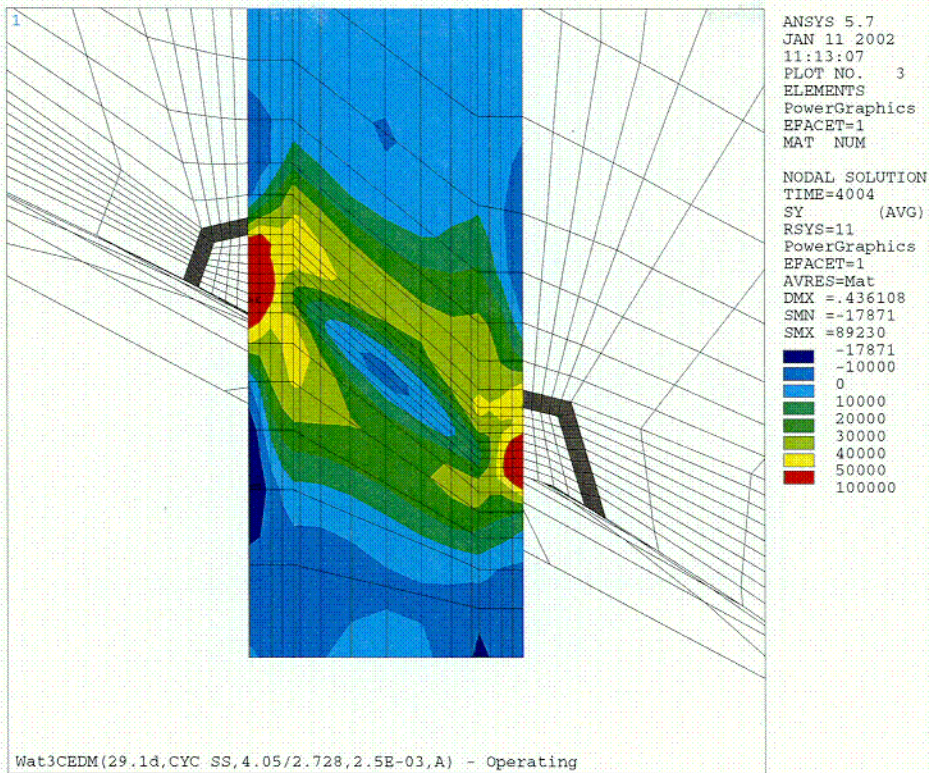
Figure 5-7   Stress Distribution at Steady State Conditions for the 29.1 Degrees CEDM Penetration (Hoop Stress is the Top Figure; Axial Stress is the Bottom Figure)
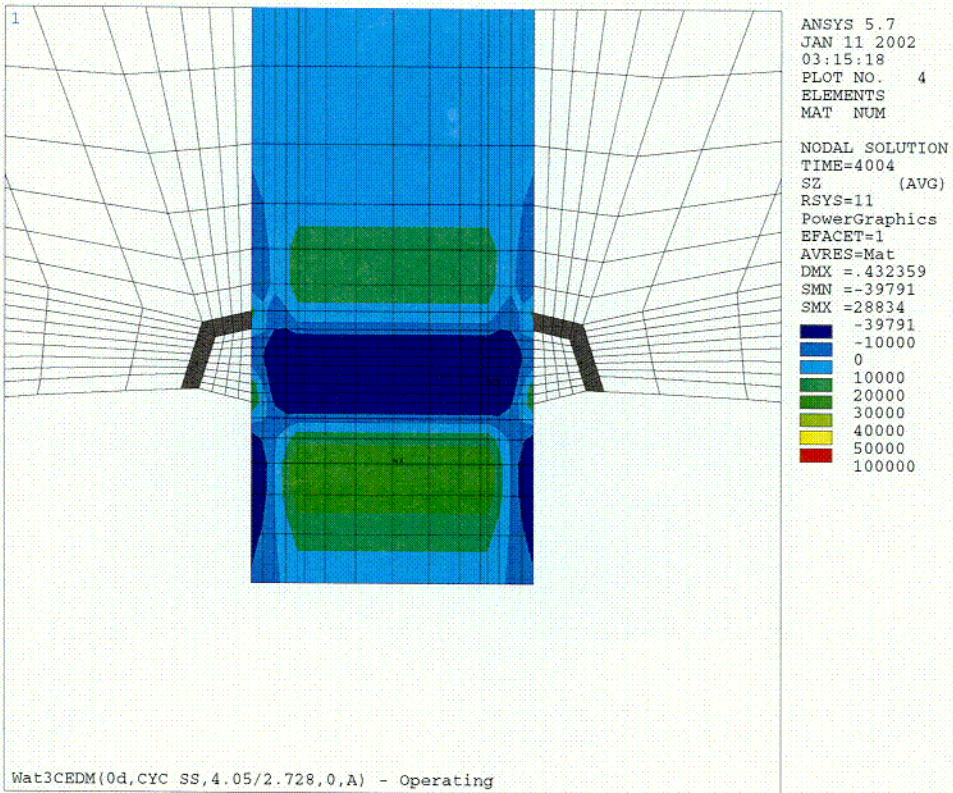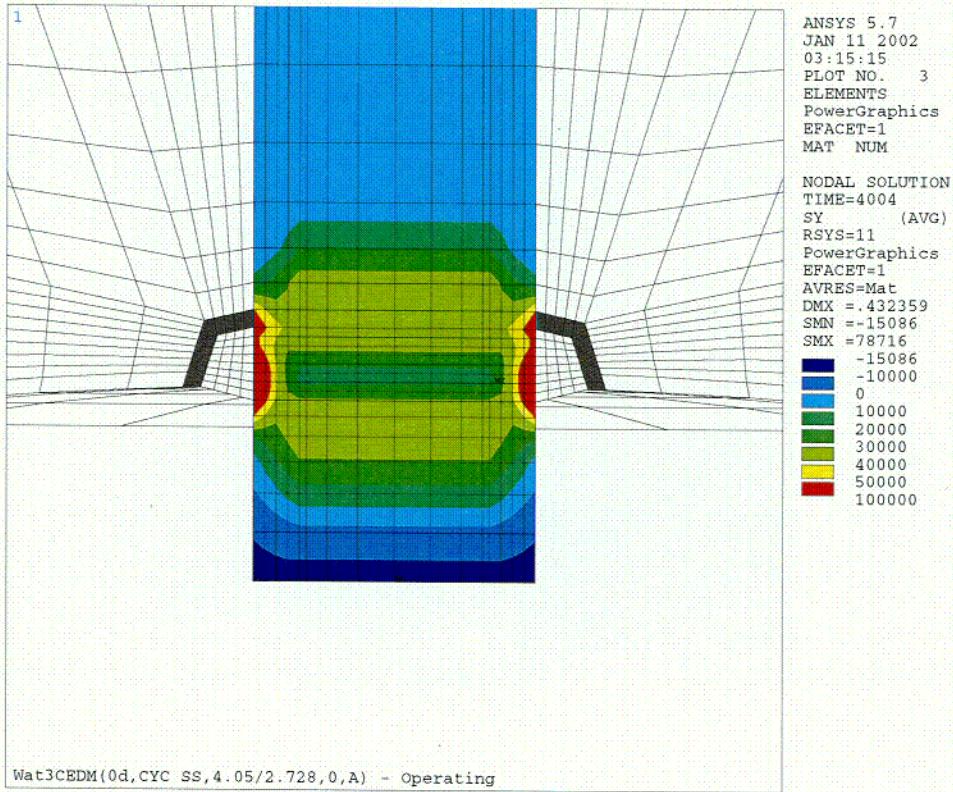
Figure 5-8   Stress Distribution at Steady State Conditions for the Center CEDM Penetration
(Hoop Stress is the Top Figure; Axial Stress is the Bottom Figure)

PV12-HV(5.3d,CYC SS,1.05/0.742,0,A) - Operating

PV12-HV(5.3d,CYC SS,1.05/0.742,0,A) - Operating
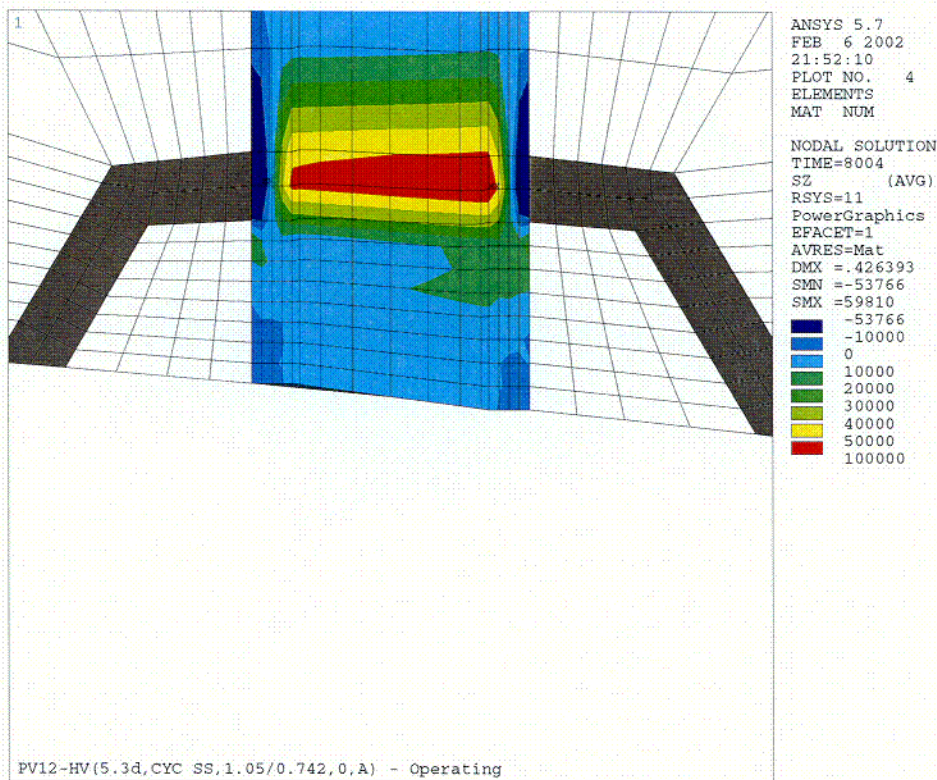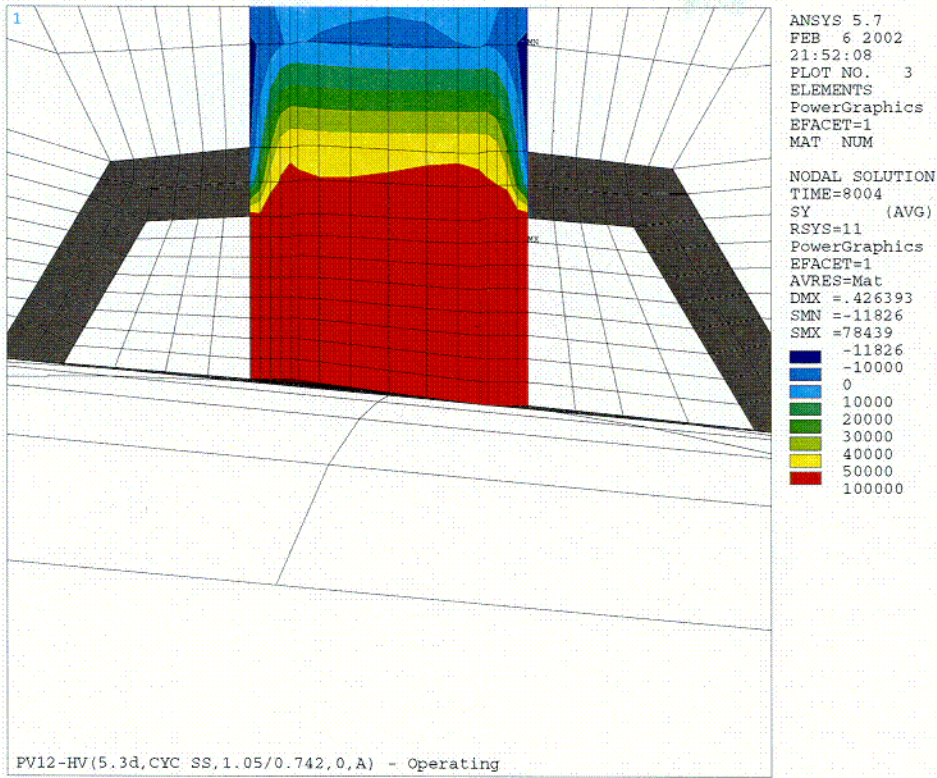
Figure 5-9   Stress Contours in the Head Vent Nozzle as a Result of Residual Stresses and Operating Pressure (Hoop Stress is the Top Figure; Axial Stress is the Bottom Figure)

```
1                                          ANSYS 5.7
                                           JAN 25 2002
                                           11:16:14
                                           PLOT NO.    2
                                           DISPLACEMENT
                                           TIME=4004
                                           RSYS=SOLU
                                           DMX =.449752

                                           *DSCA=10
                                           XV  =-1
                                           ZV  =2
                                           DIST=10.057
                                           XF  =-.231465
                                           YF  =69.289
                                           ZF  =58.121
                                           VUP =Z
                                           PRECISE HIDDEN

                                           NODAL SOLUTION
                                           TIME=4004
                                           SZ       (AVG)
                                           RSYS=SOLU
                                           DMX =.435471
                                           SMN =-48961
                                           SMX =50887
                                              -48961
                                              -10000
                                              0
                                              10000
                                              20000
                                              30000
                                              40000
                                              50000
                                              100000

Mi12 ICI(54.8d,CYC SS,5.563/4.625,2.5E-03,A) - Operating
```
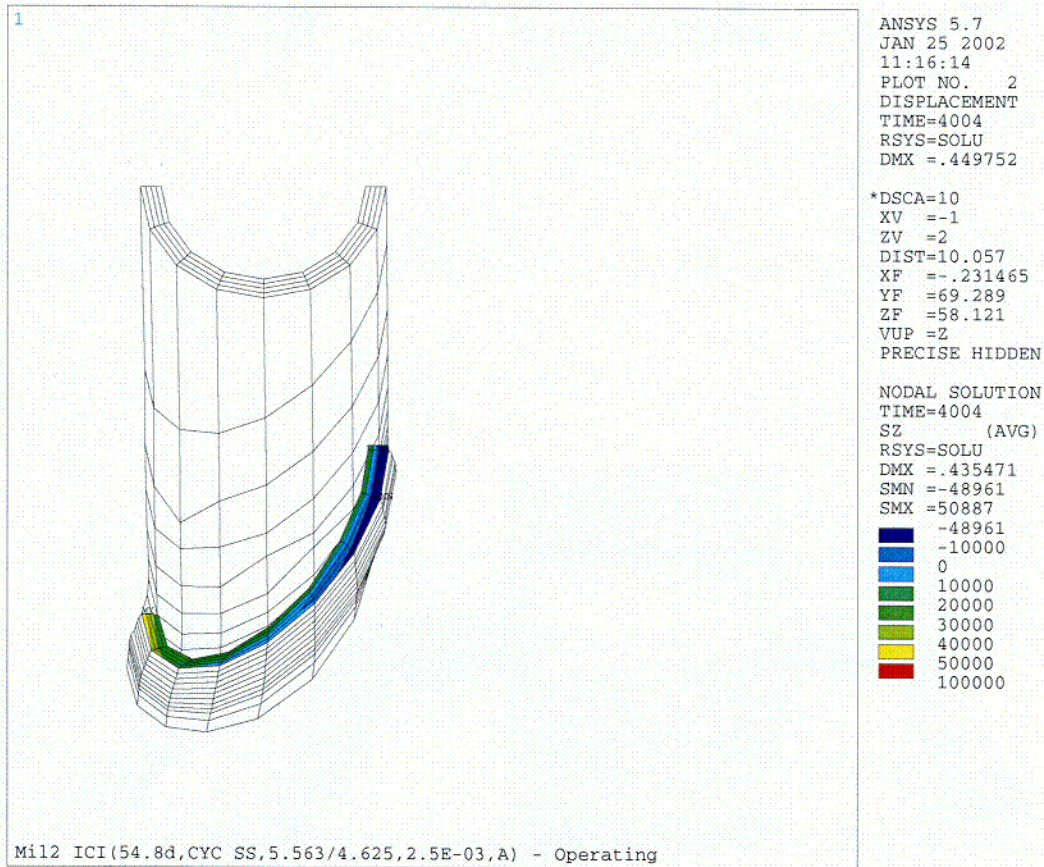
Figure 5-10   Axial Stress Distribution at Steady State Conditions for the Outermost ICI (54.8 Degrees) Penetration, Along a Plane Oriented Parallel to, and Just Above, the Attachment Weld

C09

6 FLAW TOLERANCE CHARTS

6.1 INTRODUCTION

The flaw tolerance charts were developed using the stress analysis of each of the penetration locations as discussed in Section 5. The crack growth law developed for St. Lucie Unit 1 in Section 4.2 was used for each case, and several flaw tolerance charts were developed for each penetration location. The first series of charts characterizes the growth of a part through flaw, and the second series of charts characterizes the growth of a through-wall flaw in the length direction. The allowable safe operating life of the penetration nozzle may then be directly determined, using the combined results of the two charts. All times resulting from these calculations are effective full power years, since crack growth will only occur at operating temperatures.

6.2 OVERALL APPROACH

The results of the three-dimensional stress analysis of the penetration locations were used directly in the flaw tolerance evaluation.

The crack growth evaluation for the part-through flaws was based on the worst stress distribution through the penetration wall at the location of interest of the penetration. The highest stressed location was found to be in the immediate vicinity of the weld for both the center and outermost penetrations.

The stress profile was represented by a cubic polynomial:

$$\sigma(x) = A_0 + A_1 x + A_2 x^2 + A_3 x^3 \tag{6-1}$$

where:

x = the coordinate distance into the nozzle wall
σ = stress perpendicular to the plane of the crack
A_I = coefficients of the cubic polynomial fit

For the surface flaw with length six times its depth, the stress intensity factor expression of Raju and Newman [5A] was used. The stress intensity factor $K_I (\Phi)$ can be calculated anywhere along the crack front. The point of maximum crack depth is represented by $\Phi = 0$, and this location was also found to be the point of maximum K_I for the cases considered here. The following expression is used for calculating $K_I (\Phi)$, where Φ is the angular location around the crack. The units of $K_I (\Phi)$ are $ksi\sqrt{in}$.

$$K_I(\Phi) = \left[\frac{\pi a}{Q}\right]^{0.5} \sum_{j=0}^{3} G_j \left(a/c, a/t, t/R, \Phi\right) A_j a^j \tag{6-2}$$

The boundary correction factors G_0 (Φ), G_1 (Φ), G_2 (Φ) and G_3 (Φ) are obtained by the procedure outlined in reference [5A]. The dimension "a" is the crack depth, and "c" is the semi crack length, while "t" is the wall thickness. "R" is the inside radius of the tube, and "Q" is the shape factor.

[

$]^{a,c,e}$

6.3   AXIAL FLAW PROPAGATION

CEDM and ICI Surface Flaws

The results of the calculated growth through the wall thickness of the CEDM penetration nozzles for surface flaws are shown in Figures 6-2 through 6-8 for inside surface flaws. For outside surface flaws the results are shown in Figures 6-9 and 6-10. Based on the discussion in MRP-55 report [4H], the use of stress intensity factors less than $15\,\text{MPa}\sqrt{\text{m}}$ involves assumption not currently substantiated by actual CGR data for neither CEDM nor ICI nozzle materials.

Therefore, these crack growth curves begin at a flaw depth that results in a stress intensity factor of $15\,\mathrm{MPa}\sqrt{m}$, which exceeds the threshold value of $9\,\mathrm{MPa}\sqrt{m}$. This may result in curves with different initial flaw sizes, as seen for example in Figure 6-3. Note that results are only provided for the uphill and downhill sides of each penetration nozzle; the stresses for the regions 90 degrees from these locations are compressive. If flaws are found in such a location, the results for either the uphill or downhill location, whichever is closer, can be used.

Each of these figures allows the future allowable service time to be estimated graphically, as discussed in Section 3. Results are shown for each of the penetration nozzles analyzed in each of these figures. The stresses are much higher near the attachment weld than at 0.5 inch below or above it, so separate figures have been provided for these three regions. Also, the stresses are different on the downhill side of the penetration as opposed to the uphill side, so these two cross sections have also been treated separately.

Examples have been provided in Section 7 for a range of possible flaw types, so the graphical approach can be completely understood.

CEDM and ICI Through-Wall Flaws

The projected crack growth of a through-wall flaw in the CEDM and ICI penetration nozzles are the primary concern in evaluating the structural integrity of head penetrations. In some cases, the through-wall flaw may be located sufficiently below the attachment weld that additional time may be required for the flaw to grow up to the attachment weld. To provide a means to evaluate the duration of this additional time, a series of flaw tolerance charts for through-wall flaws were prepared.

Charts were prepared for each of the penetrations evaluated, for both the uphill and downhill locations, as shown in Figures 6-12 through 6-20. In each figure, the through-wall crack length is measured from the bottom of the nozzle itself. Note that in all the cases, the crack slows down significantly as it grows above the weld, due to the decreasing magnitude of the stress field. This provides further assurance that axial flaws will not extend to a critical length which exceeds 15 inches, regardless of the duration of crack growth.

Head Vent

The only flaw tolerance chart that is necessary for the head vent region is for flaws at and above the weld, since there is no portion of the head vent which projects below the weld. Figure 6-8 provides the projected growth of a part through flaw in the head vent just above the attachment weld. The growth through the wall is relatively rapid, because the thickness of the head vent is small.

6.4 CIRCUMFERENTIAL FLAW PROPAGATION

Since circumferentially oriented flaws have been found at five plants (Bugey 3, Oconee 2, Crystal River 3, Davis Besse, and Oconee 3), it is important to consider the possibility of crack extension in the circumferential direction. The first case was discovered as part of the destructive

examination of the tube with the most extensive circumferential cracking at Bugey 3. The crack was found to have extended to a depth of 2.25 mm in a wall thickness of 16 mm. The flaw was found at the outside surface of the penetration (number 54) at the downhill side location, just above the weld.

The circumferential flaws in Oconee Unit 3 were discovered during the process of repairing a number of axial flaws, whereas the circumferential flaw in Oconee Unit 2 and Crystal River Unit 3 were discovered by UT. Experience gained from these findings has enabled the development of UT procedures capable of detecting circumferential flaws reliably.

To investigate this issue completely, a series of crack growth calculations were carried out for a postulated surface circumferential flaw located just above the head penetration weld, in a plane parallel to the weld itself. This is the only flaw plane that could result in a complete separation of the penetration nozzle, since all others would result in propagation below the weld, and therefore there is no chance of complete separation because the remaining weld would hold the penetration nozzle in place.

[

]^{a,c,e}

[

]^{a,c,e} The results of this calculation are shown in Figures 6-21 to 6-23. From Figure 6-21, it can be seen that the time required for propagation of a circumferential flaw to a point where the integrity of the CEDM penetration nozzle would be affected (330-350 degrees [12]) would be about 25 years. From Figures 6-22 and 6-23, the required time for propagation of a circumferential flaw to a point where the integrity of the ICI and head vent penetration nozzles would be affected is about 40 years and 7 years respectively. Because of the conservatism in the calculations (the time period for a surface flaw to become a through-wall flaw was conservatively ignored) it is likely to be even longer. In addition, due to uncertainties in the exact composition of the chemical environment in contact with the nozzle OD, a multiplicative factor of 2.0 is used in the CGR for all circumferential surface flaws on the OD of the head penetration nozzles located above the elevation of the J-groove weld.

6.5 FLAW ACCEPTANCE CRITERIA

Now that the projected crack growth curves have been developed, the question remains as to what flaw size would be acceptable for further service.

Acceptance criteria have been developed for indications found during inspection of reactor vessel upper head penetration as part of an industry program coordinated by NUMARC (now NEI). Such criteria are normally found in Section XI of the ASME Code, but Section XI does not require in-service inspection of these regions and therefore acceptance criteria are not available. In developing the enclosed acceptance criteria, the approach used was very similar to that used by Section XI, in that an industry consensus was reached using input from both operating utility technical staff and each of the three PWR vendors. The criteria developed are applicable to all PWR plant designs.

Since the discovery of the leaks at Oconee and ANO-1, the acceptance criteria have been revised slightly to cover flaws on the outside diameter of the penetration below the attachment weld, and flaws in the attachment weld. These revised criteria are now in draft form, but they are expected to be acceptable to the NRC, and will be used in these evaluations. The draft portions of the acceptance criteria will be noted below.

The criteria presented herein are limits on flaw sizes, which are acceptable. The criteria are to be applied to inspection results. It should be noted that determination of the future service during which the criteria are satisfied is plant-specific and dependent on flaw geometry and loading conditions.

It has been previously demonstrated by each of the owners groups that the penetration nozzles are very tolerant of flaws and there is only a small likelihood of flaw extensions to larger sizes. Therefore, it was concluded that complete fracture of the penetration nozzle is highly unlikely. The approach used here is more conservative than that used in Section XI applications where the acceptable flaw size is calculated by placing a margin on the critical flaw size. For the current

application, the critical flaw size would be far too large to allow a practical application of the approach used in Section XI applications, so protection against leakage is the priority.

The acceptance criteria presented herein apply to all the flaw types regardless of orientation and shape. Similar to the approach used in Section XI, flaws are first characterized according to established rules and then compared with acceptance criteria.

Flaw Characterization

Flaws detected must be characterized by the flaw length and preferably flaw depth. The proximity rules of Section XI for considering flaws as separate, may be used directly (Section XI, Figure IWA 3400-1). This figure is reproduced here as Figure 6-24.

When a flaw is detected, its projections in both the axial and circumferential directions must be determined. Note that the axial direction is always the same for each penetration, but the circumferential direction will be different depending on the angle of intersection of the penetration nozzle with the vessel head. The "circumferential" direction of interest here is along the top of the attachment weld, as illustrated in Figure 6-25. It is this angle which will change for each penetration nozzle and the top of the attachment weld is also the plane which could cause separation of the penetration nozzle from the vessel head. The location of the flaw relative to both the top and bottom of the partial penetration attachment weld must also be determined since a potential leak path exists when a flaw propagates through the penetration nozzle wall and up the penetration nozzle past the attachment weld. Schematic of a typical weld geometry is shown in Figure 6-26.

Flaw Acceptance Criteria

The maximum allowable depth (a_f) for axial flaws on the inside surface of the penetration nozzle, at or above the weld is 75 percent of the penetration wall thickness. The term a_f is defined as the maximum size to which the detected flaw is calculated to grow in a specified time period. This 75 percent limitation was selected to be consistent with the maximum acceptable flaw depth in Section XI and to provide an additional margin against through wall penetration. There is no concern about separation of the penetration nozzle from the vessel head, unless the flaw is above the attachment weld and oriented circumferentially. Calculations have been completed to show that the geometry of all penetrations can support a continuous circumferential flaw with a depth of 75 percent of the wall thickness.

Axial inside surface flaws found below the weld are acceptable regardless of depth as long as their upper extremity does not reach the bottom of the weld during the period of service until the next inspection. Axial flaws that extend above the weld are limited to 75 percent of the wall thickness.

Axial flaws on the outside surface of the penetration nozzle below the attachment weld are acceptable regardless of depth, as long as they do not extend into the attachment weld during the period of service until next inspection. Outside surface flaws above the attachment weld must be evaluated on a case by case basis, and must be discussed with the regulatory authority.

Circumferential flaws located below the weld are acceptable regardless of their depth, provided the length is less than 75 percent of the penetration nozzle circumference for the period of service until the next inspection. Circumferential flaws detected in this area have no structural significance except that loose parts must be avoided. To this end, intersecting axial and circumferential flaws shall be removed or repaired. Circumferential flaws at and above the weld must be discussed with the regulatory authority on a case by case basis.

Surface flaws located in the attachment welds themselves are not acceptable regardless of their depth. This is because the crack growth rate is several times faster than that of the Alloy 600 material, and also because depth sizing capability does not yet exist for indications in the attachment weld.

The flaw acceptance criteria are summarized in Table 6-1. Flaws that exceed these criteria must be repaired unless analytically justified for further service. These criteria have been reviewed and approved by the NRC, as documented in references [7, 8] with the exception of the draft criteria discussed above, for outside surface flaws and flaws in the attachment weld. These criteria are identical with the draft acceptance criteria now being considered for Section XI, for head penetrations.

It is expected that the use of these criteria and crack growth curves will provide conservative predictions of the allowable service time.

Table 6-1	Summary of R.V. Head Penetration Flaw Acceptance Criteria (Limits for Future Growth)			
	Axial		**Circumferential**	
Location	a_f	ℓ	a_f	ℓ
Below Weld (ID)	t	no limit	t	.75 circ.
At and Above Weld (ID)	0.75 t	no limit	*	*
Below Weld (OD)	t	no limit	t	.75 circ.
Above Weld (OD)	*	*	*	*

Note: Surface flaws of any size in the attachment weld are not acceptable.

* Requires case-by-case evaluation and discussion with regulatory authority.

a_f = Flaw Depth as defined in IWB 3600
ℓ = Flaw Length
t   = Wall Thickness

Table 6-2	Penetration Geometries	
Penetration Type	**Wall Thickness (in.)**	**Penetration OD (in.)**
CEDM	0.566	3.85
CEDM Counterbore * (At and Below Weld)	0.500	3.85
ICI	.469	5.563
ICI Counterbore (At and Below Weld)	.407	5.563
Head Vent	0.154	1.050

* The stress and fracture analysis carried out in this report utilized the nominal nozzle inside and outside diameters, and did not specifically account for the counterbore in the CEDM penetration nozzles. This counterbore is located at the inside of the CEDM penetration nozzles and extends from the bottom of the nozzle to a point 3 3 inch above the weld region The flaw evaluation charts are presented in terms of the flaw depth to thickness ratio, so that the use of the charts will not be affected as long as the correct thickness is used, from Table 6-2.

The effect of the slightly smaller actual wall thickness, approximately 10% smaller, on the stress and fracture evaluations was investigated. The result of the investigation showed that incorporating the counterbore changed the stresses by no more than five percent, which is within the accuracy of the finite element calculations. In addition, the effect of the wall thickness on fatigue crack growth results is negligible because the fatigue crack growth is in general of small magnitude.

Therefore, it was concluded that the counterbore can be ignored in the development of the flaw tolerance charts
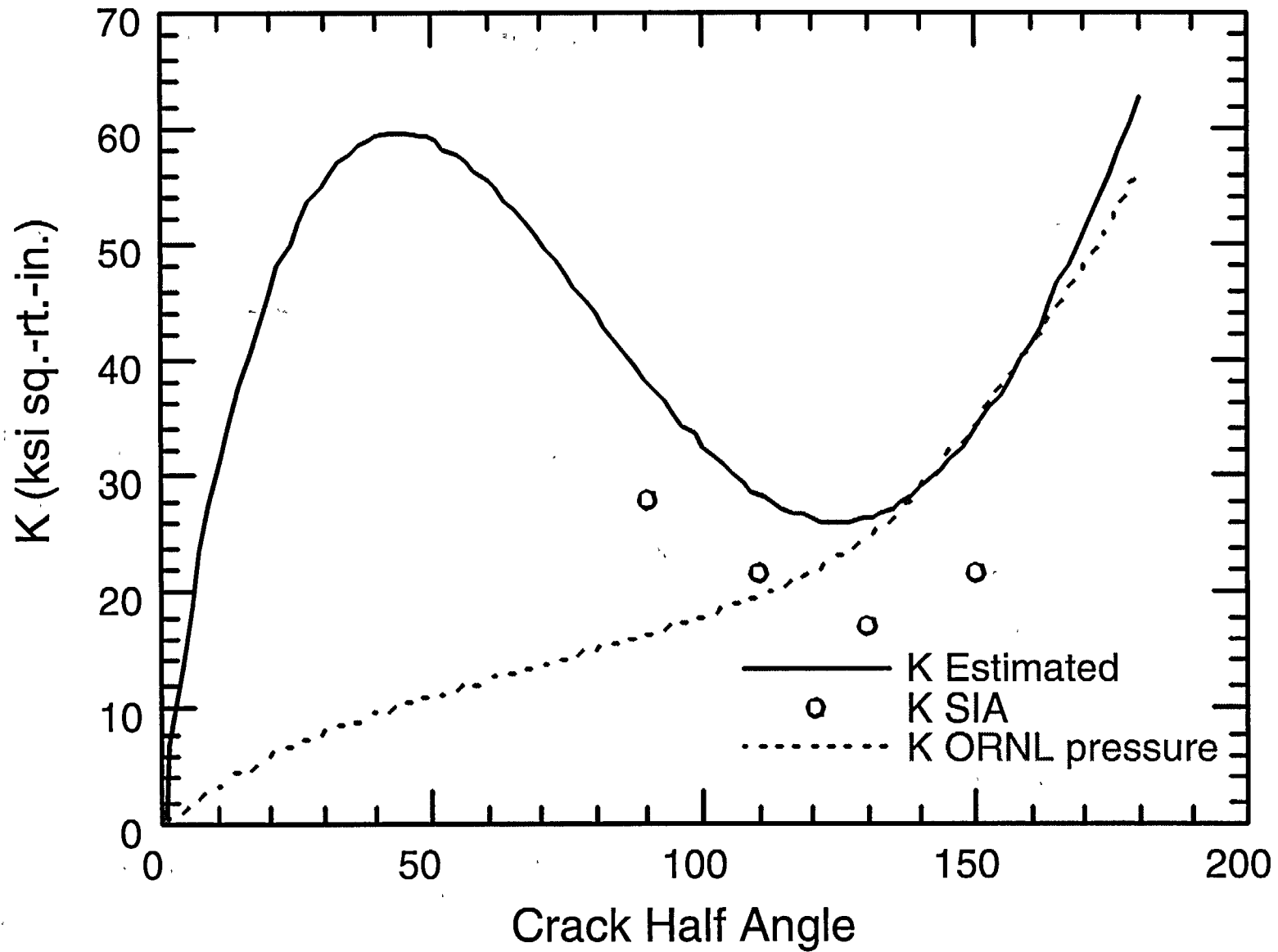
Figure 6-1 Stress Intensity Factor for a Through-Wall Circumferential Flaw in a Head Penetration

Figure 6-2 Crack Growth Predictions for Axial Inside Surface Flaws .5" Below the Attachment Weld – Nozzle Uphill Side

St. Lucie Unit 1

Nozzle Angle: 42.5 deg

Nozzle Angle: 37.1 deg

Nozzle Angle: 29.1 deg

Nozzle Angle: 54.8 deg

Nozzle Angle: 0.0 deg

a/t (Flaw Depth/Wall Thickness)

Time (Year)

Figure 6-3 Crack Growth Predictions for Axial Inside Surface Flaws .5" Below the Attachment Weld – Nozzle Downhill Side

Figure 6-4 Crack Growth Predictions for Axial Inside Surface Flaws at the Attachment Weld – Nozzle Uphill Side

Figure 6-5 Crack Growth Predictions for Axial Inside Surface Flaws at the Attachment Weld – Nozzle Downhill Side
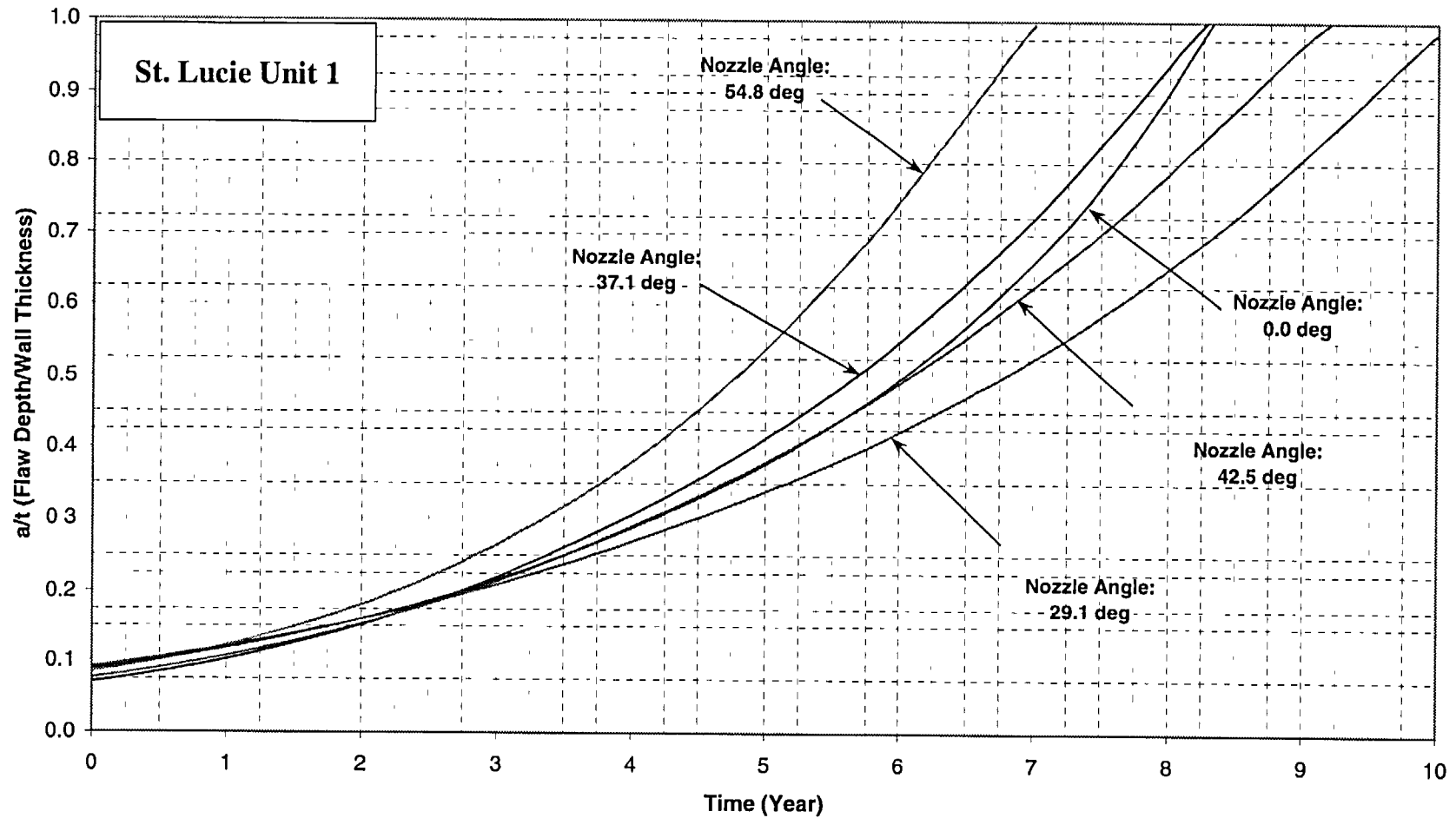
Figure 6-6 Crack Growth Predictions for Axial Inside Surface Flaws .5" Above the Attachment Weld – Nozzle Uphill Side
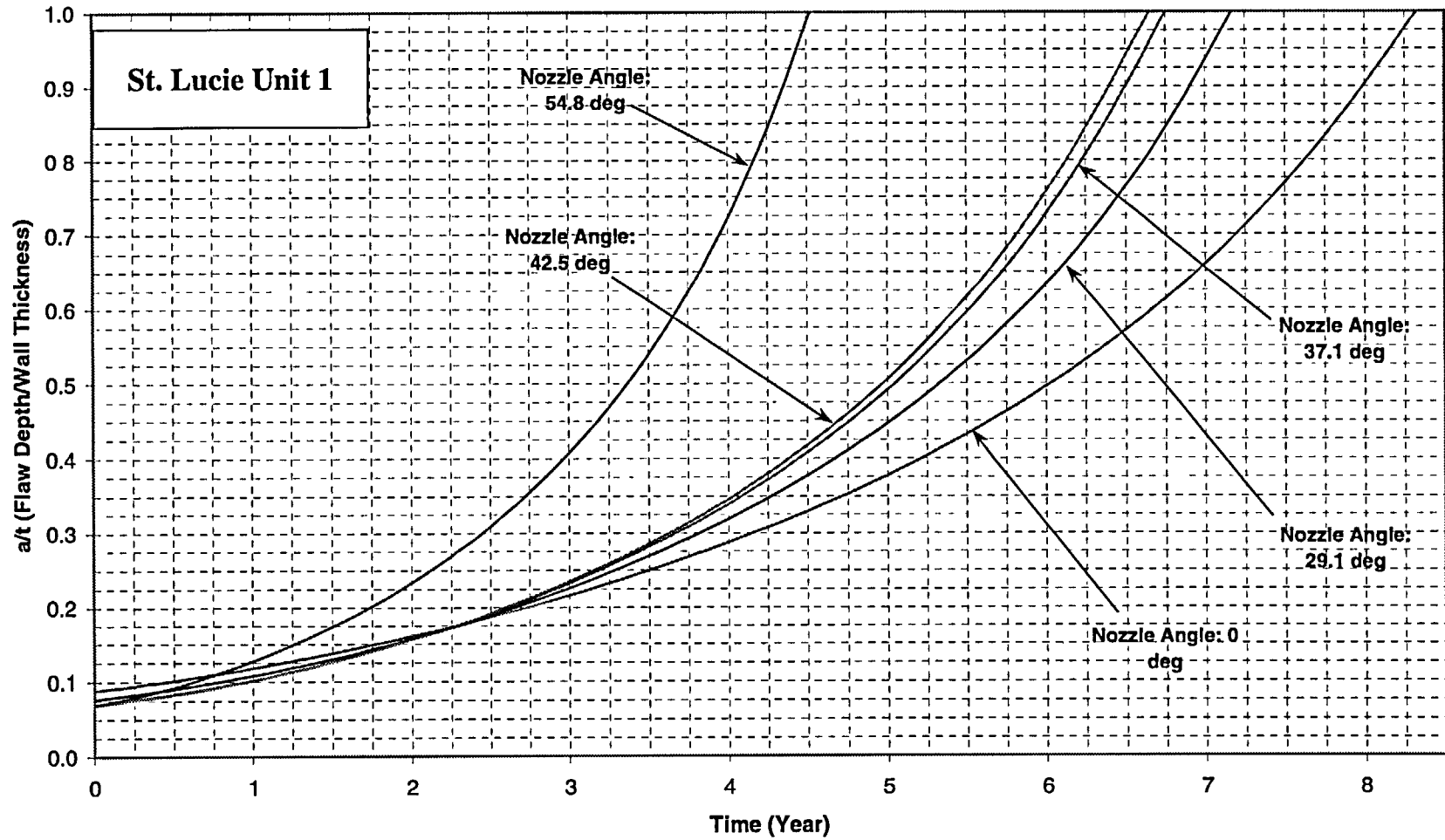
Figure 6-7 Crack Growth Predictions for Axial Inside Surface Flaws .5" Above the Attachment Weld – Nozzle Downhill Side
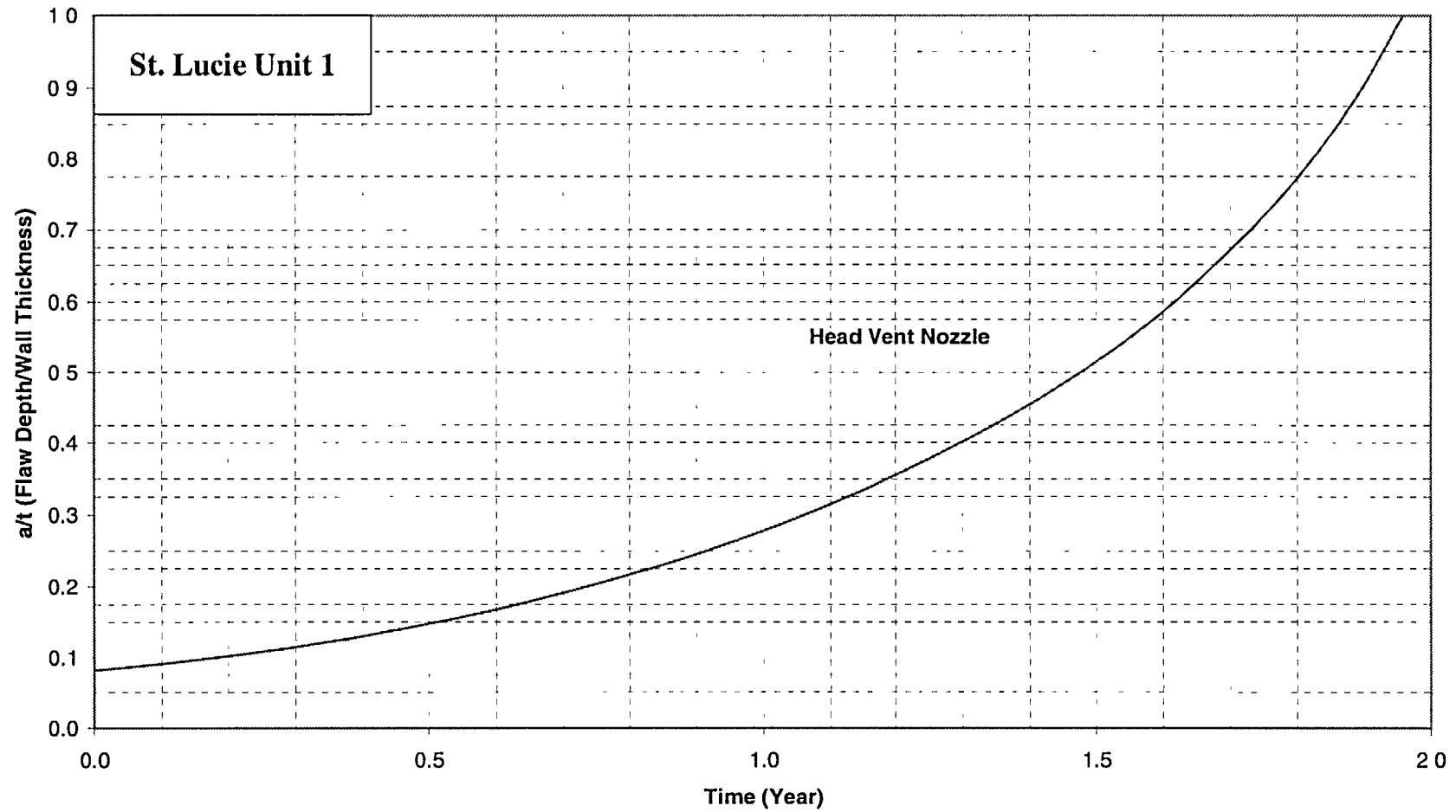
Figure 6-8 Crack Growth Predictions for Axial Inside Surface Flaws at the Attachment Weld for the Head Vent – Nozzle Downhill Side
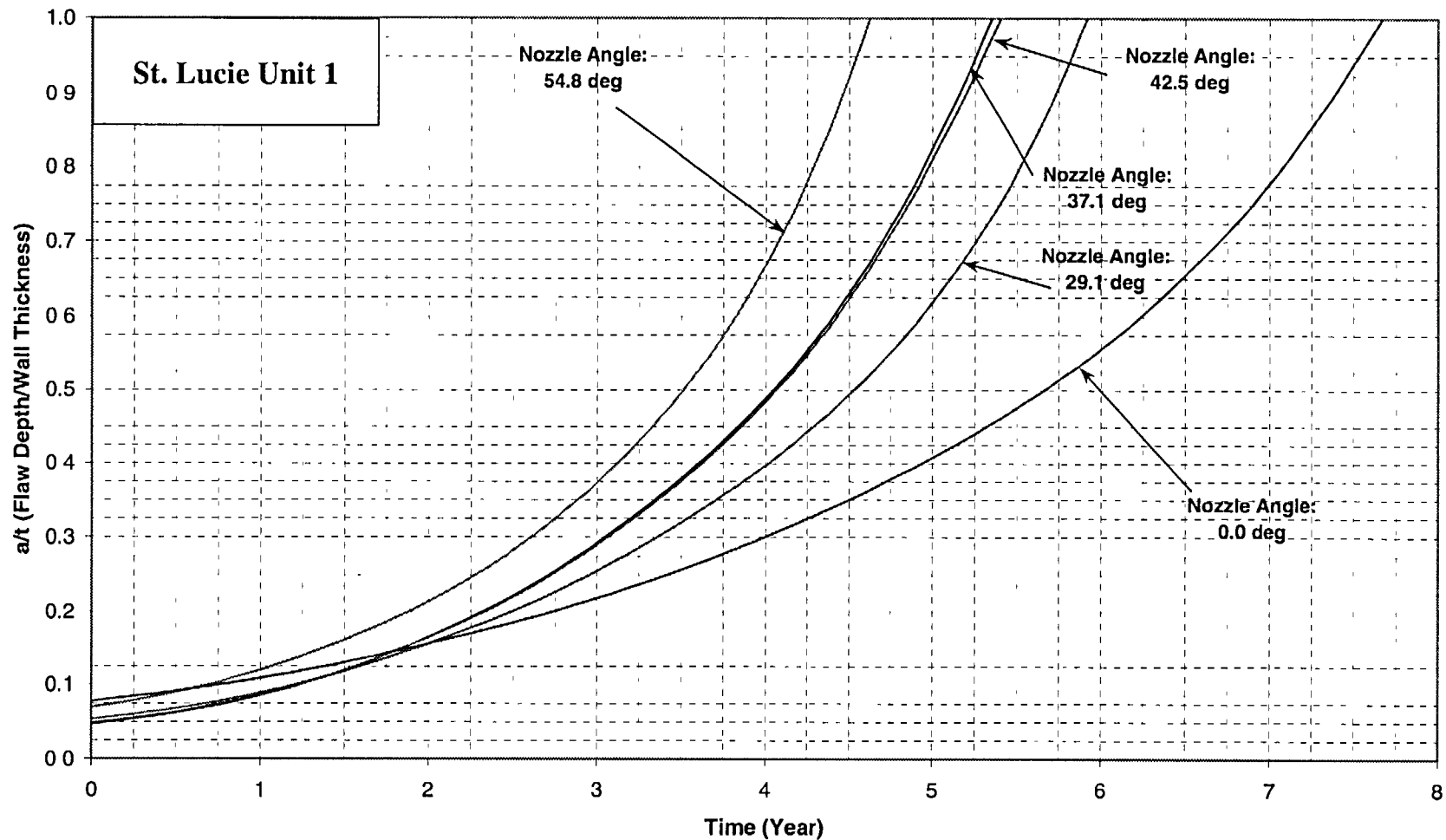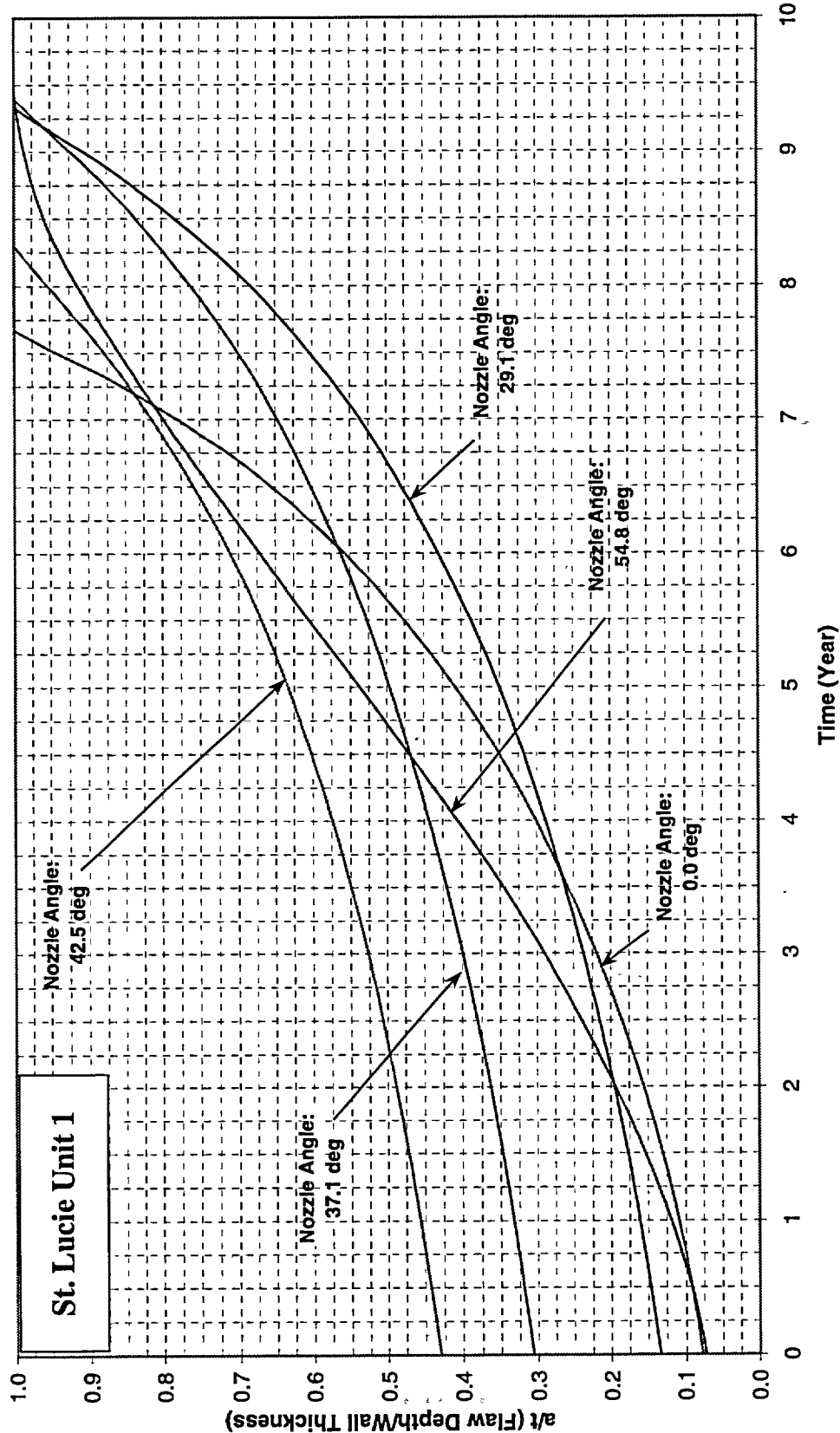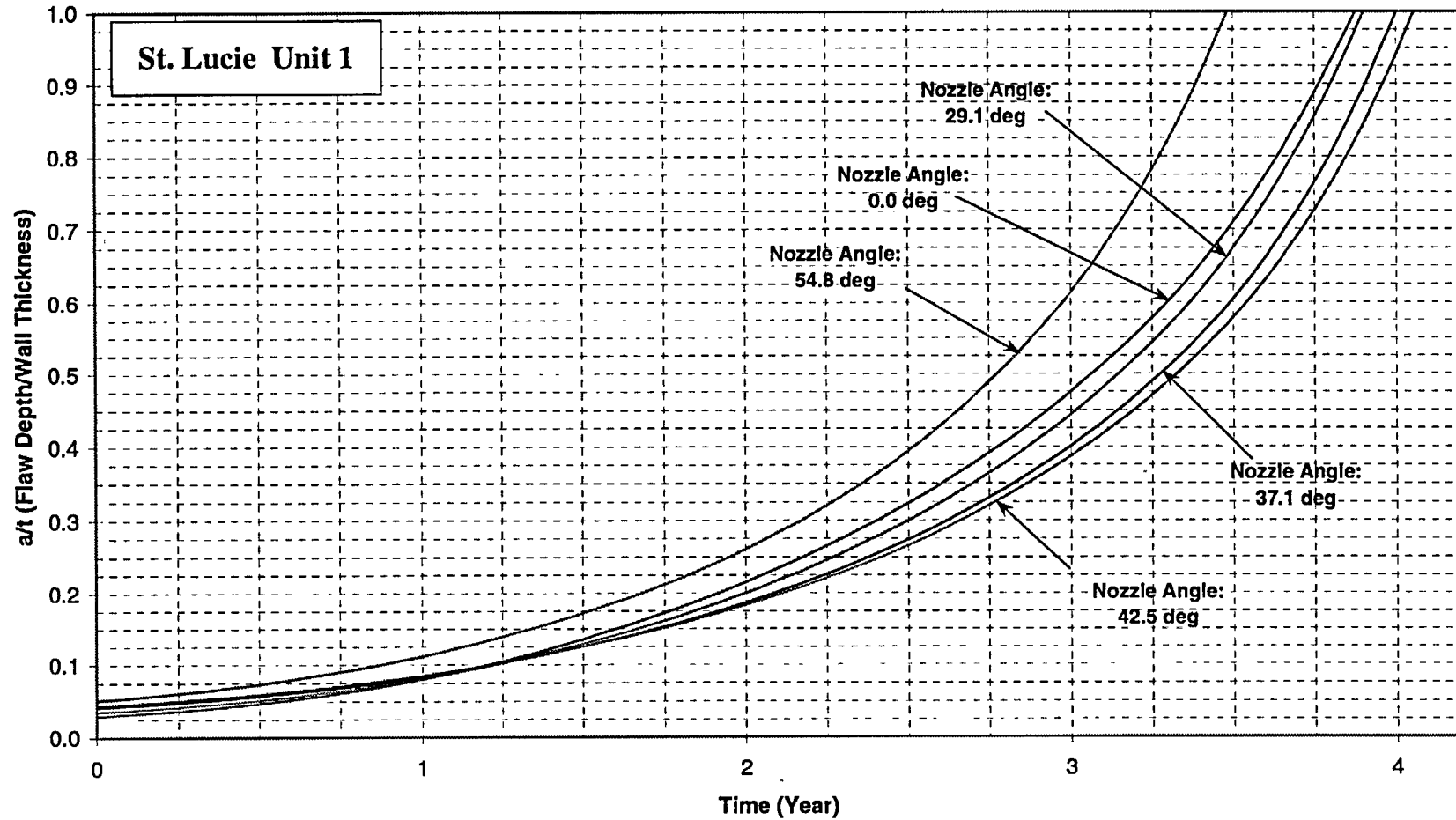
Figure 6-9 Crack Growth Predictions for Axial Outside Surface Flaws Below the Attachment Weld – Nozzle Uphill Side

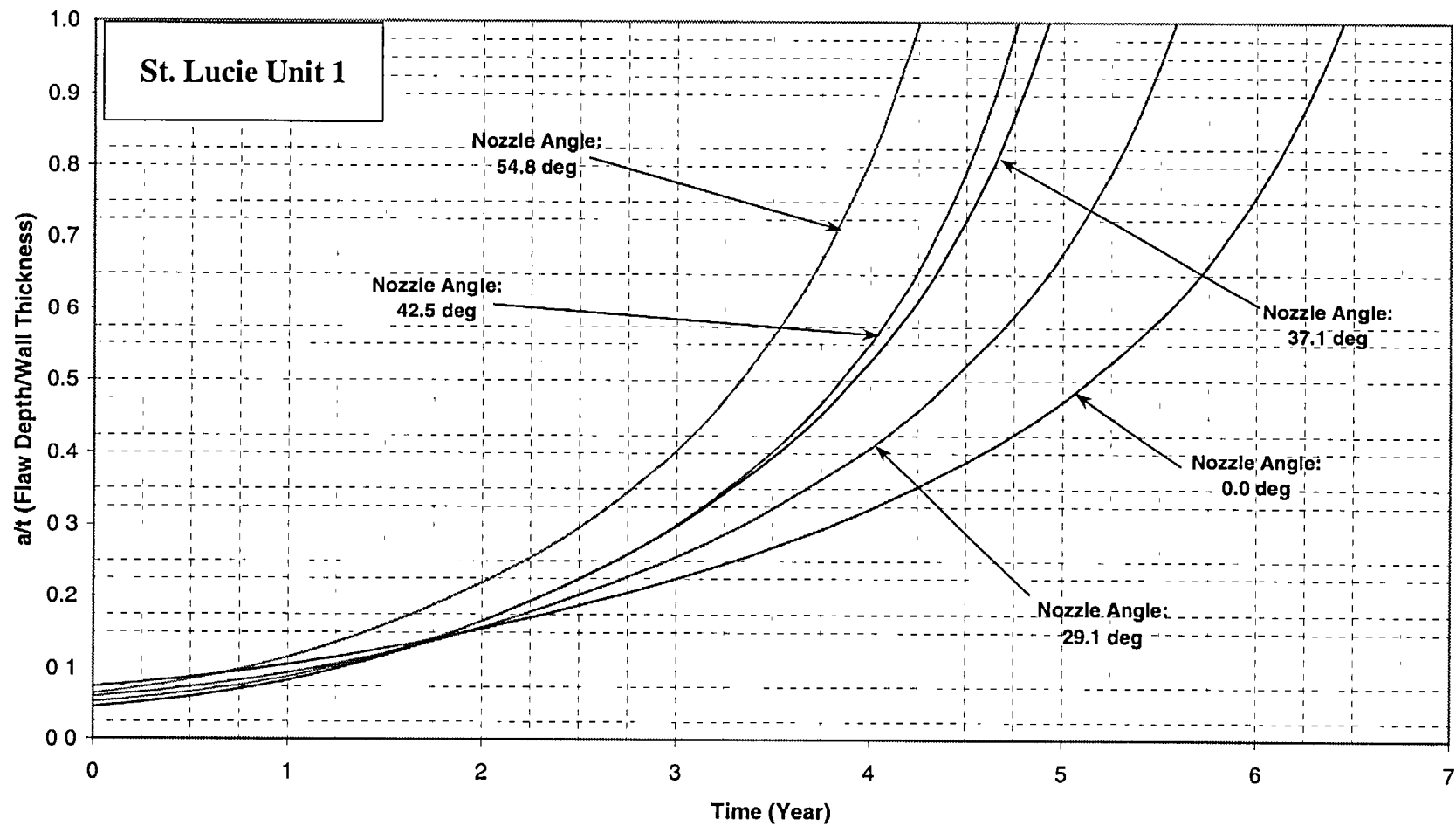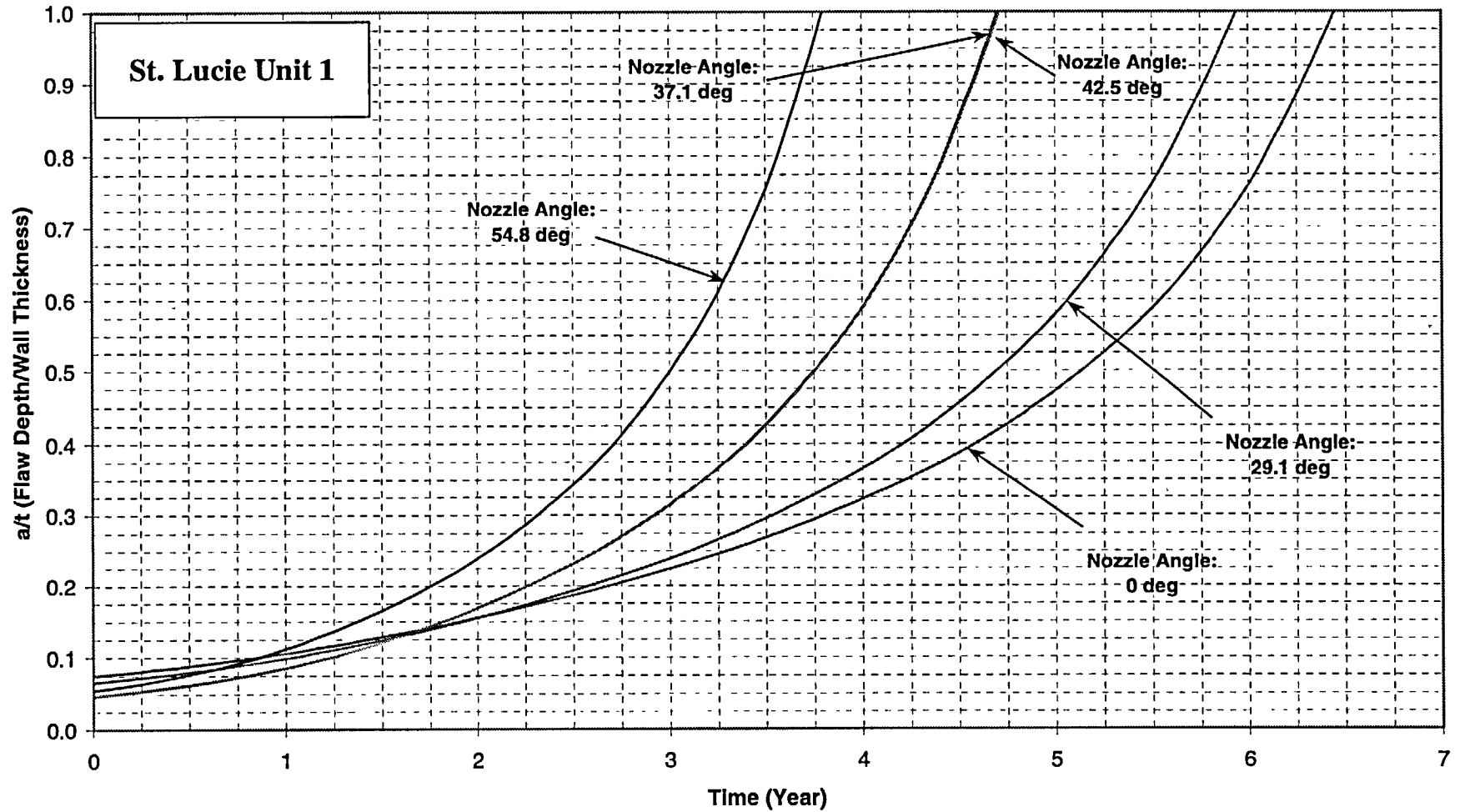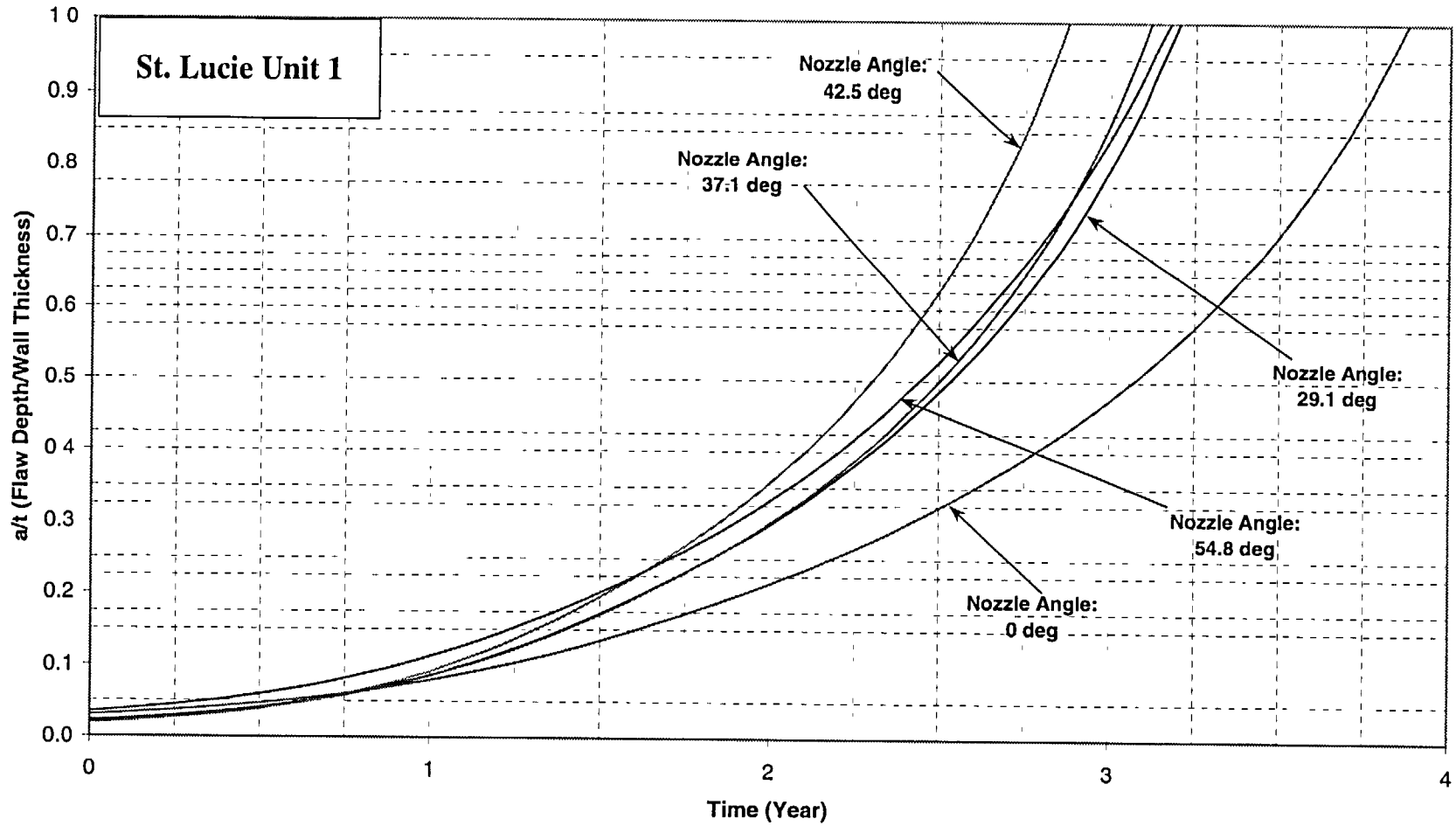**Figure 6-10 Crack Growth Predictions for Axial Outside Surface Flaws Below the Attachment Weld – Nozzle Downhill Side**
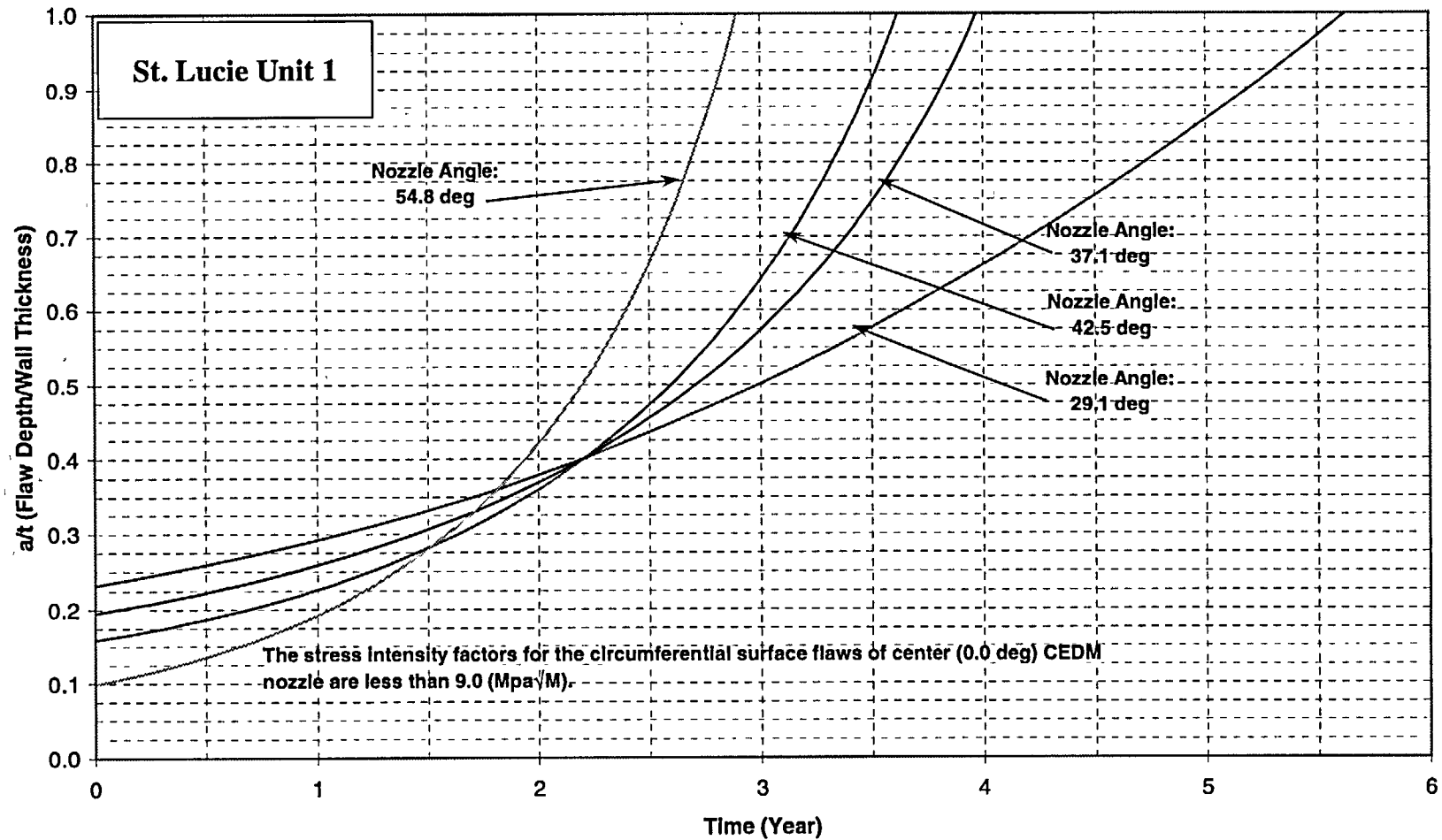
Figure 6-11 Crack Growth Predictions for Circumferential Outside Surface Flaws Along the Top of the Attachment Weld (MRP Factor of 2.0 Included)
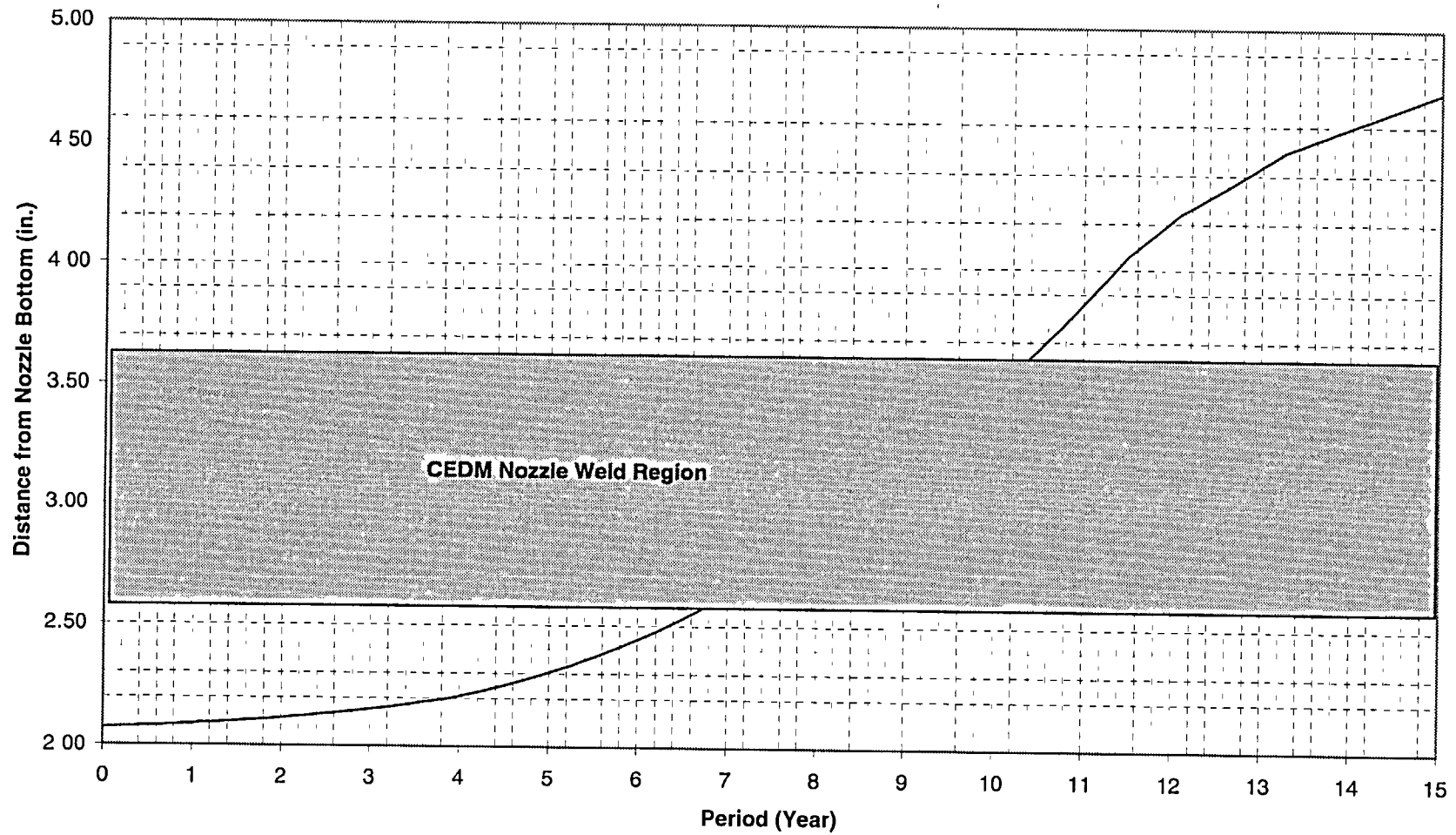
Figure 6-12 Crack Growth Predictions for Through-Wall Axial Flaws Located in the Center CEDM (0.0 Degrees) Penetration – Uphill and Downhill Side
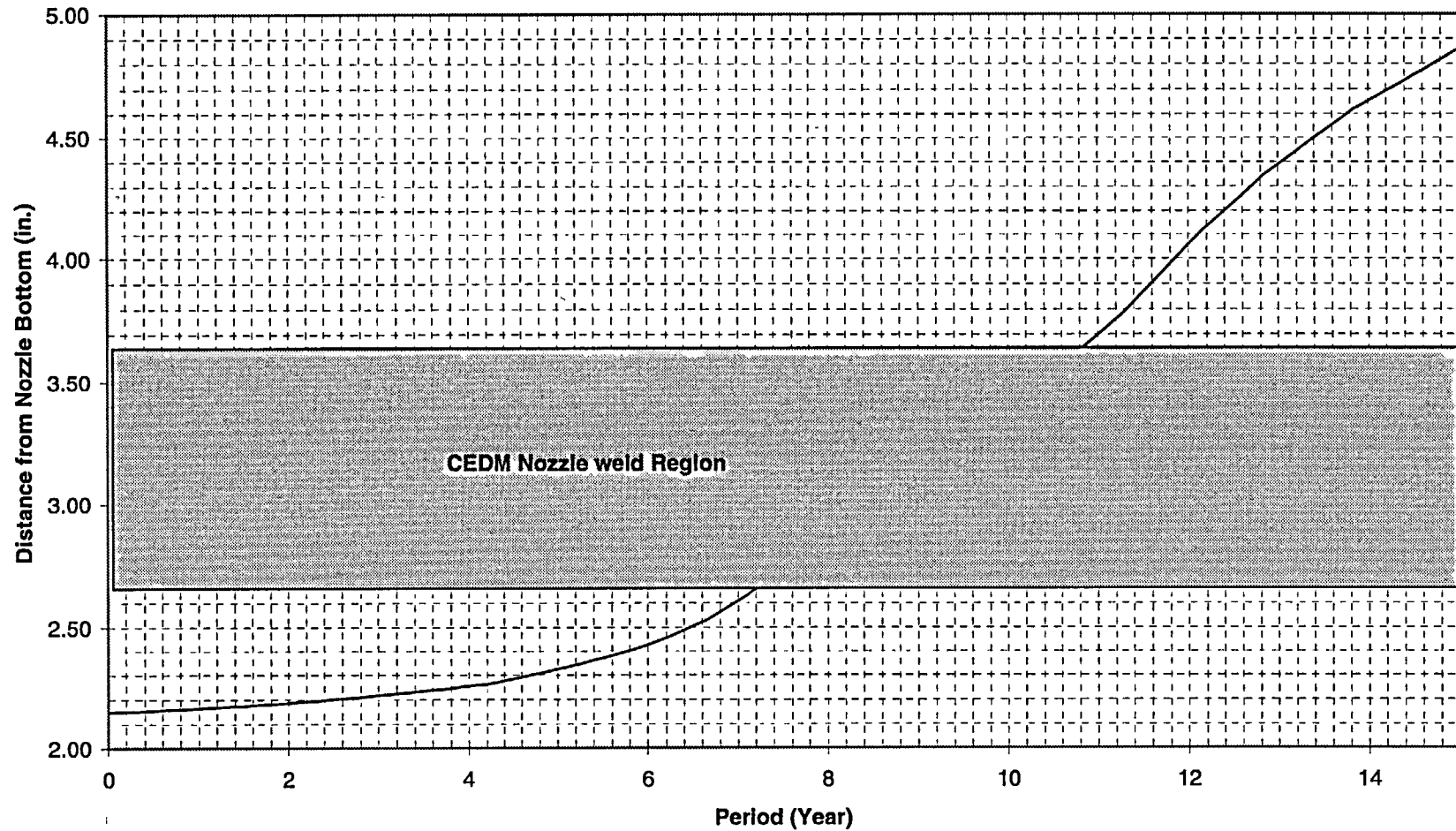
Figure 6-13 Crack Growth Predictions for Through-Wall Axial Flaws Located in the 29.1 Degree CEDM Row of Penetrations – Downhill Side
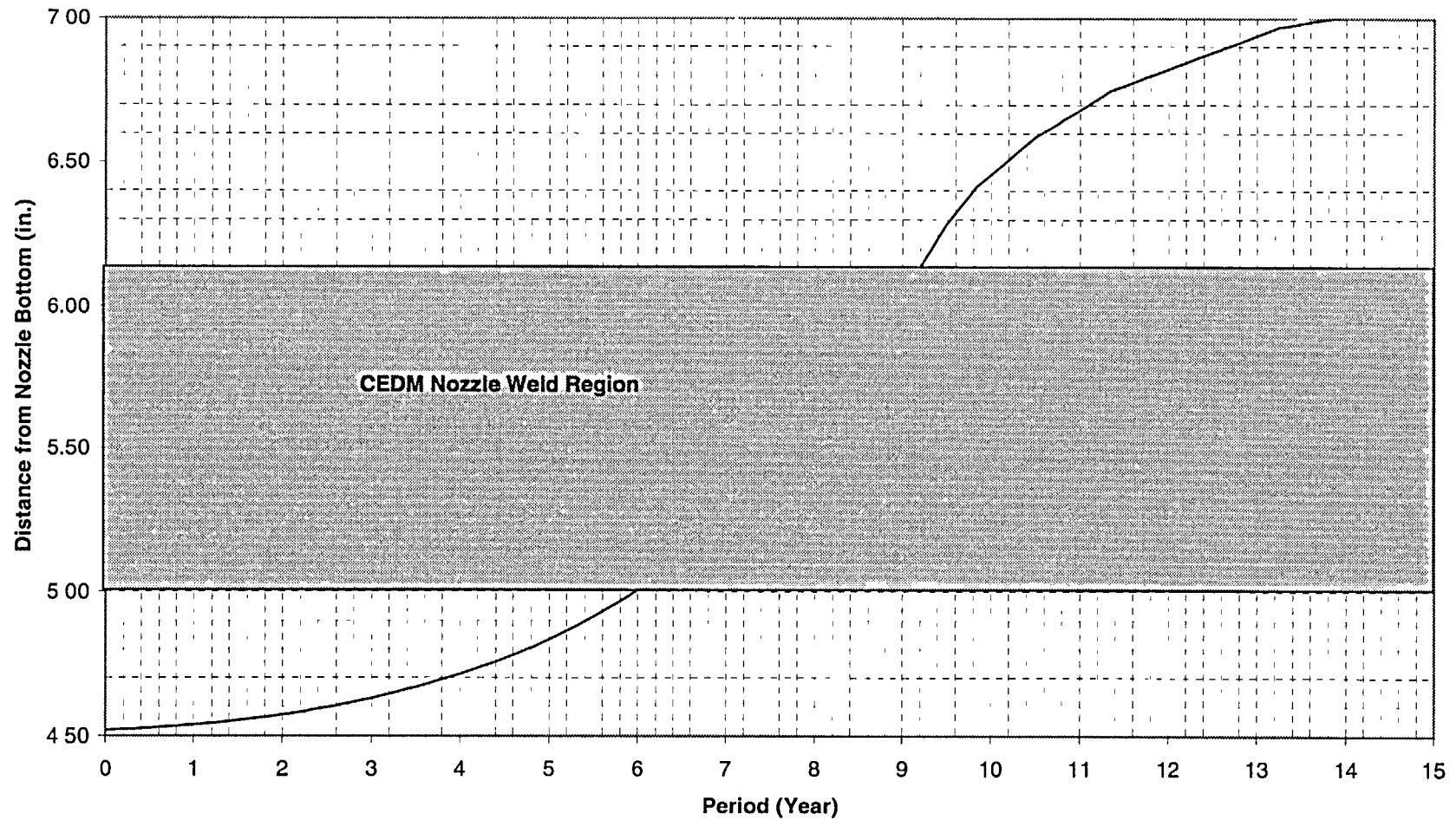
Figure 6-14 Crack Growth Predictions for Through-Wall Axial Flaws Located in the 29.1 Degrees Row of Penetrations – Uphill Side
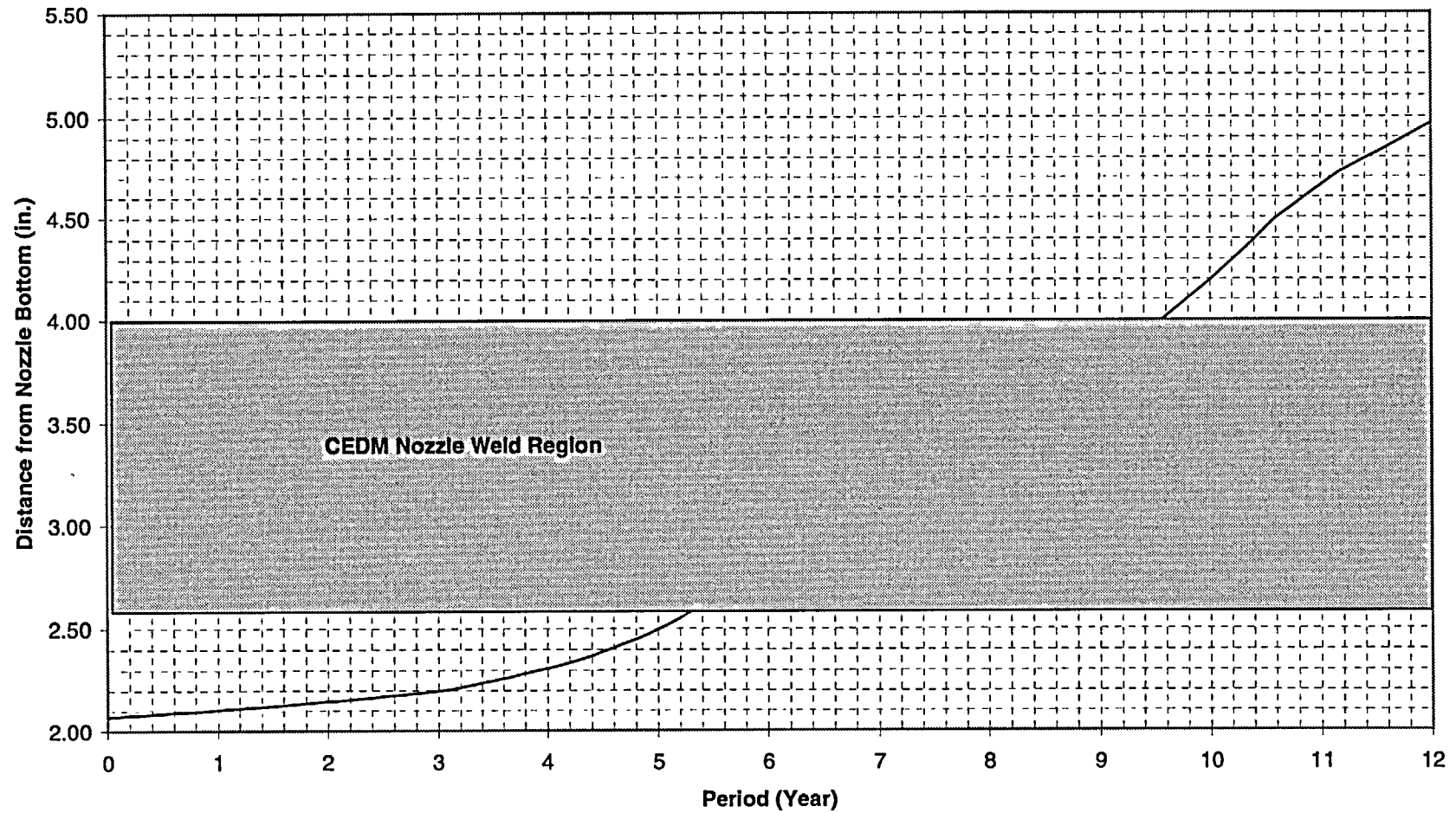
Figure 6-15 Crack Growth Predictions for Through-Wall Axial Flaws Located in the 37.1 Degrees Row of Penetrations – Downhill Side
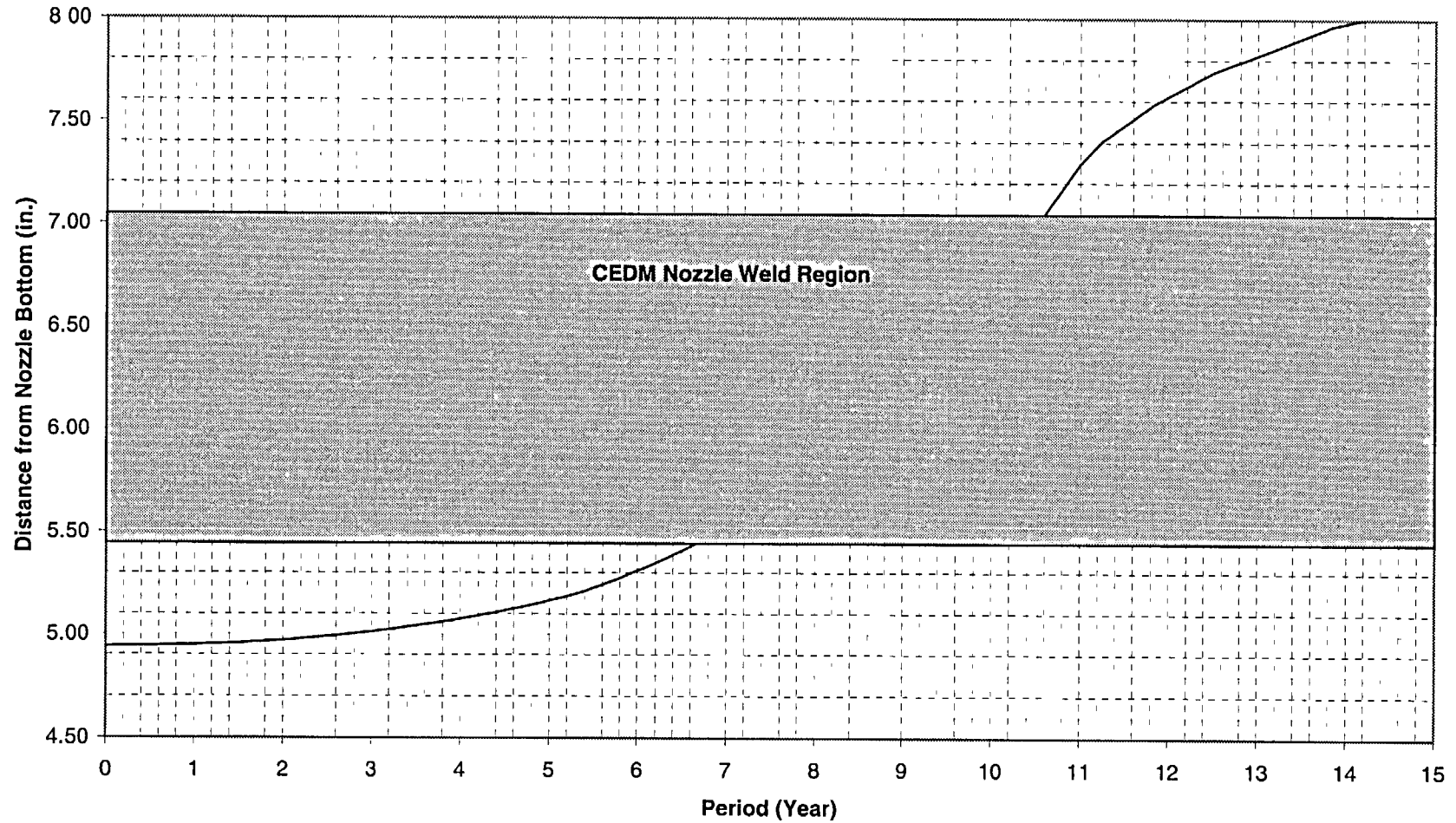
Figure 6-16 Crack Growth Predictions for Through-Wall Axial Flaws Located in the 37.1 Degrees Row of Penetrations – Uphill Side
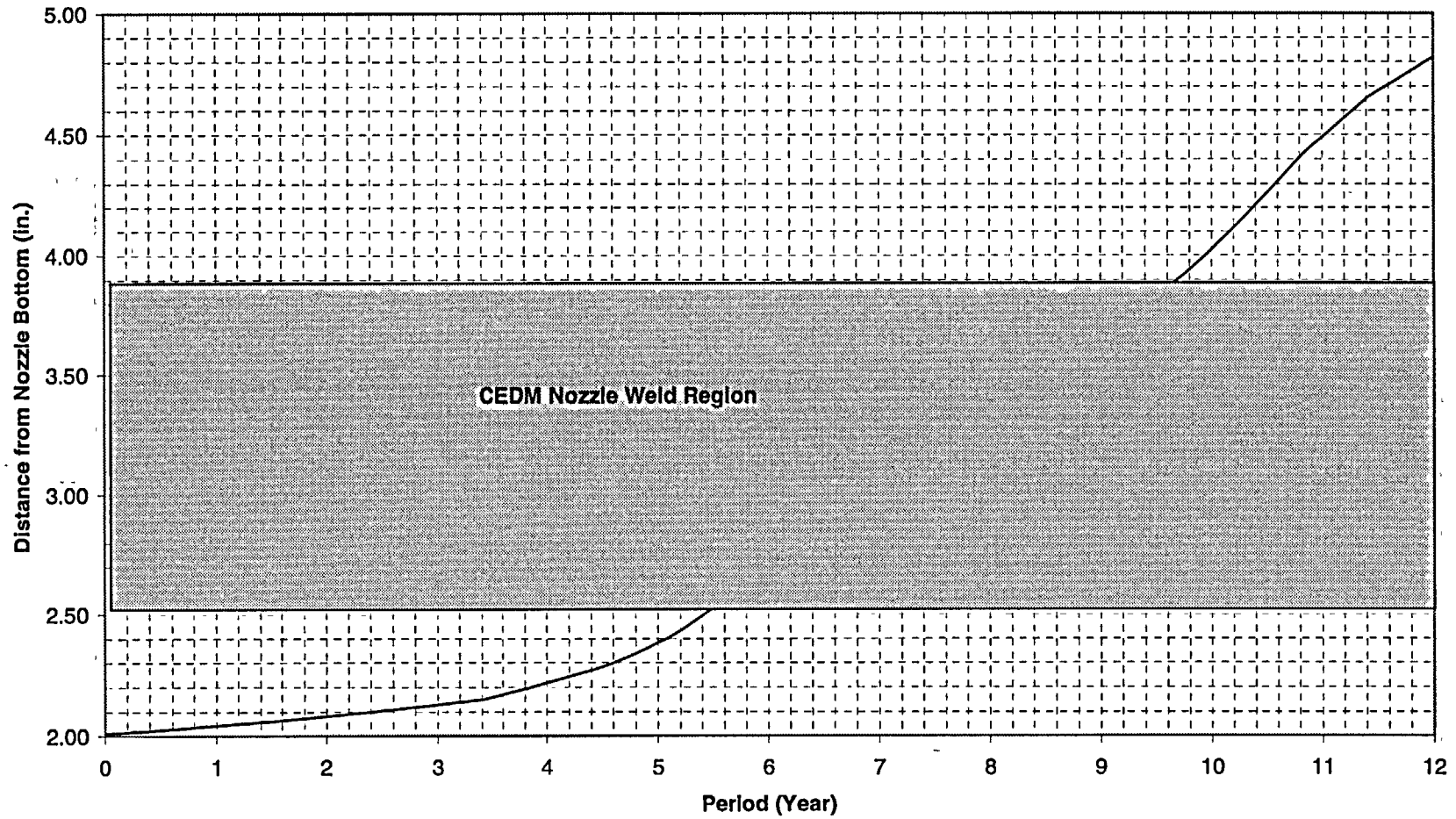
Figure 6-17 Crack Growth Predictions for Through-Wall Axial Flaws Located in the 42.5 Degrees Row of Penetrations – Downhill Side
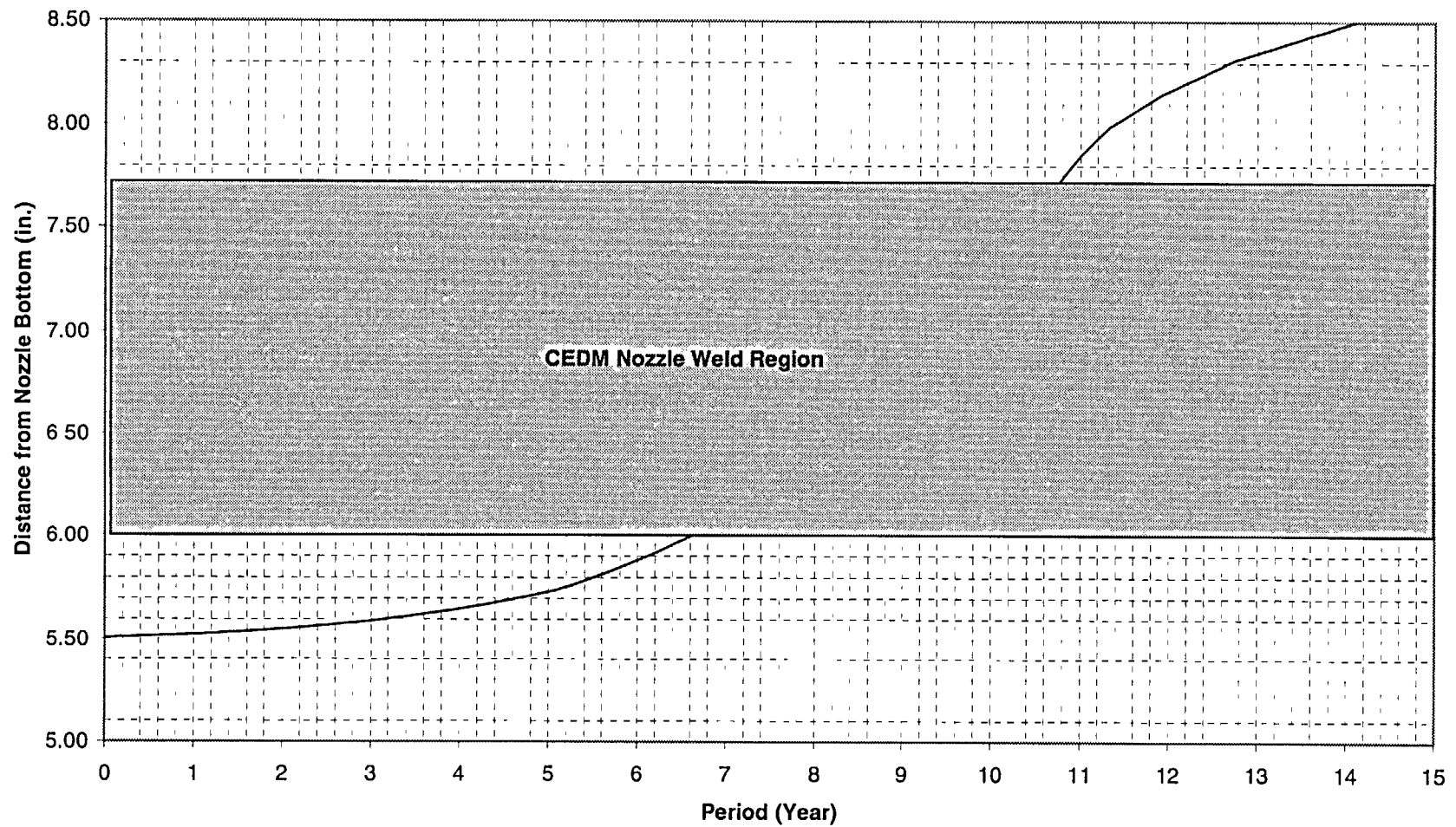
Figure 6-18 Crack Growth Predictions for Through-Wall Axial Flaws Located in the 42.5 Degrees Row of Penetrations – Uphill Side
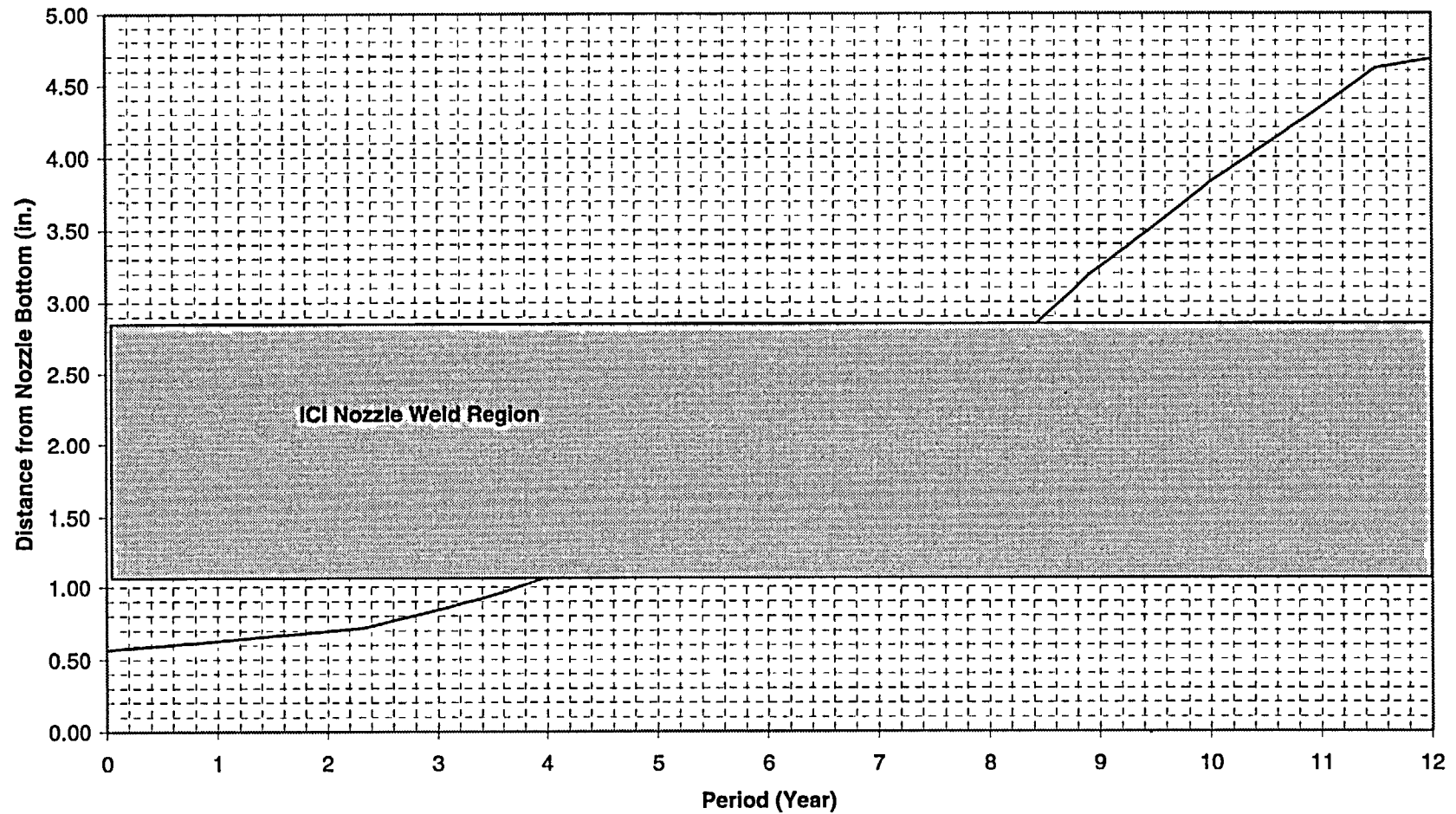
Figure 6-19 Crack Growth Predictions for Through-Wall Axial Flaws Located in the 54.8 Degrees Row of Penetrations – Downhill Side
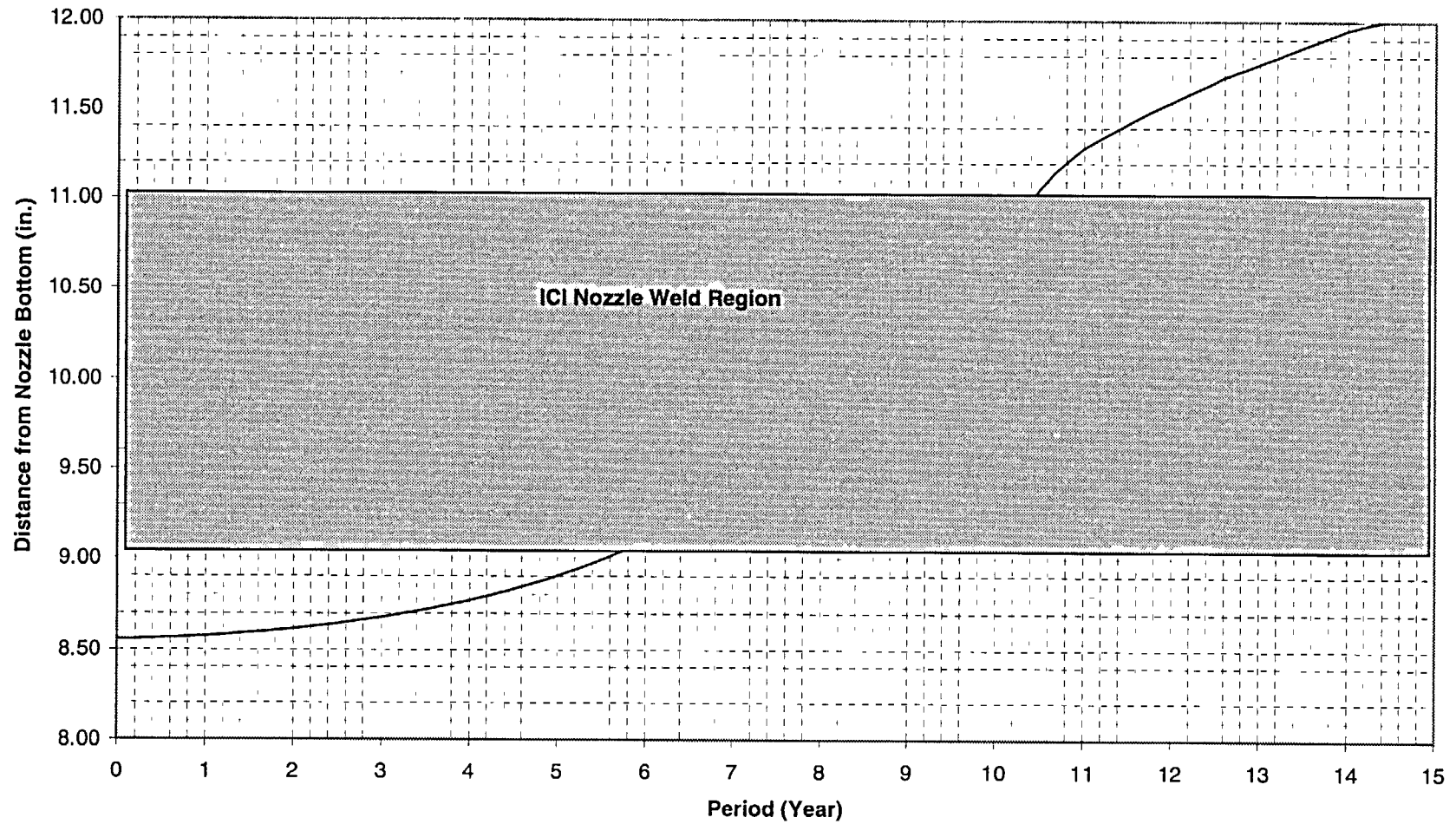
Figure 6-20 Crack Growth Predictions for Through-Wall Axial Flaws Located in the 54.8 Degrees Row of Penetrations – Uphill Side
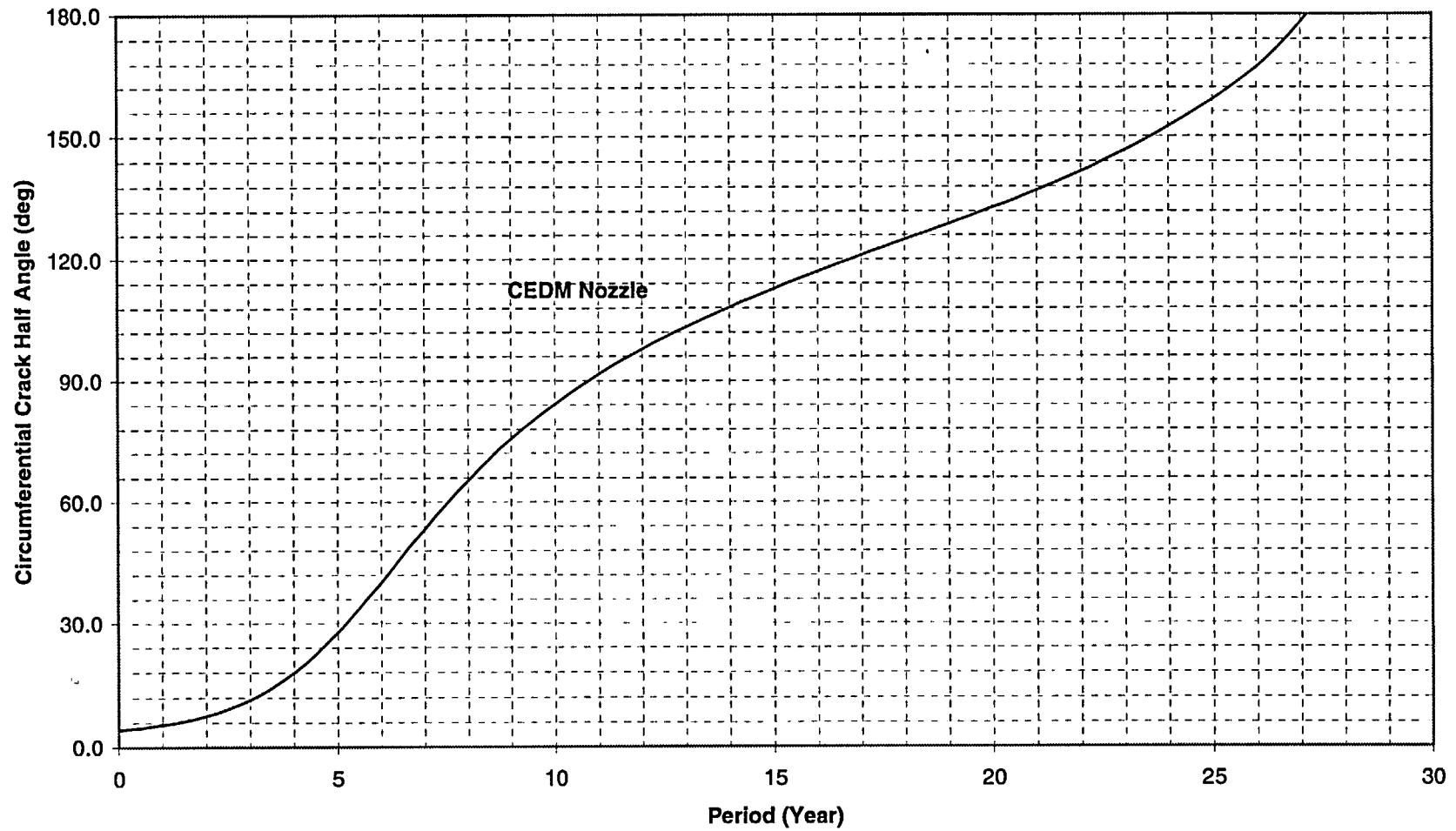
Figure 6-21 Crack Growth Predictions for Circumferential Through-Wall Flaws Near the Top of the Attachment Weld for CEDM Nozzles (MRP Factor of 2.0 Included)
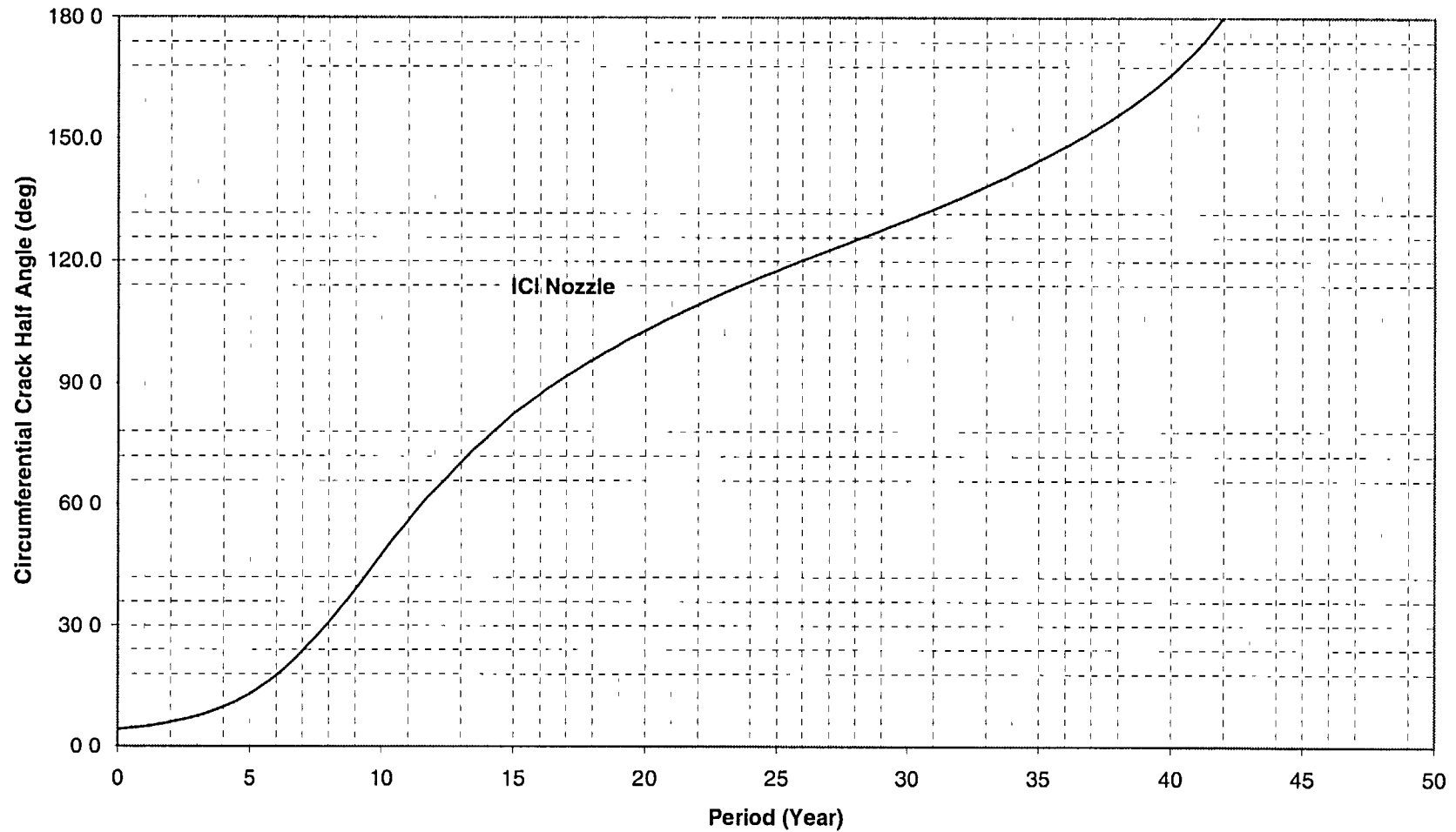
Figure 6-22 Crack Growth Predictions for Circumferential Through-Wall Cracks Near the Top of the Attachment Weld for ICI nozzles (MRP Factor of 2.0 Included)
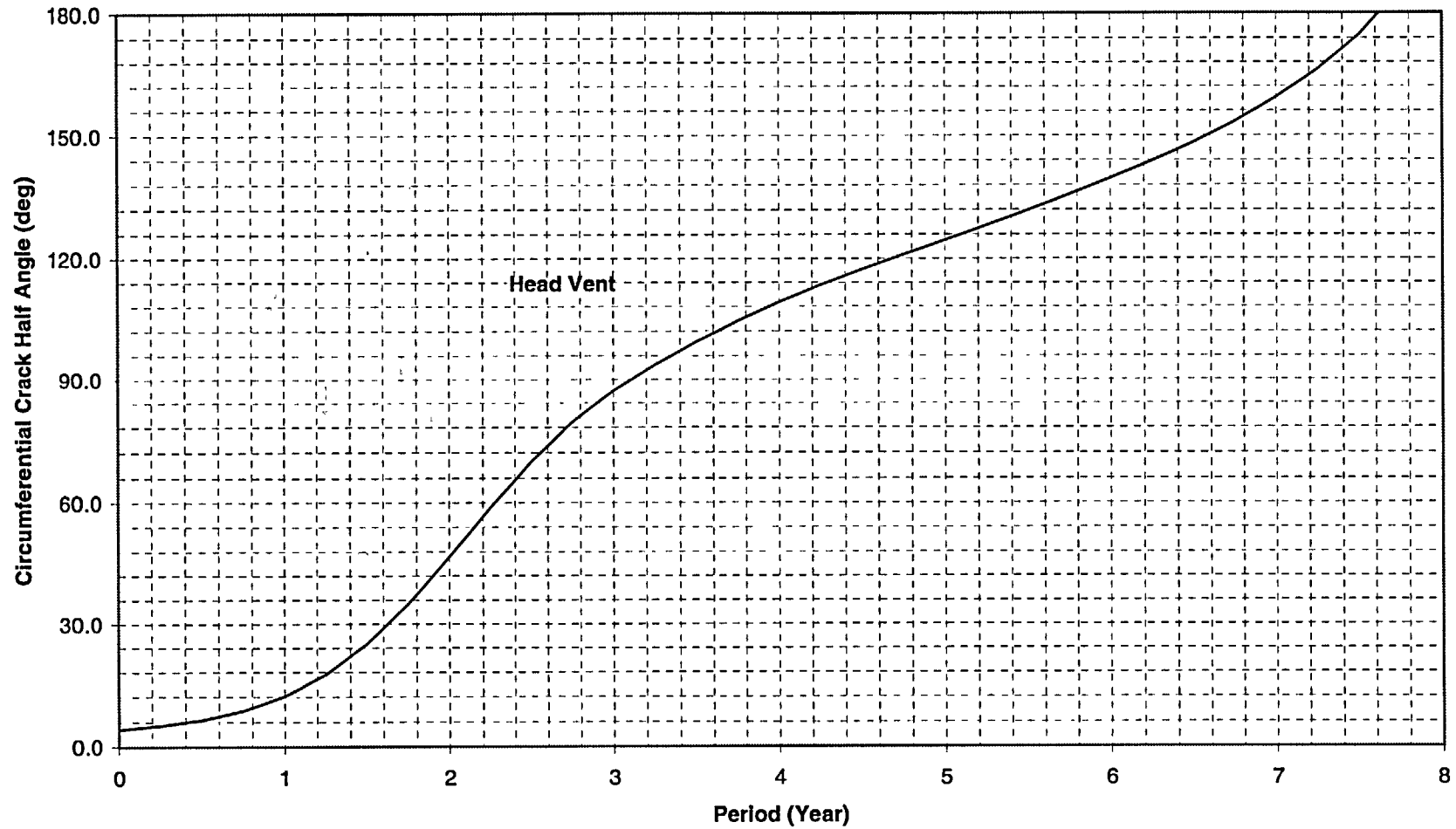
Figure 6-23 Crack Growth Predictions for Circumferential Through-Wall Flaws Near the Top of the Attachment Weld for Head Vent (MRP Factor of 2.0 Included)

(a) Single Linear Flaw

(b) Single Curvilinear Flaw

(c) Aligned Linear Flaws

$\ell_1 > \ell_2$

(d) Nonoverlapping Flaws

$\ell_1 \geqslant \ell_2$

(e) Overlapping Parallel Flaws

(f) Overlapping Flaws

(g) Nonaligned Parallel Flaws

$\ell_1 > \ell_2$

(h) Multiple Parallel Flaws
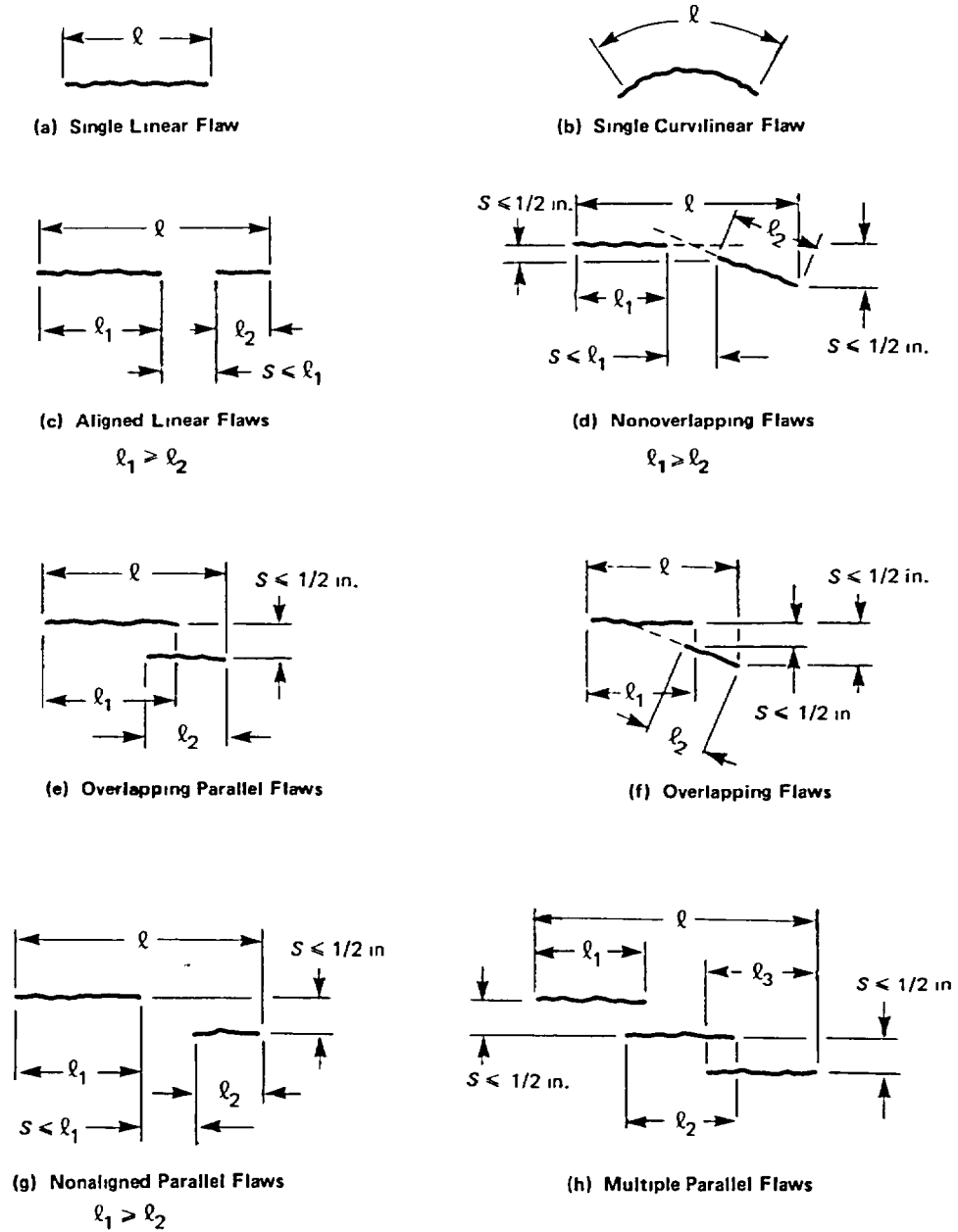
Figure 6-24 Section XI Flaw Proximity Rules for Surface Flaws (Figure IWA-3400-1)
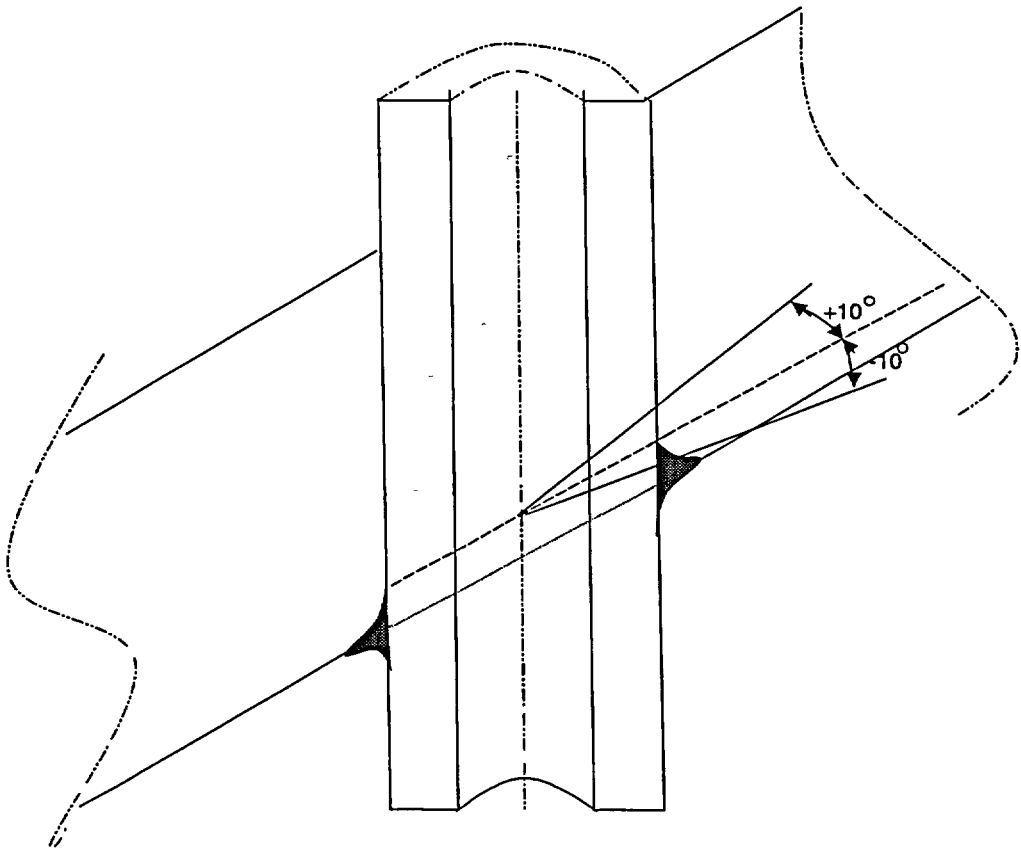
Figure 6-25 Definition of "Circumferential"

TOP OF WELD

RV Head

NOZZLE

t

BOTTOM OF WELD

c

a
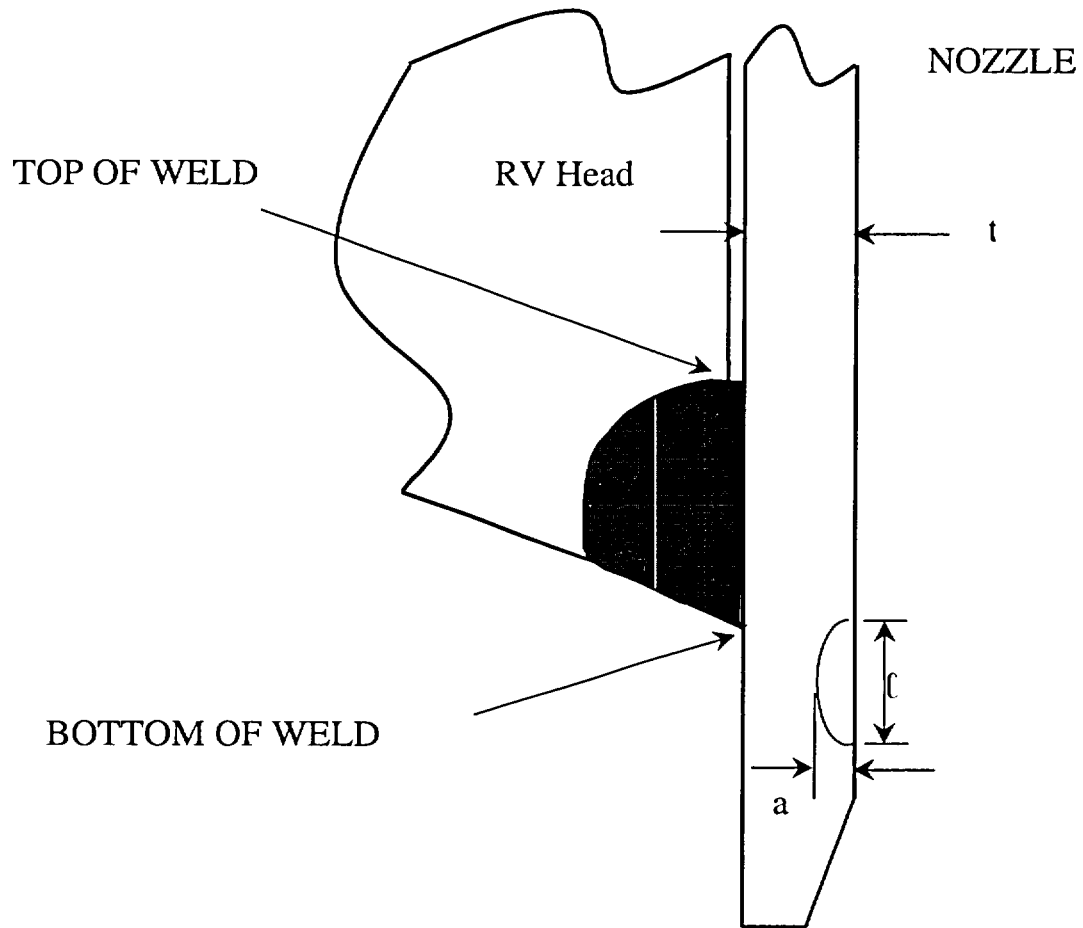
Figure 6-26 Schematic of Head Penetration Geometry

7 SUMMARY AND EXAMPLE PROBLEMS

An extensive evaluation has been carried out to characterize the loads and stresses that exist in the head penetrations at St. Lucie Unit 1. Three-dimensional finite element models were constructed, and all pertinent loads on the penetrations were analyzed [6]. These loads included internal pressure and thermal expansion effects typical of steady state operation. In addition, residual stresses due to the welding of the penetrations to the vessel head were considered.

Results of the analyses reported here are consistent with the axial orientation and location of flaws that have been found in service in a number of plants. The largest stress component is the hoop stress and the maximum stresses were found to exist at the attachment weld. The most important loading conditions were found to be those which reside on the penetration for the majority of the time. These conditions are the steady state loading and the residual stresses.

These stresses are important because the cracking that has been observed to date in operating plants has been determined to result from primary water stress corrosion cracking (PWSCC). These stresses were used in the fracture mechanics calculations to predict the future growth of flaws postulated to exist in the head penetrations. A crack growth law was developed specifically for the operating temperature of the vessel head at St. Lucie Unit 1 based on the EPRI recommendation, which is consistent with laboratory data as well as crack growth results for operating plants.

The crack growth predictions contained in Section 6 show that the future growth of cracks which might be found in the penetrations will be typically moderate, however, a number of effective full power years would be required for any significant extensions.

7.1 SAFETY ASSESSMENT

It is appropriate to examine the safety consequences of an indication that might be found. The indication, even if it were to propagate through the penetration nozzle wall, would have only minor consequences since the pressure boundary would not be broken, unless it were to propagate above the weld.

Further propagation of the indication would not change its orientation, since the hoop stresses in the penetration nozzle are much larger than the axial stresses. Therefore, it is extremely unlikely that the head penetration would be severed.

If the indication were to propagate to a position above the weld, a leak could result, but the magnitude of such a leak would be very small, because the crack could not open significantly due to the tight fit between the penetration nozzle and the vessel head. Such a leak would have no immediate impact on the structural integrity of the system, but could lead to wastage in the ferritic steel of the vessel head as the borated primary water concentrates due to evaporation. Davis Besse has demonstrated the consequence of ignoring such leaks.

Any indication is unlikely to propagate very far up the penetration nozzle above the weld since the hoop stresses decrease in this direction, causing the indication to slow down and stop before it reaches the outside surface of the head.

The high likelihood that the indication will not propagate up the penetration nozzle beyond the vessel head ensures that no catastrophic failure of the head penetration will occur. The indication will be enveloped in the vessel head itself, which precludes the opening of the crack and limits leakage.

7.2 EXAMPLE PROBLEMS

The flaw tolerance charts in Figures 6-2 through 6-23 can be used with the acceptance criteria of Section 6.5 to determine the available service life. In this section, a few examples will be presented to illustrate the use of these figures. The example cases are listed in Table 7-1. Note that the nominal thickness of 0.566 inches was used in the example problems; however, in actual application, the thickness of 0.5 inches (counterbore included) should be used where applicable. The general guidelines on the use of the flaw evaluation charts are also provided in Appendix B.

Example 1 – To determine the service life of an axially oriented inside surface flaw whose tip is located 1.2" below the weld on the uphill side of penetration no. 30, the angle of this penetration must first be determined from Table 1-1. The angle for this penetration nozzle is 29.1 degrees. The crack growth curves of Figure 6-2 are applicable and Figure 6-2 has been reproduced as Figure 7-1. In this case, the initial flaw depth is 12.5 percent of the wall thickness. A straight line is then drawn horizontally at a/t = 0.125 and intersecting the crack growth curve. Using the acceptance criteria in Table 6-1, the service life can then be determined as the remaining time for this flaw to grow to the limit of 100 percent of the wall thickness or approximately 4.5 years (labeled as Service Life in Figure 7-1). Assuming that the initial aspect ratio of 2.5:1 is maintained throughout the time that the inside surface flaw becomes a through-wall flaw, the final length of the flaw (ℓ) will be 1 415 inch The upper extremity of the flaw is now located 0 58 inch below the weld and validates the use of the crack growth curves of Figure 6-2. The upper extremity is found by subtracting half the initial ℓ from half the final ℓ, then subtracting this number from the initial distance from the weld.

Example 2 – In this case, the flaw is identical in size to that used in Example 1, but located on the outside surface and on the uphill side of penetration no. 30. The applicable curve to use is Figure 6-9. Using the acceptance criteria in Table 6-1, the determination of service life is illustrated in Figure 7-2, where we can see that the result is approximately 2.5 years.

Example 3 – The axial inside surface flaw is located at the weld and on the downhill side of penetration no. 1. From Table 1-1, the angle of this penetration nozzle is 0.0 degrees. It is assumed that the flaw maintains its aspect ratio of 5:1. The applicable curve is Figure 6-5 and used to determine the service life. In this case, the initial flaw depth is 7.5 percent of the wall thickness. Using the acceptance criteria in Table 6-1, the allowable service life can then be determined as the time for the flaw to reach a depth of 75 percent of the wall thickness. By drawing a horizontal line at a/t = 0.075 and at a/t = 0.75, the service life can be determined

through the intersection points of these lines and the crack growth curve. The resulting service life is approximately 6.0 years, as shown in Figure 7-3.

Example 4 – In this case, we have postulated an axial inside surface flaw that will require the use of two flaw charts for its evaluation because the upper extremity of this flaw will reach within 0.5 inch below the attachment weld as it propagates into the nozzle wall. The flaw has an initial depth of .078 inch and is located on the downhill side of penetration no. 30, which has an angle of 29.1 degrees. The length of the initial flaw is 0.394 inch and its upper extremity is located 1.0 inch below the attachment weld. Assuming that the initial aspect ratio of 5:1 is maintained as the flaw propagates into the nozzle wall, the final length of a through-wall flaw would be 2.83 inches long. The location of the upper extremity of this flaw would have reached within 0.5 inch below the weld as it propagates into the nozzle wall.

For this postulated flaw, the first step is to estimate the time required for the initial flaw to grow to within 0.5 inch of the weld. This can be accomplished with the use of Figure 6-3 and is reproduced here as Figure 7-4A. The crack tip is 1 inch below the weld and is assumed to grow until the tip is 0.5 inches below. The final half-length of the flaw when it reaches 0.5 inches below the weld will be the sum of the initial half-length and the 0.5 inches it has grown (0.5 +0.394/2). Multiplying this by two and then dividing by the aspect ratio gives the flaw depth when the crack tip is 0.5 inches below the weld (.279 in). The required time to reach such a flaw size is estimated as 6.5 years in Figure 7-4A. Using the flaw depth calculated previously (50 percent) as the initial flaw depth, the curves in Figure 6-5 for inside surface flaws near the weld gives the time before the flaw becomes through-wall. Using the acceptance criteria in Table 6-1, Figure 7-4B shows an additional 0.75 years of service life for a total of 7.25 years.

Example 5 – This case is an axial through-wall flaw with its upper extremity located 0.40 inches below the weld region on the uphill side of penetration no. 70. The angle of the penetration nozzle is 54.8 degrees as shown in Table 1-1. The crack growth curves of Figure 6-20 are applicable and has been reproduced as Figure 7-5. As illustrated in Figure 7-5, the service life is estimated to be approximately 4.0 years for the initial flaw to grow to the bottom of the attachment weld.

The examples show that the most important figures used in evaluating the detected flaws in the head penetrations are Figures 6-2 through 6-10 for the axial surface flaws, and Figure 6-11 for circumferential flaws postulated near the top of the attachment weld. The figures provide valuable information on the projected growth of through-wall flaws, but may be of limited practical application with the current acceptance criteria. However, there is an important safety aspect to the through-wall flaw evaluation charts in that they demonstrate that flaw propagation above the weld will be very limited.

Several guidelines are important to understand when using these flaw evaluation charts.

1.   If a flaw is found in a penetration nozzle for which no specific analysis was performed and there is a uniform trend as a function of penetration nozzle angle, interpolation between penetration nozzles is the best approach.

2.   If a flaw is found in a penetration nozzle for which no specific analysis was performed and there is no apparent trend as a function of penetration nozzle angle, the result for the penetration nozzle with the closest angle should be used.

3.   If a flaw is found which has a depth smaller than any depth shown for the penetration nozzle angle of interest, the initial flaw depth should be assumed to be the same as the smallest depth analyzed for that particular penetration nozzle.

4.   The flaw evaluation charts are applicable for aspect ratio of 6 or less. Consult with Westinghouse if the as-found flaw has an aspect ratio larger than 6.0.

No.	Orientation	Vertical Location	Circum. Location	Penetration Angle	Length (2c)	Depth (a)	a/t	Asp. Ratio	Wall Thick. (t)	Pen. No.	Source Figure
	Table 7-1			Example Problem Inputs: Initial Flaw Sizes and Locations							
1	Axial - Inside Surface	1.2" Below Weld	Uphill	29.1°	0.177"	0.071"	0.125	2.5:1	0.566"	30	6-2
2	Axial - Outside Surface	1.2" Below Weld	Uphill	29.1°	0.177"	0.071"	0.125	2.5:1	0.566"	30	6-9
3	Axial - Inside Surface	At Weld	Downhill	0.0°	0.210"	0.042"	0.075	5:1	0.566"	1	6-5
4	Axial - Inside Surface	1.0" Below Weld	Downhill	29.1°	0.394"	0.078"	0.138	5:1	0.566"	30	6-3, 6-5
5	Axial Through-Wall	0.4" Below Weld	Uphill	54.8°	--	--	--	--	0.407"	70	6-20

Note: The wall thickness used in these examples are for demonstration purposes, actual wall thickness at the location of interest must be used.

No.	Orientation	Vertical Location	Circum. Location	Penetration Angle	Length (2c)	Depth (a)	a/t	Asp. ratio	Wall Thick. (t)	Pen. No.	Source Figure
1	Axial - Inside Surface	1.2" Below Weld	Uphill	29.1°	0.177"	0.071"	0.125	2.5:1	0.566	30	6-2

Table 6-1

	Axial	
Location	a_f	l
Below Weld (ID)	t	no limit

Table 1-1

29	CEDM	29.1
30	CEDM	29.1
31	CEDM	29.1

Figure 7-1 Example Problem 1

No.	Orientation	Vertical Location	Circum. Location	Penetration Angle	Length (2c)	Depth (a)	a/t	Asp. ratio	Wall Thick. (t)	Pen. No.	Source Figure
2	Axial – Outside Surface	1.2" Below Weld	Uphill	29.1°	0.177"	0.071"	0.125	2.5:1	0.566	30	6-9

Table 6-1

Location	Axial	
	a_f	l
Below Weld (OD)	t	no limit

Table 1-1

29	CEDM	29.1
30	CEDM	29.1
31	CEDM	29.1

Figure 7-2 Example Problem 2

No.	Orientation	Vertical Location	Circum. Location	Penetration Angle	Length (2c)	Depth (a)	a/t	Asp. ratio	Wall Thick. (t)	Pen. No.	Source Figure
3	Axial - Inside Surface	At Weld	Downhill	0.0°	0.210"	0.042"	0.075	5:1	0.566	1	6-5

Table 6-1

Location	Axial	
	a_f	l
At and Above Weld (ID)	0.75 t	no limit

Table 1-1

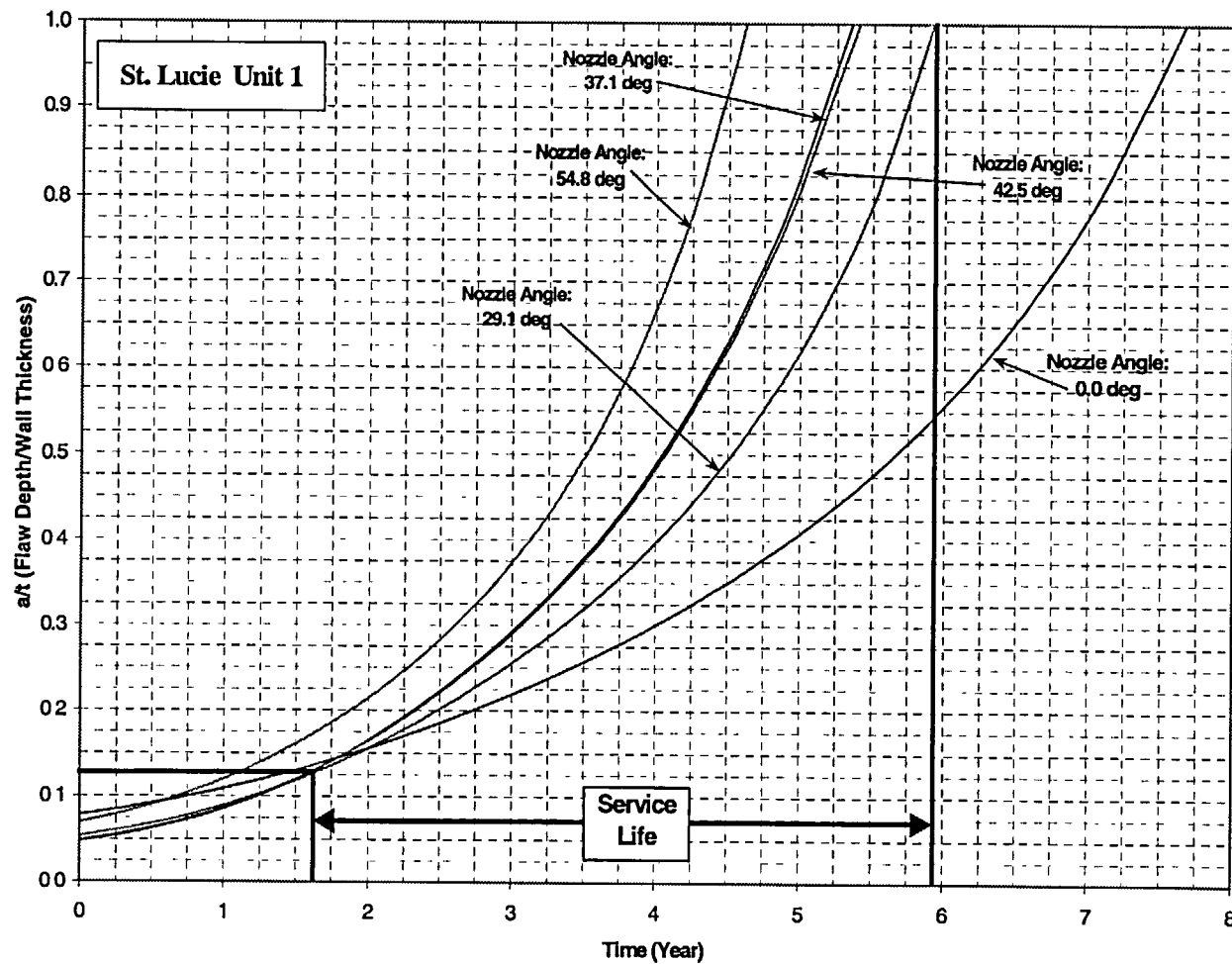| 1	CEDM	0.0
2	CEDM	11.0
3	CEDM	11.0

Figure 7-3 Example Problem 3

No.	Orientation	Vertical Location	Circum. Location	Penetration Angle	Length (2c)	Depth (a)	a/t	Asp. ratio	Wall Thick. (t)	Pen. No.	Source Figure
4	Axial - Inside Surface	1.0" Below Weld	Downhill	29.1°	0.394"	0.078"	0.138	5:1	0.566	30	6-3, 6-5

Table 6-1

Location	Axial	
	a_f	l
Below Weld (ID)	t	no limit

Table 1-1

29	CEDM	29.1
30	CEDM	29.1
31	CEDM	29.1

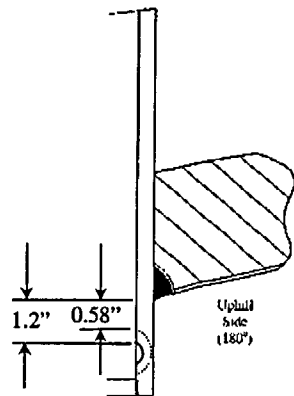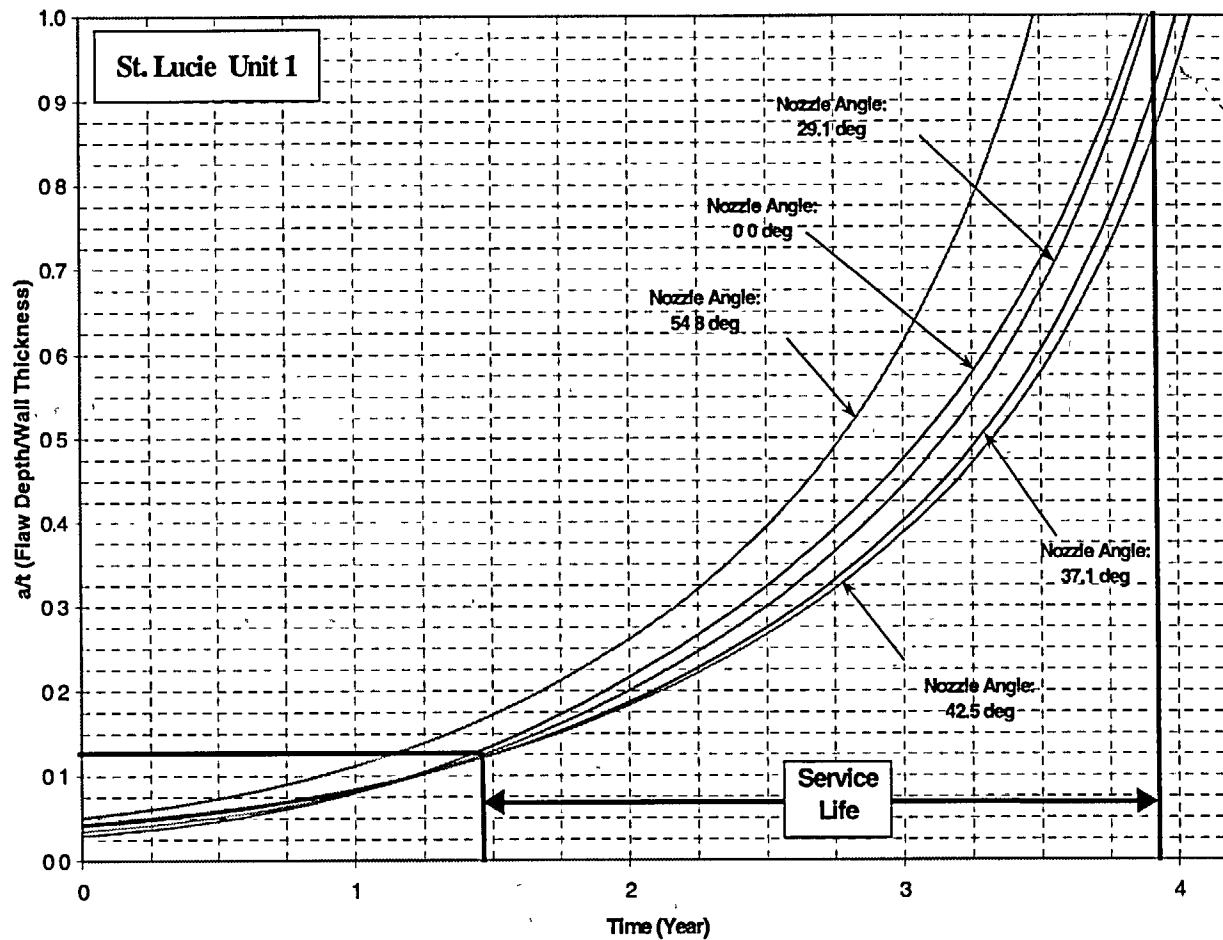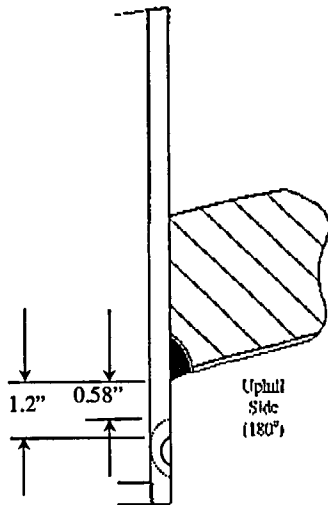Figure 7-4a Example Problem 4 (See also Figure 7-4b)

No.	Orientation	Vertical Location	Circum. Location	Penetration Angle	Length (2c)	Depth (a)	a/t	Asp. ratio	Wall Thick. (t)	Pen. No.	Source Figure
4	Axial - Inside Surface	1.0" Below Weld	Downhill	29.1°	0.394"	0.078"	0.138	5:1	0.566	30	6-3, 6-5

Table 6-1

Location	Axial	
	a_f	l
At Weld	t	.75 t

Table 1-1

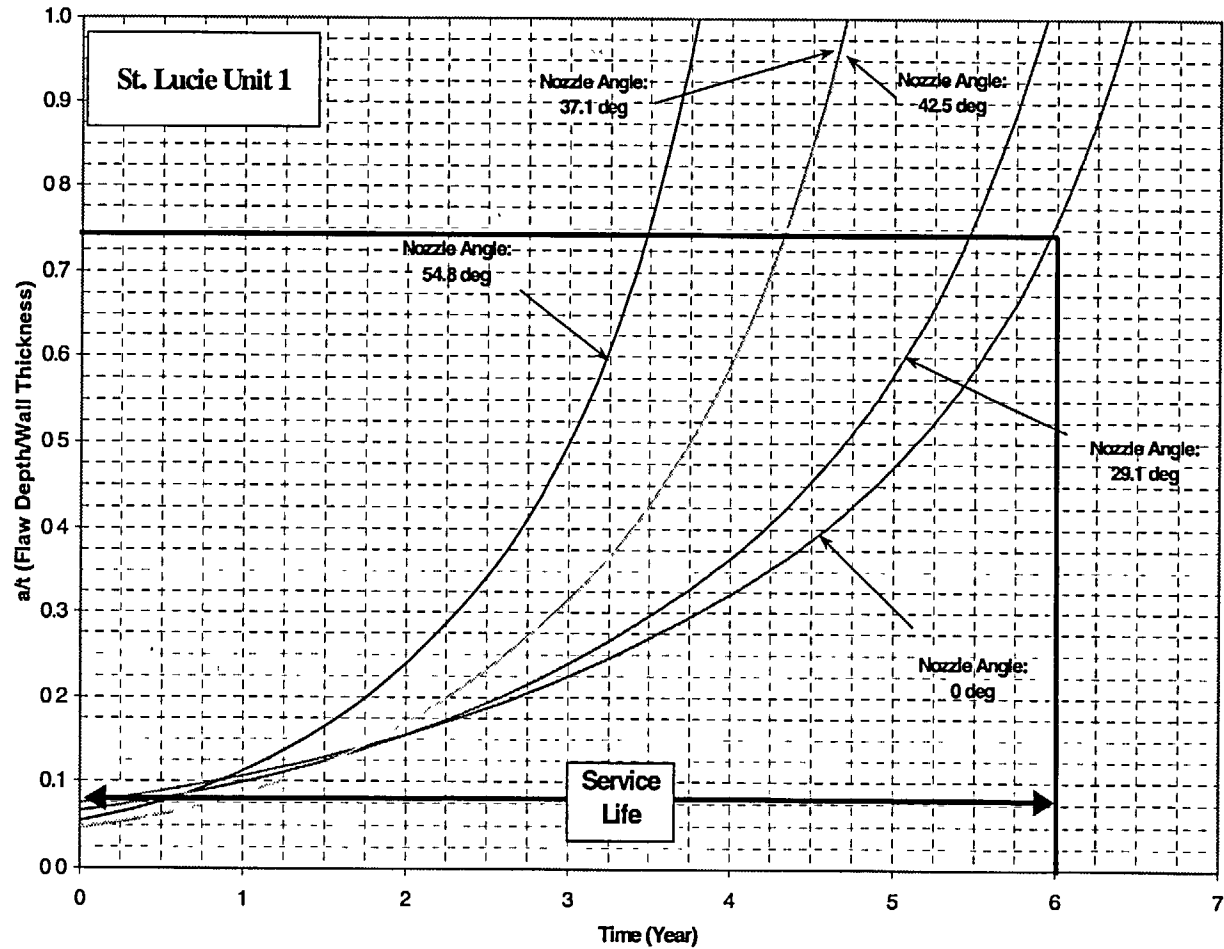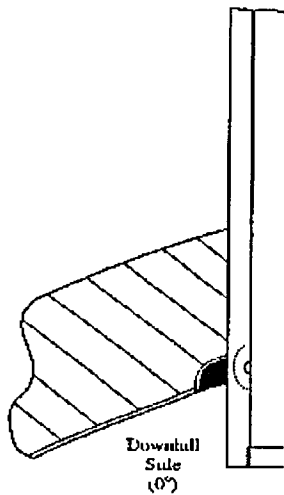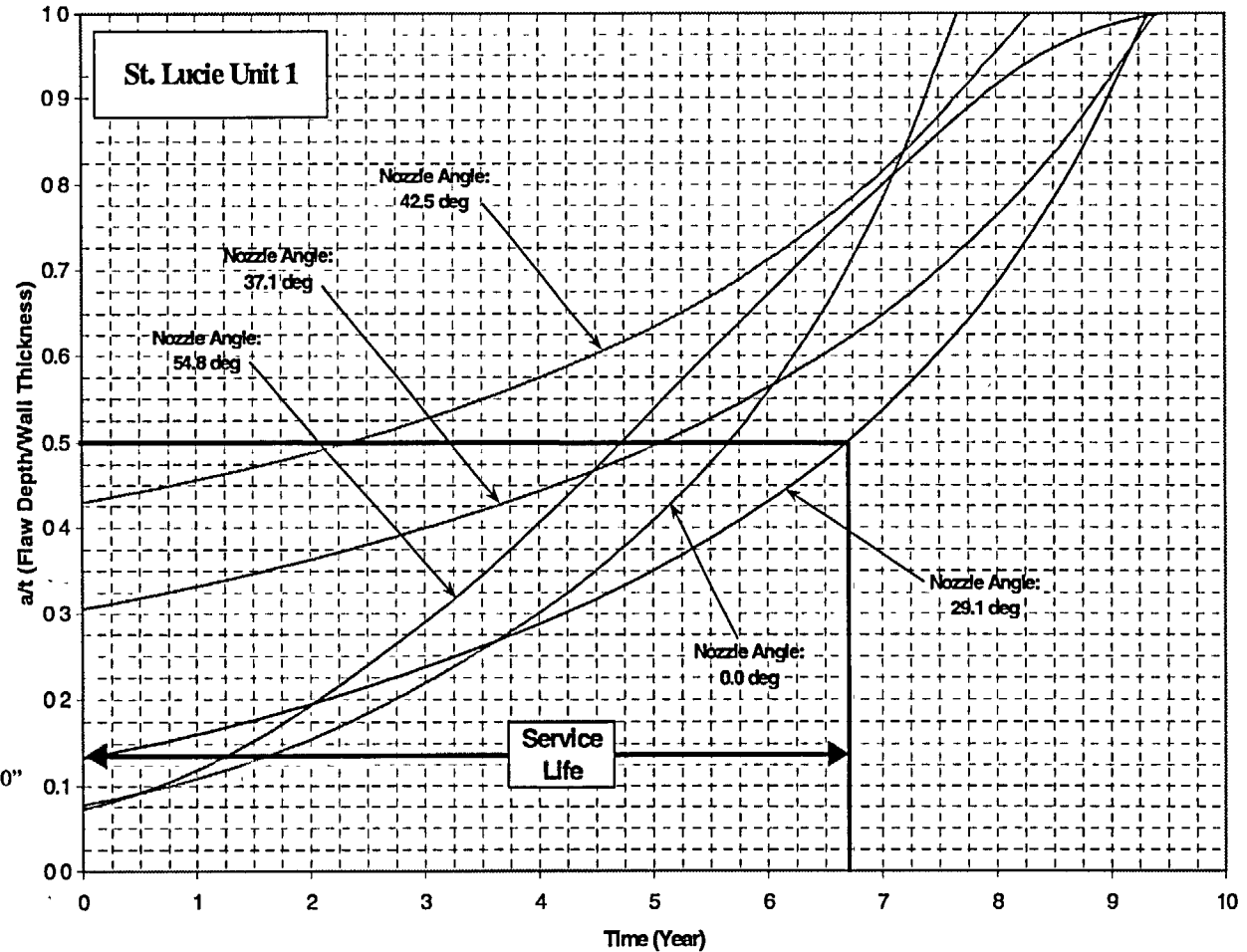| 29	CEDM	29.1
30	CEDM	29.1
31	CEDM	29.1
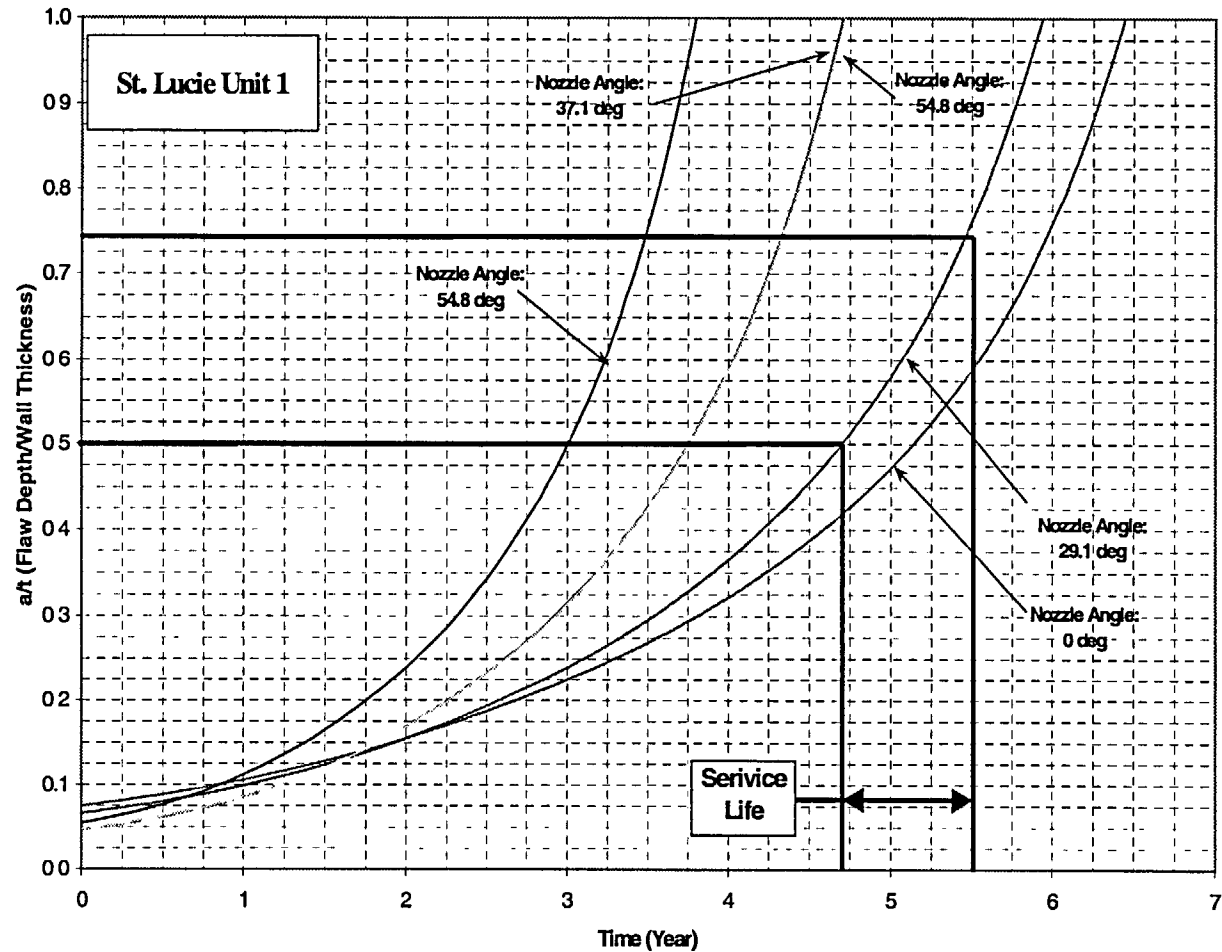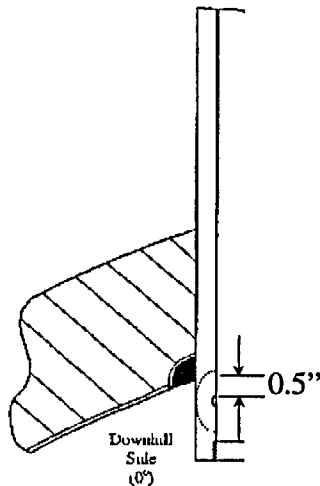
Figure 7-4b Example Problem 4 (See also Figure 7-4a)

No.	Orientation	Vertical Location	Circum. Location	Penetration Angle	Length (2c)	Depth (a)	a/t	Asp. ratio	Wall Thick. (t)	Pen. No.	Source Figure
5	Axial Through-Wall	0.4" Below Weld	Uphill	54.8°	--	--	--	--	.469	70	6-20

Table 6-1

Location	Axial	
	a_f	l
Below Weld (ID)	t	Bottom Weld

Table 1-1

69	CEDM	42.5
70	ICI	54.8
71	ICI	54.8
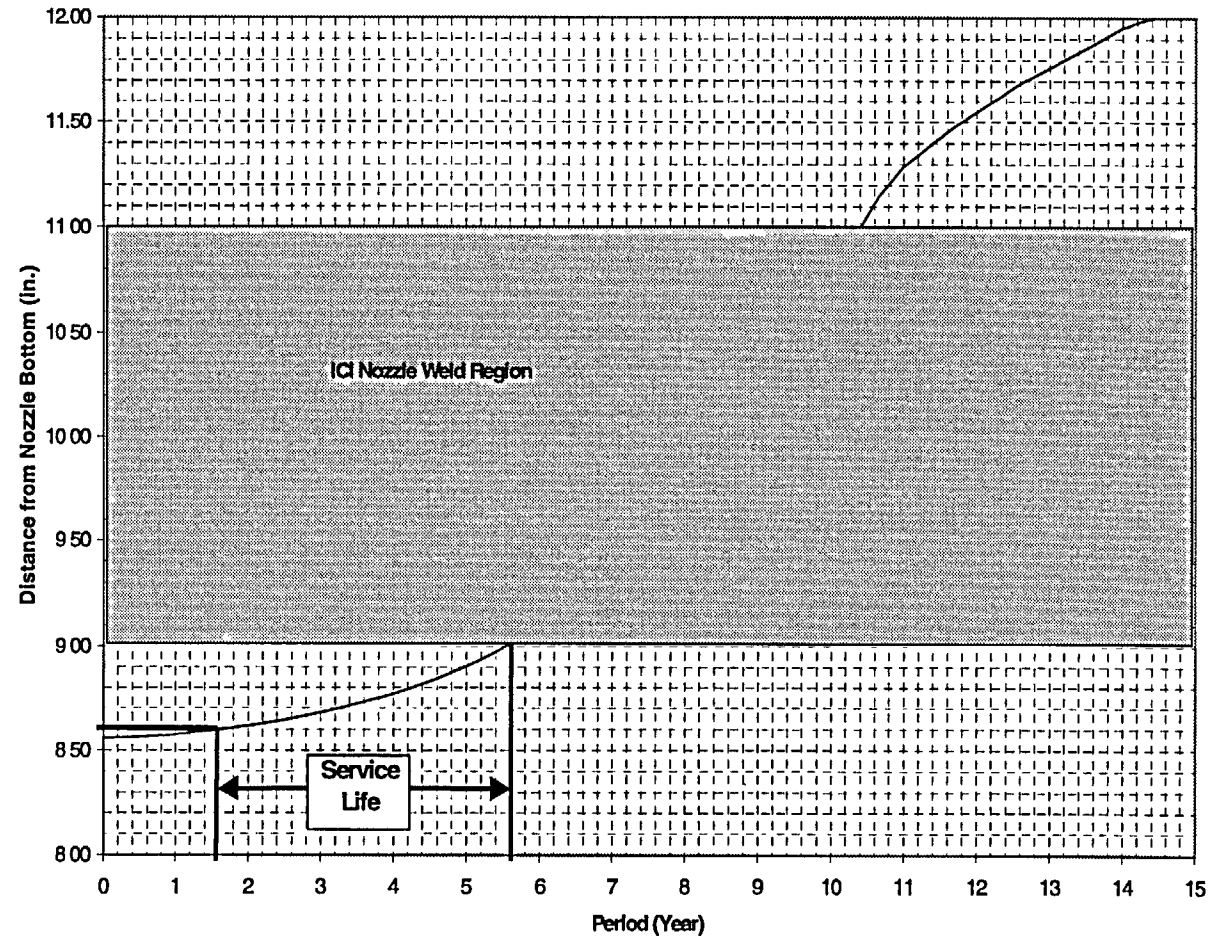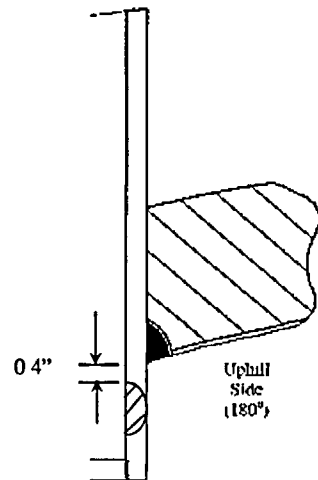
Figure 7-5 Example Problem 5

8   REFERENCES

1.   Scott, P. M., "An Analysis of Primary Water Stress Corrosion Cracking in PWR Steam Generators," in Proceedings, Specialists Meeting on Operating Experience With Steam Generators, Brussels Belgium, Sept. 1991, pages 5, 6.

2.   McIlree, A. R., Rebak, R. B., Smialowska, S., "Relationship of Stress Intensity to Crack Growth Rate of Alloy 600 in Primary Water," Proceedings International Symposium Fontevraud II, Vol, 1, p. 258-267, September 10-14, 1990.

3.   Cassagne, T., Gelpi, A., "Measurements of Crack Propagation Rates on Alloy 600 Tubes in PWR Primary Water, in Proceedings of the 5th International Symposium on Environmental Degradation of Materials in Nuclear Power Systems-Water Reactors," August 25-29, 1991, Monterey, California.

4A.   *Crack Growth and Microstructural Characterization of Alloy 600 PWR Vessel Head Penetration Materials,* EPRI, Palo Alto, CA. 1997. TR-109136.

4B.   Vaillant, F. and C. Amzallag. "Crack Growth Rates of Alloy 600 in Primary Water," Presentation to the EPRI-MRP Crack Growth Rate (CGR) Review Team, Lake Tahoe, NV, presented August 10, 2001, and revised October 11, 2001

4C.   Vaillant, F. and S. Le Hong. *Crack Growth Rate Measurements in Primary Water of Pressure Vessel Penetrations in Alloy 600 and Weld Metal 182,* EDF, April 1997. HT-44/96/024/A.

4D.   Framatome laboratory data provided by C. Amzallag (EDF) to MRP Crack Growth Rate Review Team, October 4, 2001 (Proprietary to EDF).

4E.   Cassagne, T., D. Caron, J. Daret, and Y. Lefevre. "Stress Corrosion Crack Growth Rate Measurements in Alloys 600 and 182 in Primary Water Loops Under Constant Load," *Ninth International Symposium on Environmental Degradation of Materials in Nuclear Power Systems-Water Reactors* (Newport Beach, CA, August 1-5, 1999), Edited by F. P. Ford, S. M. Bruemmer, and G S. Was, The Minerals, Metals & Materials Society (TMS), Warrendale, PA, 1999.

4F.   Studsvik laboratory data provided by Anders Jenssen (Studsvik) to MRP Crack Growth Rate Review Team, October 3, 2001 (Proprietary to Studsvik).

4G.   [   ]a,c,e

4H.   "Materials Reliability Program (MRP) Crack Growth Rates for Evaluating Primary Water Stress Corrosion Cracking (PWSCC) of Thick Wall Alloy 600 Material," EPRI MRP Report MRP-55, May 30, 2002.

4I.   "Crack Growth Rate Tests of Alloy 600 in Primary PWR Conditions," Communication from M. L. Castaño (CIEMAT) to J. Hickling (EPRI), March 25, 2002.

4J.   G∴mez-BriceZo, D., J. LapeZa, and F. Bl<zquez. "Crack Growth Rates in Vessel Head Penetration Materials," *Proceedings of the International Symposium Fontevraud III: Contribution of Materials Investigation to the Resolution of Problems Encountered in Pressurized Water Reactors* (Chinton, France, September 12-16, 1994), French Nuclear Energy Society, Paris, 1994, pp. 209-214.

4K.   G∴mez-BriceZo, D. and J. LapeZa. "Crack Growth Rates in Vessel Head Penetration Materials," *Proceedings: 1994 EPRI Workshop on PWSCC of Alloy 600 in PWRs* (Tampa, FL, November 15-17, 1994), EPRI, Palo Alto, CA, TR-105406, August 1995, pp. E4-1 through E4-15.

4L.   G∴mez-BriceZo, D., et al. "Crack Propagation in Inconel 600 Vessel Head Penetrations," Eurocorr 96, Nice, France, September 24-26, 1996.

4M.   CastaZo, M. L., D. G∴mez-BriceZo, M. Alvarez-de-Lara, F. Bl<zquez, M. S. Garcia, F. Hem<ndez, and A. Largares. "Effect of Cationic Resin Intrusions on IGA/SCC of Alloy 600 Under Primary Water Conditions," *Proceedings of the International Symposium Fontevraud IV: Contribution of Materials Investigation to the Resolution of Problems Encountered in Pressurized Water Reactors* (France, September 14-18, 1998), French Nuclear Energy Society, Paris, 1998, Volume 2, pp. 925-937.

5A.   Newman, J. C. and Raju, I. S., "Stress Intensity Factor Influence Coefficients for Internal and External Surface Cracks in Cylindrical Vessels," in <u>Aspects of Fracture Mechanics in Pressure Vessels and Piping</u>, PVP Vol. 58, ASME, 1982, pp. 37-48.

5B.   Hiser, Allen, "Deterministic and Probabilistic Assessments," presentation at NRC/Industry/ACRS meeting, November 8, 2001.

6A.   [
                                                              ] a,c,e

6B.   [
                                                              ] a,c,e

6C.   [
                                                              ] a,c,e

7.   USNRC Letter, W. T. Russell to W. Raisin, NUMARC, "Safety Evaluation for Potential Reactor Vessel Head Adapter Tube Cracking," November 19, 1993.

8.   USNRC Letter, A. G. Hansen to R. E. Link, "Acceptance Criteria for Control Rod Drive Mechanism Penetrations at Point Beach Nuclear Plant, Unit 1," March 9, 1994.

9.   Materials Reliability Program Response to NRC Bulletin 2001-01 EPRI MRP Report 48 (TP 1006284), August 2001.

10. "CEOG Program to Address A; pw 600 Cracking of CEDM Penetrations Subtask 1 Nozzle Evaluation," CE NSPD-903-P, CEOG Task 730, Combustion Engineerng Owners Group, February 1993.

11. "CE Drawing No. E-233-498, Miscellaneous Details, 172" I.D. PWR

12. CEOG Report # CEN-614, "Safety Evaluation of the Potential for and Consequences of Reactor Vessel Head Penetration Alloy 600 OD Initiated Nozzle Cracking," December 1993

APPENDIX A

ALLOWABLE AREAS OF LACK OF FUSION: WELD FUSION ZONES

There are two fusion zones of interest for the head penetration nozzle attachment welds, the penetration nozzle itself (Alloy 600) and the reactor vessel head material (A533B ferritic steel). The operating temperature of the upper head region of the St. Lucie Unit 1 is 311°C (591°F) and the materials will be very ductile. The toughness of both materials is quite high and any flaw propagation along either of the fusion zones will be totally ductile.

Two calculations were completed for the fusion zones, one for the critical flaw size, and the second one for the allowable flaw size, which includes the margins required in the ASME code. The simpler case is the Alloy 600 fusion zone, where the potential failure will be a pure shearing of the penetration as the pressurized penetration nozzle is forced outward from the vessel head, as shown in Figure A-1.

The failure criterion will be that the average shear stress along the fusion line exceeds the limit shear stress. For the critical flaw size, the limiting shear stress is the shear flow stress, which is equal to half the tensile flow stress, according to the Tresca criterion. The tensile flow stress is the average of the yield stress and ultimate tensile stress of the material. The criterion for Alloy 600 tubes in the upper head region is:

Average shear stress < shear flow stress = 26.85 ksi

This value was taken from the ASME Code, Section III, Appendix I, at 600°F.

For each penetration, the axial force, which produces this shear stress, results from the internal pressure. Since each penetration has the same outer diameter, the axial force is the same. The average shear stress increases as the load carrying area decreases (the area of lack of fusion increases). When this increasing lack of fusion area increases the stress to the point at which it equals the flow stress, failure occurs. This point may be termed the critical flaw size. This criterion is actually somewhat conservative. Alternatively, use of the Von Mises failure criterion would have set the shear flow stress equal to 60 percent of the axial flow stress, and would therefore have resulted in larger critical flaw sizes.

The allowable flaw size, as opposed to the critical flaw size discussed above, was calculated using the allowable limit of Section III of the ASME Code, paragraph NB 3227.2. The criterion for allowable shear stress then becomes:

Average shear stress < 0.6 S_m = 13.98 ksi

where:

S_m = the ASME Code limiting design stress from Section III, Appendix I.

The above approach was used to calculate the allowable flaw size and critical flaw size for the outermost and center penetrations. The results show that a very large area of lack of fusion can be tolerated by the

head penetrations, regardless of their orientation. These results can be illustrated for the outermost CEDM penetration.

The total surface contact area for the fusion zone on the outermost head penetration is 17.4 in^2. The calculations above result in a required area to avoid failure of only 1.45 in^2, and using the ASME Code criteria, the area required is 2.79 in^2. These calculations show that as much as 83.9 percent of the weld may be unfused, and the code acceptance criteria can still be met.

To envision the extent of lack of fusion allowed, Figure A-2 was prepared. In this figure, the weld fusion region for the outermost penetration has been shown in an unwrapped, or developed view. The figure shows the extent of lack of fusion allowed in terms of limiting lengths for a range of circumferential lack of fusion. This figure shows that the allowable vertical length of lack of fusion for a full circumferential unfused region is 84 percent of the weld length. Conversely, for a region of lack of fusion extending the full vertical length of the weld, the circumferential extent is limited to 302 degrees. The extent of lack of fusion which would cause failure is labeled "critical" on this figure, and is even larger. The dimensions shown on this figure are based on an assumed rectangular area of lack of fusion.

The full extent of this allowable lack of fusion is shown in Figure A-3, where the axes have been expanded to show the full extent of the head penetration-weld fusion line. This figure shows that a very large area of lack of fusion is allowed for the outer most penetration. Similar results were found for the center penetration, where the weld fusion area is somewhat smaller at 16.1 in^2.

A similar calculation was also carried out for the fusion zone between the weld and the vessel head, and the result is shown in Figure A-4. The allowable area of unfused weld for this location is 84.8 percent of the total area. This approach to evaluating the fusion zone with the carbon steel vessel head is only approximate, but may provide a realistic estimate of the allowable. Note that even a complete lack of fusion in this region would not result in penetration nozzle ejection, because the weld to the head penetration would prevent the penetration nozzle from moving up through the vessel head.

The allowable lack of fusion for the weld fusion zone to the vessel head using the approximate approach may be somewhat in doubt, because of the different geometry, where one cannot ensure that the failure would be due to pure shear. To investigate this concern, additional finite element models were constructed with various degrees of lack of fusion discretely modeled, ranging from 30 to 65 percent. The stress intensities around the circumference of the penetration were calculated to provide for the effects of all the stresses, as opposed to the shear stress only, as used above. When the average stress intensity reaches the flow stress (53.7 ksi), failure is expected to occur. The code allowable stress intensity is 1.5 S_m, or 35 ksi, using the lower of the Alloy 600 and ferritic allowables at 316°C (600°F).

The results of this series of analyses are shown in Figure A-5, where it is clear that large areas of lack of fusion are allowed. As the area of lack of fusion increases, the stresses redistribute themselves, and that the stress intensity does not increase in proportion to the area lost. These results seem to confirm that shear stress is the only important stress governing the critical flaw size for the vessel head fusion zone as well.
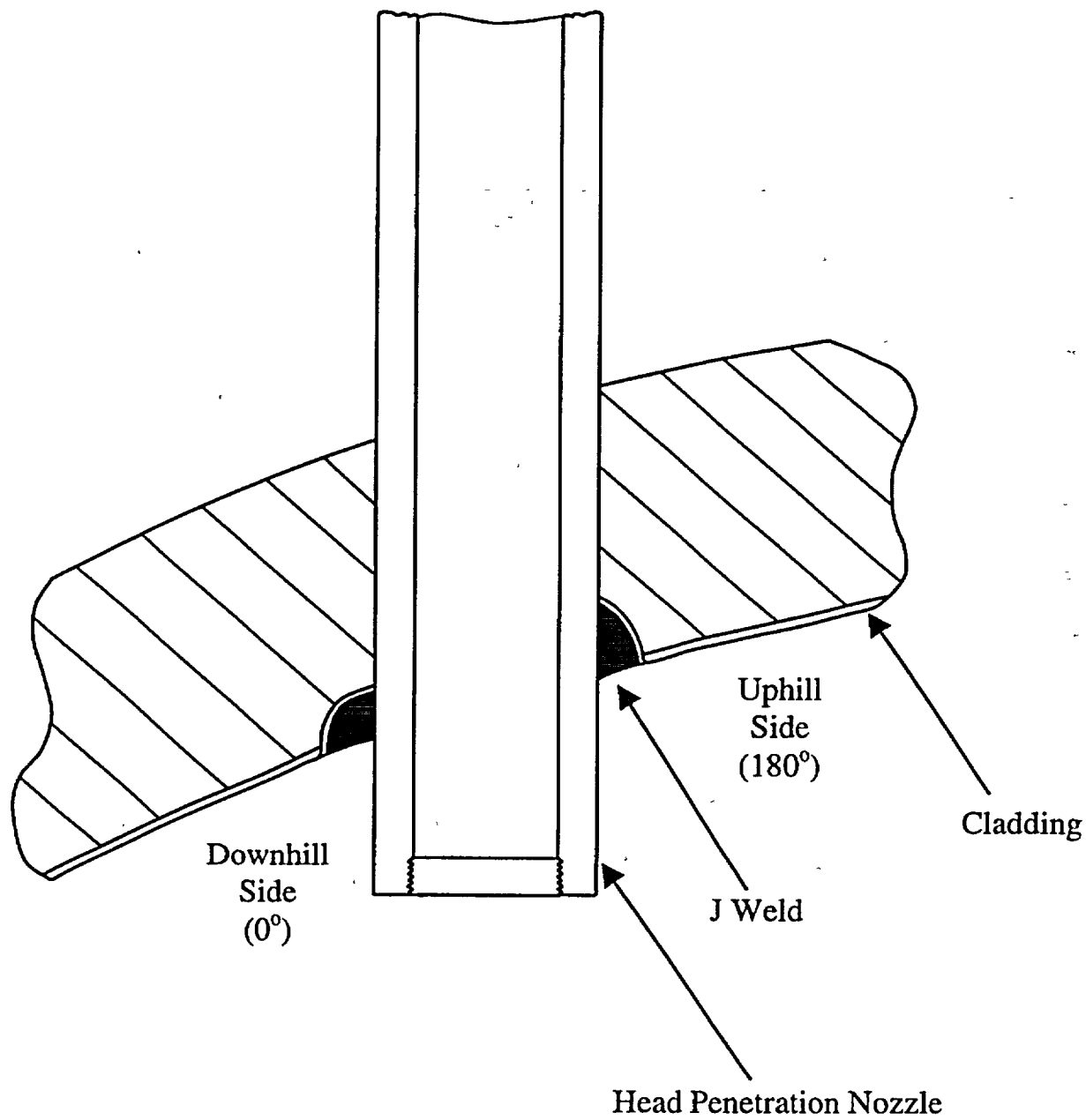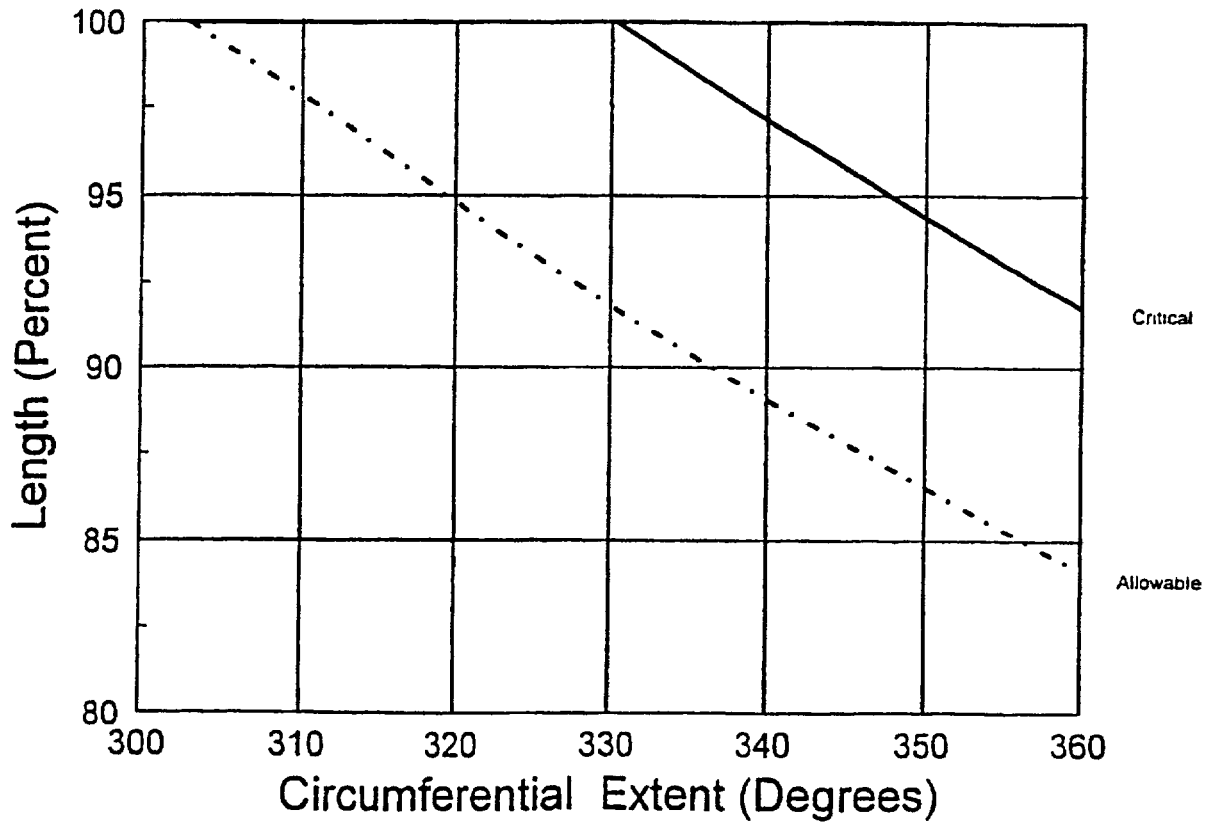
Figure A-1 Typical Head Penetration

Figure A-2   Allowable Regions of Lack of Fusion for the Outermost Penetration Tube to Weld Fusion Zone: Detailed View
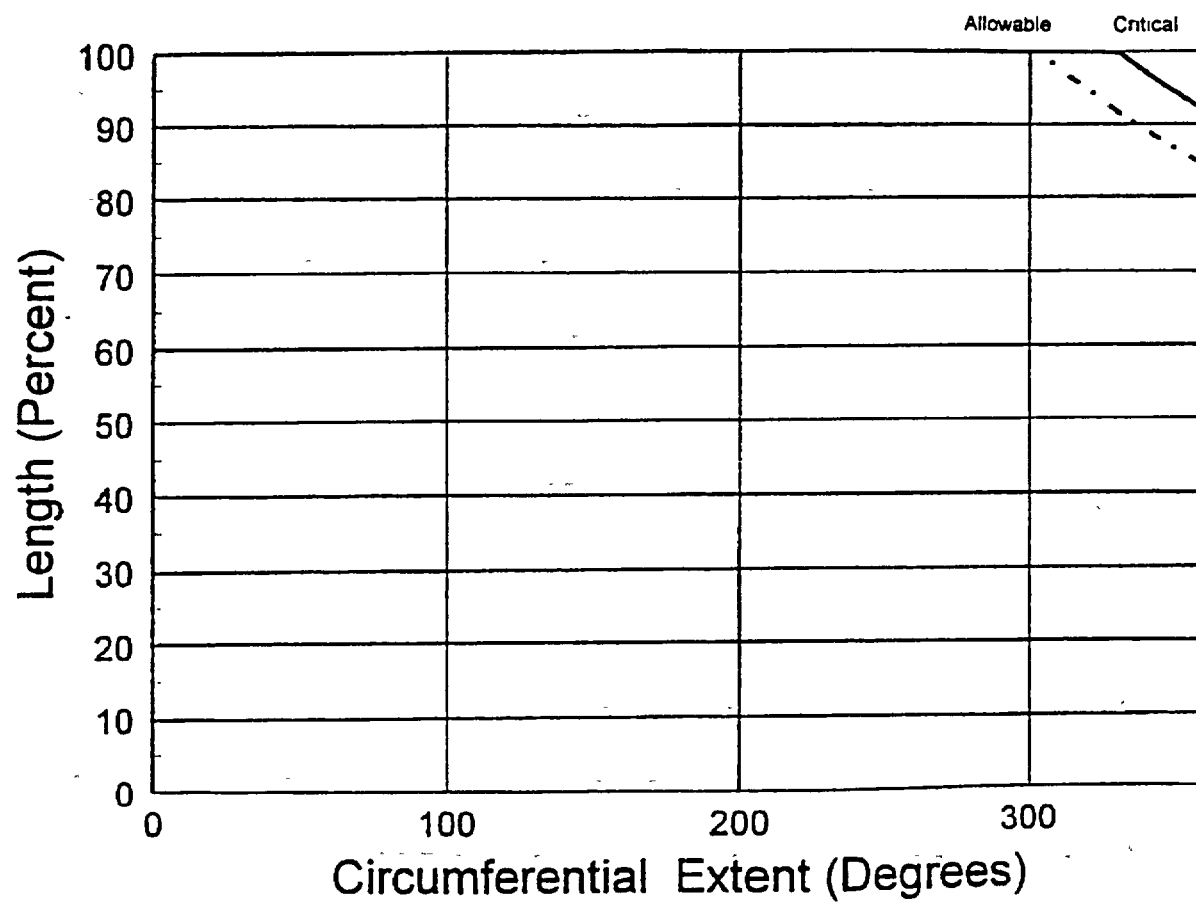
Figure A-3   Allowable Regions of Lack of Fusion for the Outermost Penetration Tube to Weld Fusion Zone
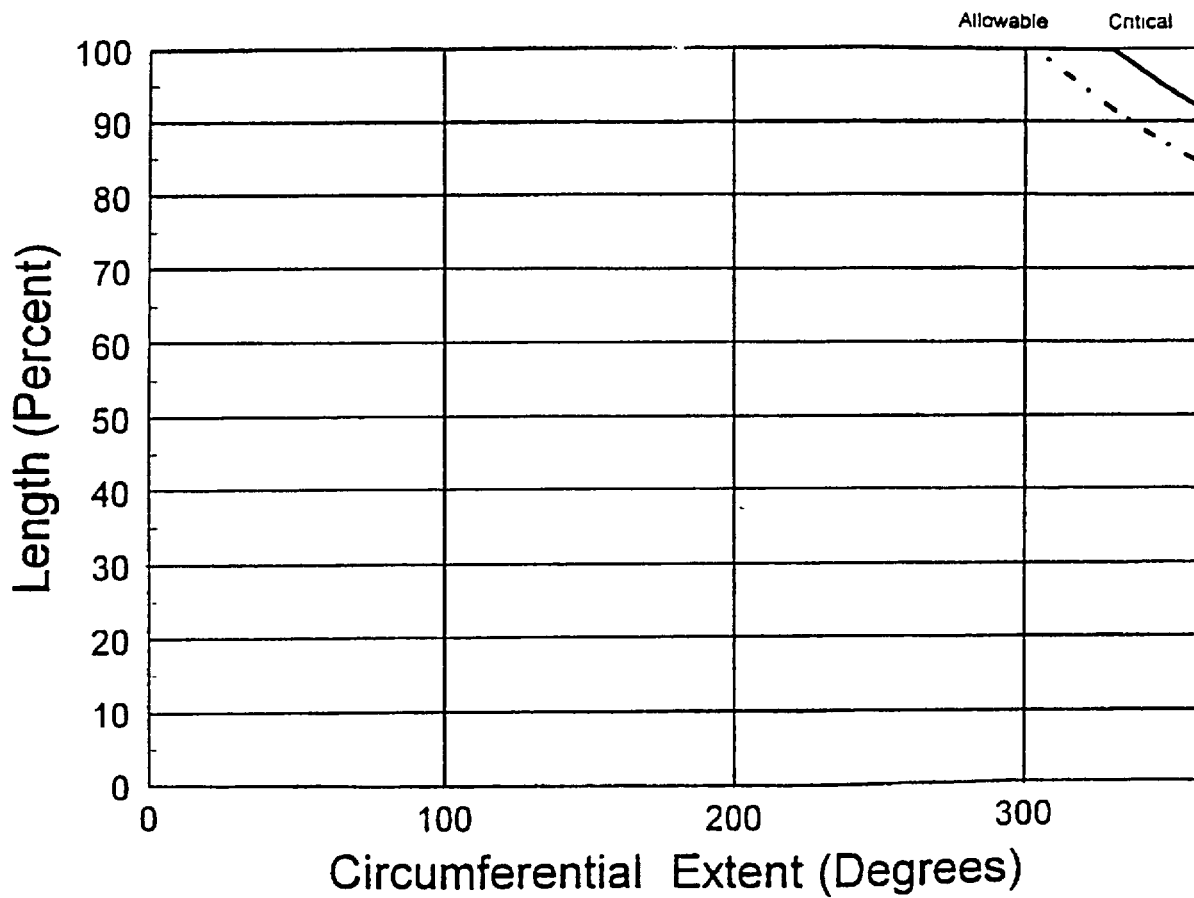
Figure A-4 Allowable Regions of Lack of Fusion for all Penetrations: Weld to Vessel Fusion Zone
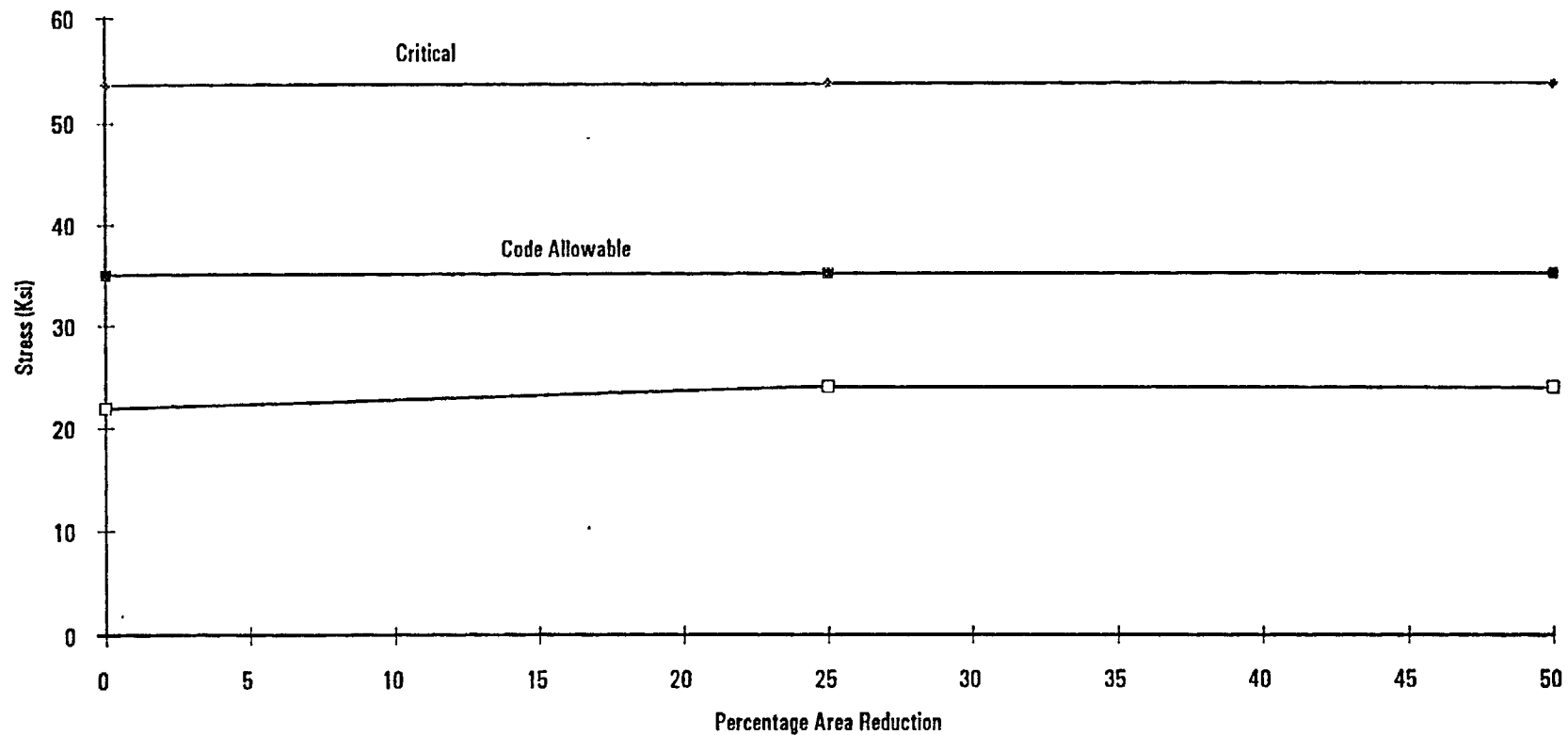
Figure A-5 Allowable Regions of Lack of Fusion for the Weld to Vessel Fusion Zone

APPENDIX B

FLAW TOLERANCE EVALUATION GUIDELINES

Step 1: Determine Location and Orientation of the Flaw

- Axial or Circumferential
- Inside or Outside Surface
- Above, At or Below Attachment Weld
- Uphill or Downhill

Step 2: Identify the Applicable Flaw Tolerance Chart(s)

- 0.5" Below Weld
- At or Near the Weld
- 0.5" Above Weld

Step 3: Identify Penetration Number for the Flawed Penetration Nozzle

Step 4: Go to Table 1-1 to obtain the Penetration Nozzle Locality Angle

Step 5: Determine the Ratio a/t of Flaw Depth (a) to Wall Thickness (t)

Step 6: Determine the Initial Reference Time for the Flaw

- Draw a horizontal line intersecting the vertical axis at the value of a/t

- Draw a vertical line downwards at the point where the horizontal line intersects the applicable penetration nozzle locality angle curve

- The initial reference time for the flaw is where the vertical line intersects the horizontal axis

Step 7: Go to Table 6-1 to Determine Acceptance Criteria

- Determine the acceptable a/t ratio

Step 8: Determine the Final Reference Time for the Flaw

- Draw a horizontal line intersecting the vertical axis at the value of the allowable a/t

- Draw a vertical line downwards at the point where the horizontal line intersects the applicable penetration nozzle locality angle curve

- The final reference time for the flaw is where the vertical line intersects the horizontal axis

Step 9: Determine the Remaining Service Life

- Remaining Service Life = Final Reference Time - Initial Reference Time

Additional Guidelines

1. Flaws in Penetration Nozzles with Locality Angles Not Shown on Flaw Tolerance Charts

   a. use interpolation (if there is an uniform trend as a function of nozzle angle)
   b. use the curve with the closest nozzle locality angle (if there is no apparent trend)

2. Flaw with Flaw Depth Smaller than Shown on the Flaw Tolerance Charts

   a. assume flaw depth the same as the smallest flaw depth analyzed

3. The flaw evaluation charts are applicable for aspect ratio of 6 or less. Consult with Westinghouse if the as-found flaw has an aspect ratio larger than 6.0.